Forging Specimen Design

for

Magnesium Alloys

by

Guo Yu

A thesis

presented to the University of Waterloo

in fulfillment of the

thesis requirement for the degree of

Master of Applied Science

in

Mechanical Engineering

Waterloo, Ontario, Canada, 2016

AUTHOR'S DECLARATION

I hereby declare that I am the sole author of this thesis. This is a true copy of the thesis, including any required final revisions, as accepted by my examiners.

I understand that my thesis may be made electronically available to the public.

Abstract

The automotive industry is seeking every possible way to reduce the vehicle weight in order to achieve better fuel efficiency. Forged magnesium (Mg) alloys, due to low density and high stiffness-to-weight ratio, have potential to replace the current structural materials. Forging of Mg alloys is not new, however, forging process finite element simulation and design guidelines are needed to help design the final product.

Three materials in two conditions were under investigation – extruded/cast AZ31, extruded/cast AZ80, and extruded/cast ZK60. Simple uniaxial compression tests were conducted in longitudinal and transverse directions of the cylindrical billets to examine their forging behaviour. By comparing the experimental results to an isotropic simulation result, it was observed that anisotropy was pronounced at forging temperature and could not be ignored. An anisotropic material model in finite element simulation was necessary to capture material's real-life behavior. Hill's anisotropic material model in DEFORM 3D was therefore selected for this design project.

Hill's material model in DEFORM 3D not only required material's rate-sensitive flow stress data, but also 6 anisotropic coefficients that need to be generated from compressive yield stresses and shear yield stresses. Shear hat tests were conducted for extruded materials in order to produce these anisotropic coefficients. Complete material models were created for all extruded materials at their own optimal forging conditions.

A small-scale forging sample designed for the 110-ton press was necessary to validate the material model and simulation results. The first design iteration was based on existing axisymmetric design in literature. The second attempt was proposed based on a rib-web geometry forging specimen. The final design improved the second one to accommodate for more test samples. Both the geometric and load comparisons between simulation and experiment were promising.

The model was then used to design a simplified forging sample to test material forgeability and access forging process parameters. The simplified forging sample was intended to fit in between lab-scale specimens and the final component. A few trial geometries were proposed and evaluated based on material flow and die complexity. A symmetric I-beam geometry with distinct rib features was selected as the final design. Simulations of all extruded materials were carried out to compare with the experiments. The material model served its purpose but can still be improved based on the geometric comparison.

Acknowledgements

I would like to express my gratitude to my supervisor, Professor Steve Lambert, for giving me the opportunity to work on this project and for his invaluable support and guidance throughout my research.

I wish to thank Jonathan McKinley for the valuable suggestions on simulation and tooling design, and Bruce Williams for the discussion of forging conditions.

I am thankful to Yuqyan Ding, Mark Whitney, Lucian Blaga for their technical assistance. I would also like to thank Alex Strong, Andrew Gryguc, Paresh Prakash, Rick Wong, Amir Hadadzadeh for the helpful discussions.

I sincerely thank my parents for their encouragement; this journey would not be possible without their continuous support.

Lastly and most importantly, I owe my deepest gratitude to my lovely wife, Jun, for her understanding and dedication to our small family. This accomplishment would not have been possible without her devotion and love.

Table of Contents

List of Figures

ix

List of Tables

Nomenclature

$\sigma_{11}, \sigma_{22}, \sigma_{33}$	Principal stresses	[MPa]
$\sigma_{12}, \sigma_{23}, \sigma_{31}$	Shear stresses	[MPa]
F,G,H,L,M,N	Hill's anisotropic coefficients	[Unitless]
$\bar{\sigma}_0$	Equivalent stress	[MPa]
σ_{max}	Maximum principal stress	[MPa]
σ_i	Effective stress	[MPa]
ε_i	Effective strain	[mm/mm]
C	Critical damage value	[Unitless]
F	Compressive force	[kN]
d_0	Initial diameter of Gleeble billet	[mm]
h_0	Initial height of Gleeble billet	[mm]
σ	True stress	[MPa]
ε	True strain	[mm/mm]
$\dot{\gamma}$	Shear strain rate	[strain/s]
v	Shear velocity	[mm/s]
h	Shear region height	[mm]
A	Shear region area	[mm^2]
m	Shear factor	[Unitless]
μ	Coefficient of friction	[Unitless]
w	Width of flash	[mm]
t	Thickness of flash	[mm]

Chapter 1

Introduction

The automotive industry is seeking every possible way to reduce vehicle weight in order to improve overall fuel efficiency. Magnesium alloys, due to low density and high stiffness to weight ratio, have gained popularity in recent years. Most magnesium applications in automobiles are in the form of sheet metal or body panels, not structural components. It is desired to replace aluminum or steel structural components with magnesium to further reduce weight. Therefore, in this project, a front suspension component is to be forged from magnesium alloys to take the place of a current cast aluminum control-arm. The candidate materials include 3 magnesium alloys in 2 conditions: AZ31 (extrusion and cast), AZ80 (extrusion and cast), and ZK60 (extrusion and cast).

This work was carried out in collaboration with various researchers at Waterloo as well as CanmetMATERIALS, with oversight from Multimatic Technical Corporation and Ford. It was funded through the Automotive Partnership Canada [1]. The Waterloo team is divided into 6 tasks to conduct research on different aspects of the project: design (this group), forging, fatigue, residual stresses, corrosion and residual stress measurement.

Due to limited experience with magnesium forging technology, the forging process design, including forging geometry, must proceed with extra care. Thus, instead of directly forging a control-arm, a decision has been made to design and forge small-scale test specimens to help characterize material behavior during the forging process and to fine-tune the forging parameters. The presented work addresses the design target with a number of forging tests and with the help of finite element simulations.

1.1 Objectives

The ultimate goal of this work is to create a forging model that can supplement physical tests and to design a simplified forging specimen to test material behavior and process parameters. The objectives are listed and explained below.

- Create forging model in finite element simulation

   The forging model consists of a material model, boundary conditions (interfacial coefficient of friction, heat transfer), and forging process parameters. Forging process parameters include

temperature selection, material selection, shape design, and die design. Proper material model is essential to a successful simulation. The forging simulation software DEFORM 3D has a built-in material model to capture anisotropic behavior. Material characterization tests are necessary to determine the parameters in such a material model.

- Study material forgeability

Forgeability means a material's ability to form a workpiece without defects while forming all features of a product. Forgeability can be assessed using forging load, die filling and final surface condition. Forgeability is important not only because it affects how easy or difficult it is to form a specific product, but also has an impact on forging load, which is limited by the equipment at CanmetMATERIALS. The forgeability of all 6 materials can be compared using same test geometry and forging condition.

- Validate simulation using small-scale tests

Prior to using simulation to help design the simplified specimen, validation of the FE model was conducted to assess its reliability. Validation can be done by comparing forging load and forging geometry. A lower-resolution forging specimen needs to be designed for this validation purpose.

- Design simplified forging specimen

The simplified forging specimen is intended to fit in between the small-scale Gleeble specimens, used to examine material behavior, and the completed component. It should have adequate dimensions to accommodate material characterization specimens but small in size to minimize complexity and save die cost. Experiences gained in the small-scale forgings should transfer to geometry and process design for the final product.

1.2 Thesis Overview

This thesis consists of five major parts: literature review, material characterization and modelling, preliminary tests, 110-ton forging, and 500-ton forging.

Chapter 2 focuses on a literature review. A shear test to determine coefficients for material model is introduced. Previous forging simulations using FE software is reviewed. A damage criterion in simulation to predict material failure is presented. Successful forging design and design parameters are briefly discussed.

Chapter 3 discusses material properties and the modelling approach. Small-scale Gleeble forging is briefly introduced. The shear test to generate anisotropic material data is discussed. Sample preparation and experimental setup are explained and the test results are presented. Hill's anisotropic material model in DEFORM 3D is described and the method to calculate the coefficients is discussed.

Chapter 4 introduces three types of preliminary tests to investigate forging parameters. The first test is the "pancake" test which compresses a cylindrical billet axially to form a disk. Simulation and test load results are compared. The second test is the ring compression test, used to determine the friction behaviour. The experimental setup and billet geometry are explained. The procedure to create the friction calibration curve in simulation is introduced. The third test is the "flatbread" test, which compresses the billet in the transverse direction and therefore is more representative of the component configuration. The importance of anisotropic material simulation is examined. Details of the test setup, simulation parameters and forging results are presented.

Chapter 5 covers the geometry design, tooling design, experiment setup, numerical simulation and validation of the specimen used in the 110-ton press. The evolution of geometric design as well as the final tooling design are discussed. Test parameters and material preparation are also included. Geometric and load comparisons between tests and simulations are conducted. These tests served as an additional way to validate the simulation and also provided insight into material forgeability.

Chapter 6 describes the design of a simplified I-beam forging sample for use in the 500 tone press, using the complete anisotropic material model. Three designs were considered and the design compromises are explained. Tooling design ideas and parameters are briefly discussed. The experimental procedure is described followed by simulation and test comparison.

Finally, chapter 7 summarizes the design work and provides recommendations for future work.

Chapter 2
Literature Review

2.1 Overview

While magnesium (Mg) alloys are lightweight and have good structural properties, they have poor cold workability at room temperature due to their HCP structure and limited basal slip systems. Non-basal slip systems can be activated at warm forging temperatures above 250 $^{\circ}$C to increase their workability, so forging is limited to temperatures between about 300 and 500 $^{\circ}$C. Material data is available in the literature for AZ31B Mg alloy [2]. For our actual materials, uniaxial compression tests were conducted within the research group[1] to explore the material behavior of the alloys. Flow stress data in the extrusion direction (ED) and the transverse direction (TD) of the material stock were therefore available within the group.

2.2 Hill's Anisotropic Material Model and Shear Hat Test

Anisotropy is another challenge when dealing with Mg alloys. Although the intensity of anisotropy decreases with temperature, it is observable and should be considered in the design process. Thus an anisotropic material model in the simulation was necessary to replicate their real-life behavior. Due to the lack of material data at this stage of the project, it was desired to use a simple material model. A material model that is easy to use in simulation can provide great help in geometry and tooling design.

In DEFORM 3D, material anisotropy can be captured by using different yield functions. There are three types of yield functions available in the software: Von Mises, Hill's quadratic (6 coefficients - FGHLMN, R value, polycrystalline plasticity model) and Lankford coefficient (R value). Von Mises is the default setting in the software for an isotropic material.

According to DEFORM documentation [3], Hill's quadratic (R value) and Lankford coefficient (R value) models are "useful for material flow along an axial direction with small reduction of thickness" which are not suitable for bulk metal forging process.

That leaves us with two options – Hill's 6 coefficients FGHLMN or a Polycrystal Plasticity model.

---

[1] Amir Hadadzadeh, Paresh Prakash, and Rick Wong, supervised by Professor Mary Wells

The FGHLMN model requires 6 coefficients to define material flow in the three main directions and three shear directions. The quadratic polycrystalline plasticity model not only needs 6 coefficients but also relies on texture information to work, including inputs of crystal type and texture type. Texture mesh type also needs to be defined for the Rodrigues space [4].

As material data was limited at the early stage of the project, the Hill's FGHLMN model was a clear choice. Kobold et al. [5] have used same material model to simulate wrought AZ80 successfully in DEFORM 3D for both experimental trials and industrial-scale part.

Rodney Hill [6] developed this yield criterion for anisotropic materials in 1948. The quadratic yield function has the form of

$$F(\sigma_{22} - \sigma_{33})^2 + G(\sigma_{33} - \sigma_{11})^2 + H(\sigma_{11} - \sigma_{22})^2 + 2L\sigma_{23}^2 + 2M\sigma_{31}^2 + 2N\sigma_{12}^2 = 1 \qquad \text{(1)}$$

where σ_{ij} are stresses and F,G,H,L,M,N are constants that need to be determined from uniaxial compression and shear tests.

If X,Y,Z are the tensile yield stresses in the orthogonal directions, i.e., $X=\sigma_{11}$, $Y=\sigma_{22}$, $Z=\sigma_{33}$, then F,G,H can be obtained from these relationships:

$$\left. \begin{aligned} 2F &= \frac{1}{Y^2} + \frac{1}{Z^2} - \frac{1}{X^2}, \\ 2G &= \frac{1}{Z^2} + \frac{1}{X^2} - \frac{1}{Y^2}, \\ 2H &= \frac{1}{X^2} + \frac{1}{Y^2} - \frac{1}{Z^2}. \end{aligned} \right\} \qquad \text{(2)}$$

L,M,N can be determined from the shear yield stresses R, S, T where $R=\sigma_{12}$, $S=\sigma_{23}$, $T=\sigma_{31}$:

$$2L = \frac{1}{R^2}, \quad 2M = \frac{1}{S^2}, \quad 2N = \frac{1}{T^2}. \qquad \text{(3)}$$

However, the coefficients calculated using this method have units of MPa². DEFORM software uses dimensionless coefficients and F=G=H=1 with L=M=N=3 corresponds to isotropic material.

Finnie and Heller [7] proposed the following relationships to solve for the dimensionless coefficients:

$$F = \bar{\sigma}_0^2 \left(\frac{1}{(\sigma_{22})^2} + \frac{1}{(\sigma_{11})^2} - \frac{1}{(\sigma_{33})^2} \right)$$

$$G = \bar{\sigma}_0^2 \left(\frac{1}{(\sigma_{11})^2} + \frac{1}{(\sigma_{33})^2} - \frac{1}{(\sigma_{22})^2} \right)$$

$$H = \bar{\sigma}_0^2 \left(\frac{1}{(\sigma_{33})^2} + \frac{1}{(\sigma_{22})^2} - \frac{1}{(\sigma_{11})^2} \right)$$

$$L = \frac{\bar{\sigma}_0^2}{(\sigma_{23})^2}, \quad M = \frac{\bar{\sigma}_0^2}{(\sigma_{13})^2}, \quad N = \frac{\bar{\sigma}_0^2}{(\sigma_{12})^2}$$

(4)

where $\bar{\sigma}_0$ is calculated using

$$\bar{\sigma}_0^2 = 1/3 \left((\sigma_{11})^2 + (\sigma_{22})^2 + (\sigma_{33})^2 \right)$$

(5)

For isotropic yield function, F=G=H=1 and L=M=N=3. In DEFORM 3D, F, G, H were preset to 0.5 and L, M, N were set to 1.5. Hence the calculated coefficients need to be divided by 2 before inputting into the software.

Compressive flow stress data were available from the Gleeble tests. However, a different test was required to obtain the remaining shear data for Hill's anisotropic model. One of the common bulk material shear tests is the so called "shear hat test". Meyer and Hartmann [8] proposed a hat-shaped specimen in 1977 to measure shear stress in compression setups such as the Hopkinson bar. Meyer et al. further developed the hat specimen in 1994 [9] to adapt to a drop hammer system. Recent studies [10] [11] [12] have used the hat specimens in both quasi-static and dynamic loading conditions to determine shear stresses.

Pepelnjak et al. [13] analyzed the shear hat test using FEM on materials including Mg alloy AZ80. Peirs et al. [14] conducted numerical simulations for various hat-specimen geometries and concluded that for specimens with r1/r2=0.975 (Figure 2.1), the compression force is a good measurement of shear stress and the shear stress is homogeneous during the test process. The effect of corner radius in the shear zone was also studied. Rounded corners due to machining can increase the force required to trigger shear localization, hence can affect the accuracy of the shear stress calculation. Fine tools should be used to achieve small radius during sample machining.
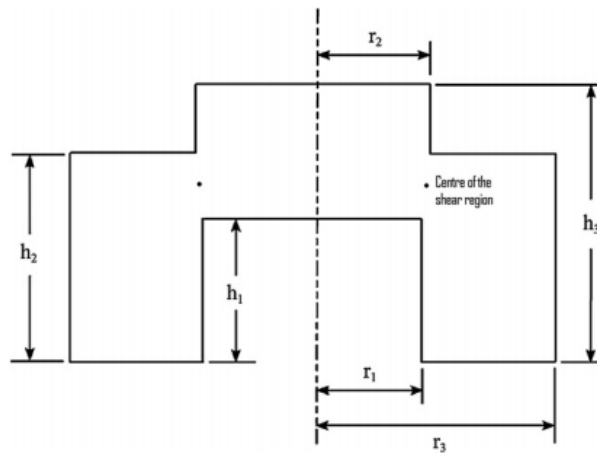
Figure 2.1: Shear hat specimen with r1/r2=0.975 [14]

2.3 Forging Simulation

Proper use of finite element (FE) simulation in metal forming area can dramatically reduce design cost and time. Many researchers [15-21] have applied FE simulation in forging of Mg alloys and proved its reliability through geometric comparison. Others [22-24] successfully designed lab scale samples with the help of FE simulation. Still others [26-28] implemented FEM as a tool for forging preform design. Pepelnjak et al. [29] compared forging simulation results of 3 popular FE packages - due to the large deformation of elements in the forging process, software with remeshing capability or ALE (Arbitrary Lagrangian Eulerian) / CEL (Combined Eulerian Lagrangian) algorithms are clearly better options.

Kobold et al. [5] documented a detailed process of creating anisotropic material model for Mg alloy AZ80 in DEFORM 3D software which was then applied in simulation of an industrial scale component. Their approach was used herein.

2.4 Damage Criterion

A finite element simulation is not complete without a material failure criterion. In bulk metal forming processes, especially forging, material failure often occurs as ductile fracture. The propagation of a crack is of less interest when compared to failure initiation as the main focus in forging design is to avoid any defects from happening. Many criteria are available in the DEFORM 3D software to predict material failure initiation, Figure 2.2.

7
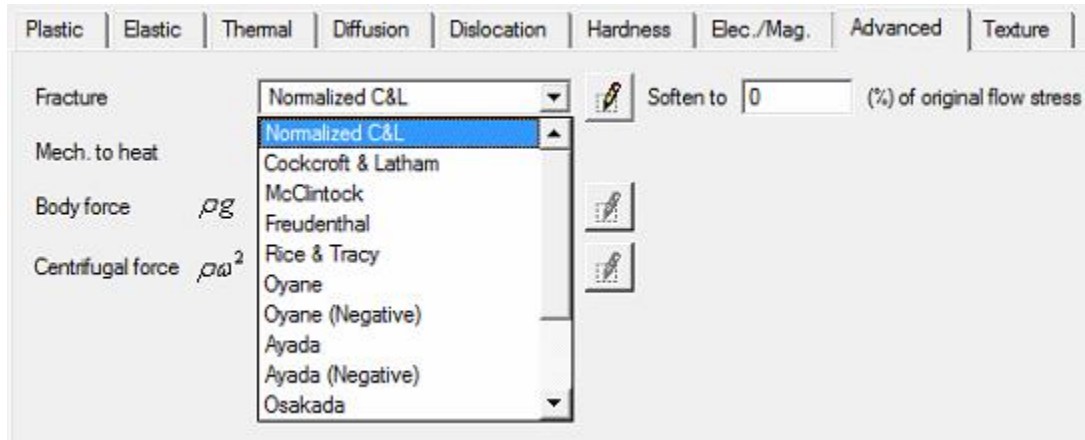
Figure 2.2: Fracture criteria in DEFORM software

The normalized Cockroft & Latham criterion [28] is one of the failure models in DEFORM. It assumes that the largest principal stress has the most significant impact on crack initiation, and integrates the greatest principle stress normalized by the effective stress over effective strain, Equation 2.1 below, to obtain an estimate to damage.

$$\int_0^{\varepsilon_i(t)} \frac{\sigma_{\max}}{\sigma_i} \, d\varepsilon_i(t) \geqslant C$$

(6)

where σ_{max} is the maximum principal stress, σ_i is the effective stress, ε_i is the effective strain, and C is the critical damage value.

Christianse et al. [30] and Rao [31] studied a number of ductile failure models and concluded that the normalized Cockroft & Latham criterion was among the most reliable models and was able to predict damage location consistently for rate-sensitive materials. Kakimoto and Arikawa [32] employed this criterion and successfully modeled brittle and ductile fracture in tensile tests. Gontarz et al. [33] designed an AZ80 wheel hub forging process with this criterion to avoid defects. Gontarz et al. [16] applied the criterion to help locate defects on the component. Kim and Lee [34] and Xue et al. [35] proposed critical damage values for AZ31 and AZ80 using different approaches. According to [34], AZ31 at 500 °C had a critical damage value around 0.5 for strain rates ranging from 0.001 to 0.1. Xue et al. [35] claimed that AZ80's critical value was between 0.26 and 0.46 at 400 °C for strain rates of 0.001 to 0.1. No information was available for ZK60.

8

In DEFORM, the pre-determined critical damage value C has to be assigned to the material (Figure 2.3).

Normalized Cockcroft & Latham

$$\int_{.}^{\cdot\bar{\varepsilon}_{f}} \frac{\sigma^{*}}{\bar{\sigma}} d\bar{\varepsilon}$$
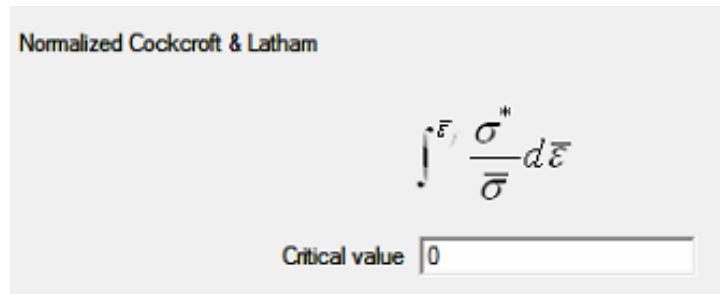
Critical value 0

Figure 2.3: Critical value definition for Normalized Cockroft & Latham Criterion in DEFORM

During numerical simulation, an element is deleted in the remesh process when its damage value exceeds this critical value. However, since we are interested in keeping the max damage value below critical in the entire process rather than to predict the geometry of the cracked region, DEFORM 3D allows us to calculate the damage value without removing elements by setting both the "critical value" and "soften to" value to 0 in the "Advanced" material tab. By doing so, the max damage value in the process can be manually compared to the critical value pre-determined from experiments or the literature.

2.5 Forging Design

Forging is a very old metal processing technique that relies heavily on designer's experience and operator's craftsmanship. Forging design has been an expensive process consisting of costly prototyping and endless trial-and-error design iterations. The forging cost and difficulty generally increase with part complexity. A part with simple geometry could be forged in a single forming step but more stages are necessary for complicated geometries [36] (Figure 2.4). It is not rare in industry to use more than 3 forging steps to produce a component.

The forging design process should begin with the geometry of the final component. The designer takes into account different aspects of the process, including shape complexity, material behavior, forging equipment, target post-forging property, and overall cost of the product, to finish the process design [37].
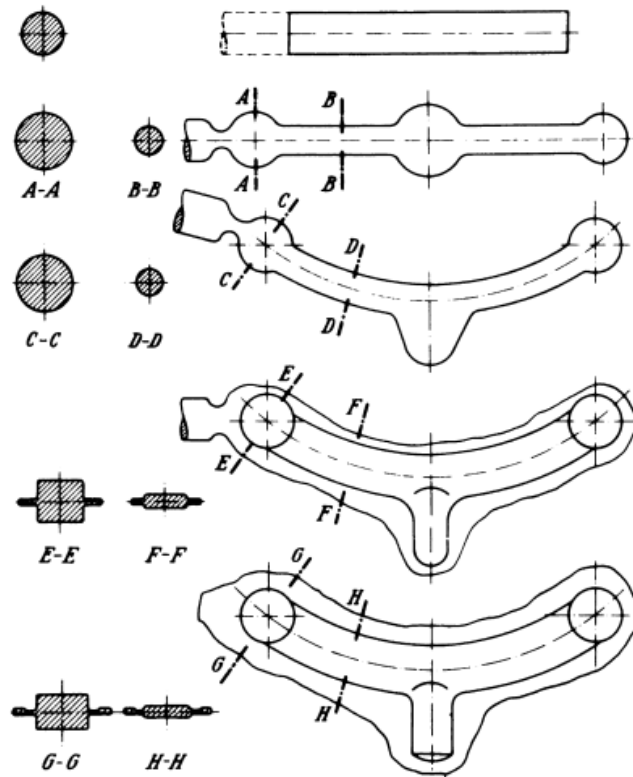
Figure 2.4: Multi-stage forging of a [36]

Die design is the next step and is critical to a flawless product. Flashland geometry, draft angles, corner and fillet radii, parting plane location are basic elements in die design. Proper selection of die geometry can enhance material flow, and hence improve grain structure in the final component. Continuous fiber structure in the loading direction of a component can improve its load-carrying capability and reduce the chance of failure under load [38].

Figure 2.5 illustrates the effect of parting plane location on grain flow within an I-beam. Discontinuous grains are present in the upper design at the stress concentrated corner after machining whereas the other design does not have the same issue.

Parting line in middle of part

Final Form

Avoid fibre exit at high stress concentrations after machining

Parting line on top edge of workpiece

Improved fibre structure at roundings
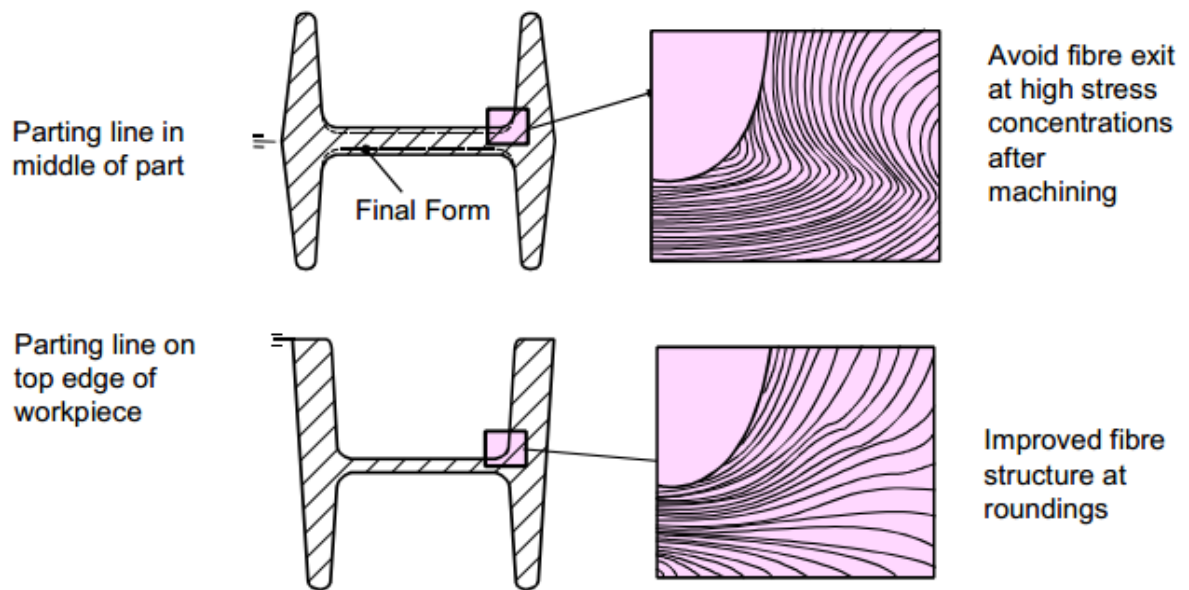
Figure 2.5: Grain flow of an I-beam geometry [38]

With the desired final geometry, the designer can estimate the volume of the product and have a rough idea of the initial billet size and percentage of flash. Flash geometry then needs to be optimized in the die design process. Flash terminologies are illustrated in the figure below.

Flash   Top die   Forging

Gutter

Flash land   Bottom die   Trim line

C_L
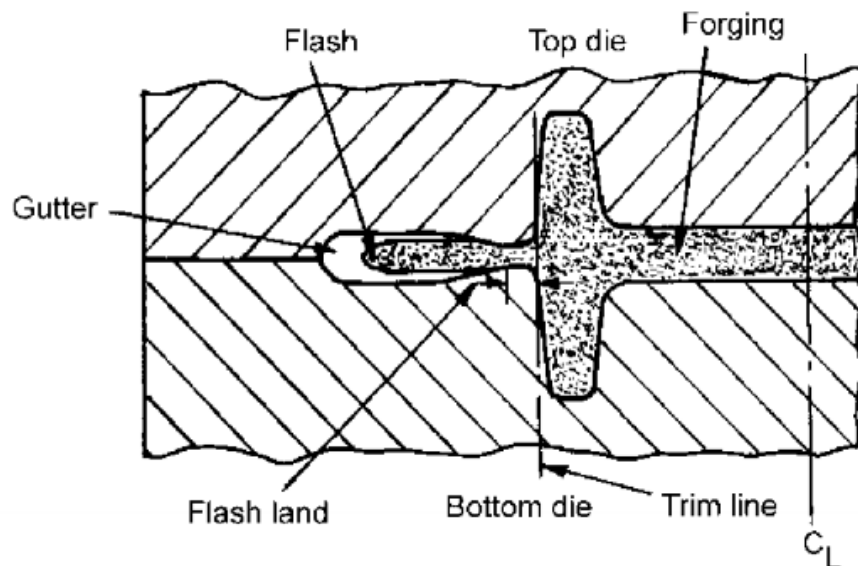
Figure 2.6: Flash design terminologies [39]

11

The flash dimensions are crucial to a forging, as a thin and wide flashland acts as a restriction to the material flow. This promotes better die filling for tall and thin rib cavitys, on the other hand, it increases the stress on the die which may cause tooling failure. For short and wide rib features, a thicker and narrower flashland is preferred to reduce forging load [40] (Figure 2.7).

Limited design data is available for Mg alloy flash design, hence a flash thickness design diagram for steel forgings was borrowed as a reference [41] (Figure 2.8). With the help of this chart, the thickness and width of the flashland can be correlated to the weight of the product.

According to literature [42], 3 degrees of draft angle was recommended for Mg alloys for easy extraction. Corner radius of 1.6mm, fillet radii of 4.8mm and web thickness of 3.2mm are not uncommon for forging of Mg alloys.

Figure 2.7: Typical flashland design [40]

Figure 2.8: Flash geometry design guideline for steel [41]

Chapter 3
Material Properties and Modelling

3.1 Overview

Three Mg alloys were selected as candidate materials in this project - AZ31, AZ80, ZK60. Each alloy came in the extruded or as-cast condition from Magnesium Elektron company. The forging group[2] conducted studies on 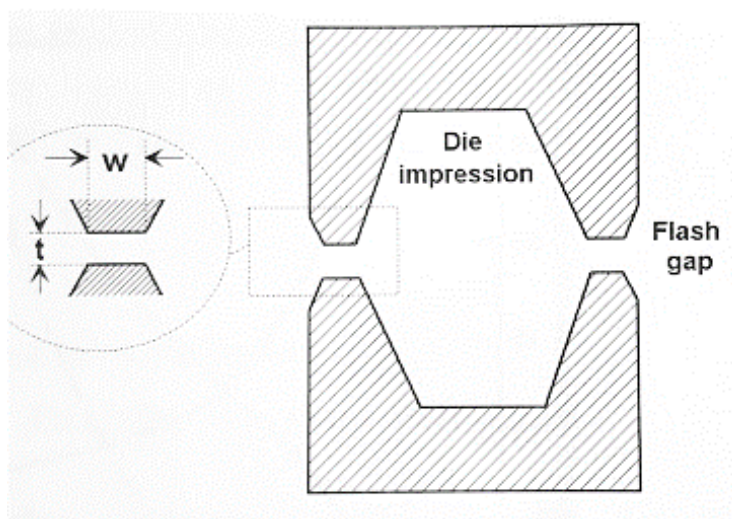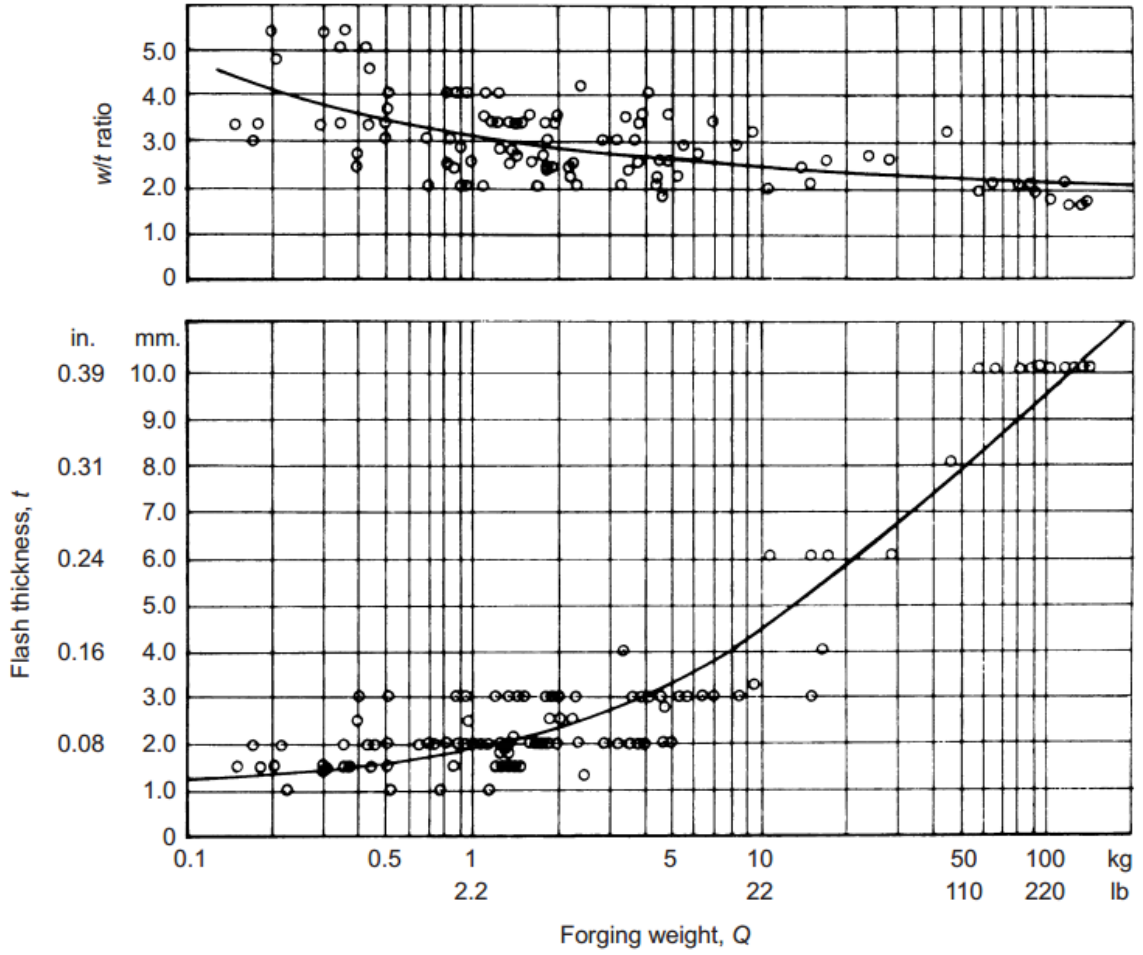flow stress, DRX (Dynamic Recrystallization) behavior, and anisotropy of each material. The effect of heat treatment on the alloys was also studied.

In a forging numerical simulation, a material model is required to capture the material flow behavior and response during deformation process. An isotropic material model assumes the flow stresses of the alloy to be equal in all directions, and thus requires only one flow stress curve as input for a given strain rate and temperature. These were obtained for the various materials by members of the forging group. An anisotropic model however, in DEFORM 3D, assumes different flow stresses in the three orthogonal directions – X,Y,Z, by using Hill's anisotropic model (Hill's 48). One flow stress curve and six anisotropic coefficients for each strain rate and temperature condition were necessary to successfully implement the anisotropic material model. The shear stress components for these were obtained by the author with the help of Mark Whitney using the shear hat specimen on the Gleeble.

The flow stress of materials can be achieved by doing small-scale compression tests using a Gleeble (Figure 3.1). Three of the Hill's anisotropic coefficients are calculated from yield values of flow stresses in the major directions from these compression tests. The other three coefficients are calculated from shear yield stresses from 'top-hat' specimens.

---

[2] Amir Hadadzadeh, Paresh Prakash, and Rick Wong, supervised by Professor Mary Wells
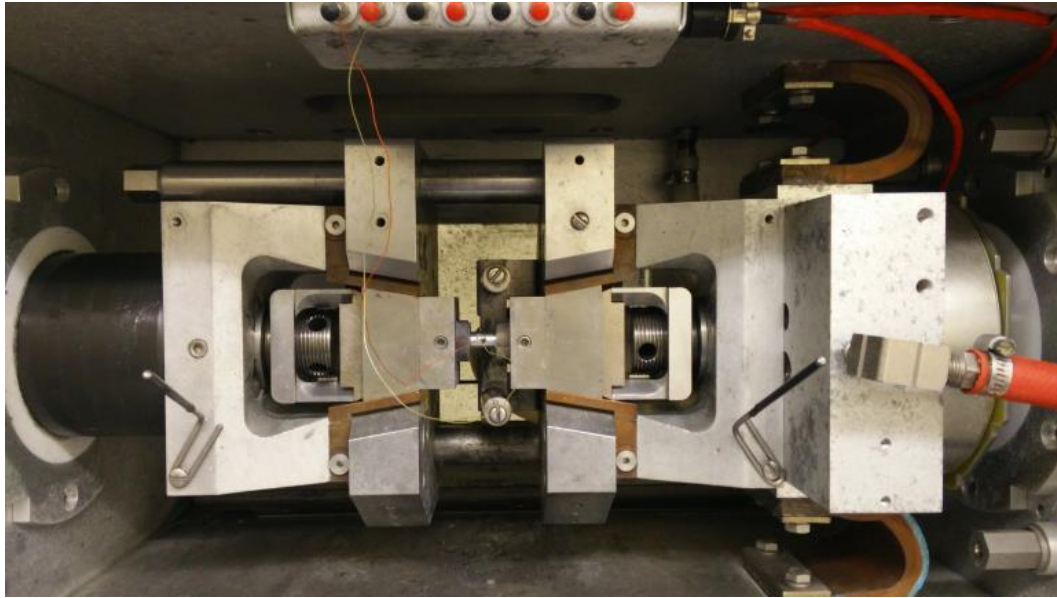
Figure 3.1: Gleeble compression test

3.2 Small-scale Gleeble Forging

The Gleeble was able to provide true stress – true strain data after the test using the following equations:

$$\sigma = \frac{F}{\left[\dfrac{\dfrac{\pi d_o^2}{4} h_o}{h_o + \Delta h}\right]}$$

$$\varepsilon = \ln\left(\frac{h_o + \Delta h}{h_o}\right)$$

(7)

These data were not directly usable for simulation due to the area change of the billet during compression. The barreling of the billet caused by surface friction (Figure 3.2(a)), and the ovaling (Figure 3.2(b)) due to material anisotropy had to be corrected before the stress-strain curve could be used in simulations. Figure 3.3 shows a comparison between corrected and uncorrected flow stresses for ZK60@250ºC. The correction method used by the forging group can be found in literature [43].

15

Figure 3.2: Deformation of extruded AZ80 during uniaxial compression @300ºC & 0.1 strain/s

(a) Barreling (b) Ovaling
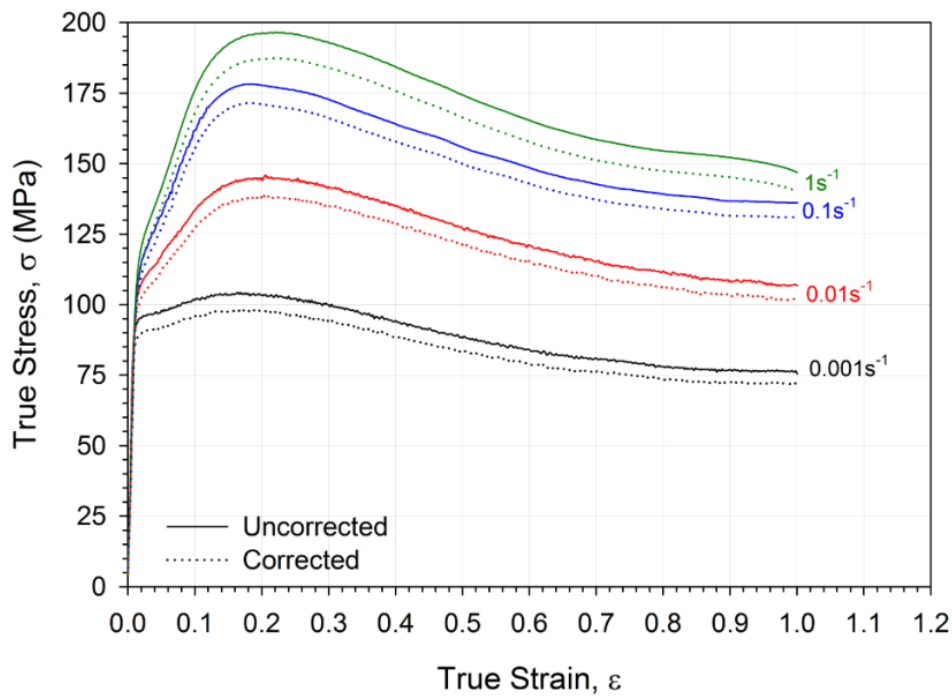
Figure 3.3 : Comparison of corrected & uncorrected flow stresses of ZK60@250ºC

3.3 Shear Hat Test

The hat-sample geometry discussed in section 2 was selected for this project based on the following considerations:

1. r1/r2=0.975, the compression force is a good measurement of shear stress
2. Shear stress calculation is straight-forward using load data and area of shear zone
3. The sample is small enough to be machined from the Ø63.5mm material in both extrusion and transverse directions

4. The sample can fit on Gleeble to produce material shear data at compression test temperatures for consistency
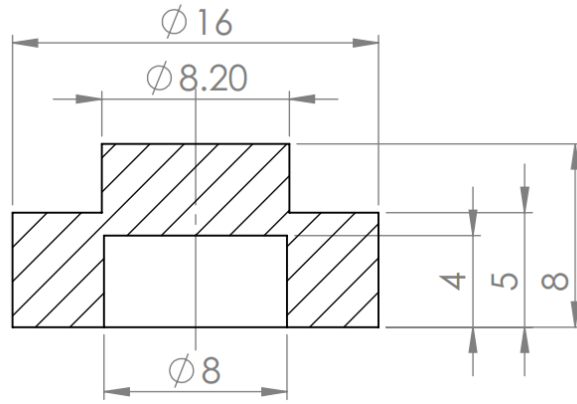
Figure 3.4 : Shear hat sample with dimensions

(a)   (b)
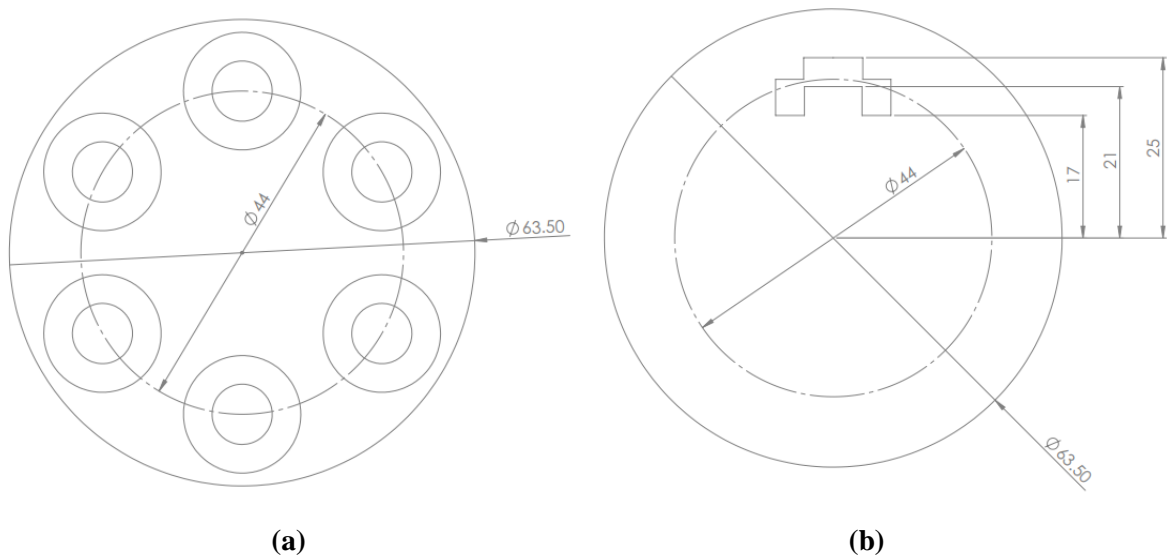
Figure 3.5 : Shear hat sample locations (a) Extrusion direction (b) Transverse direction

Hat samples with dimensions in Figure 3.4 were machined from the Ø63.5mm extruded materials in the extrusion direction and transverse direction. Extrusion direction samples had their center located on a 44mm ring on the extruded bar (Figure 3.5(a)). The transverse samples were placed such that the shear zone was on the 44mm ring (Figure 3.5(b)). This 44mm sample location was used for consistency with the Gleeble compression test sample locations on the extruded rod.

Based on the forging group's study of optimal forging condition for each material, the following test temperatures were selected: AZ31 was at 500 ºC, ZK60 was at 450 º C, AZ80 was at 400 º C. Shear strain rates for each material were 0.01/s, 0.1/s or 1/s, calculated using the following equation:

$$\dot{\gamma} = \frac{v}{h} \tag{8}$$

where v is velocity in the shear direction and h is the height of the shear zone.

In our case, v was the Gleeble die displacement rate in mm/s, h was calculated using r2-r1=0.1mm. To achieve the rates of 0.01/s, 0.1/s and 1/s, the die displacement rates of Gleeble were set to 0.001mm/s, 0.01mm/s and 0.1/s correspondingly.

As only the yield of shear stress was of our interest, the hat samples did not have to be compressed too much after yielding, Figure 3.6. The tests stopped at a die displacement of 1mm. Actual testing was conducted by Mark Whitney.

The graph below (Figure 3.7) shows data collected from the extrusion direction sample of AZ80 under a shear rate of 0.1/s at 400 º C. The shear zone area was estimated using a cylindrical surface area A=2πrh=25.45mm^2 where r was taken as the average of r1 and r2, and h was 1mm. The shear yield stress was calculated using the yield load divided by the shear zone area.

Yield load was determined to be 0.54kN from the test result. Hence the shear yield stress in this case was 0.54kN/25.45mm^2=21.07MPa.
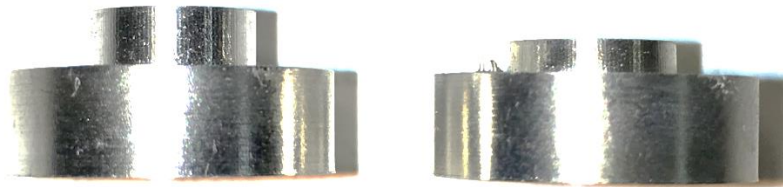

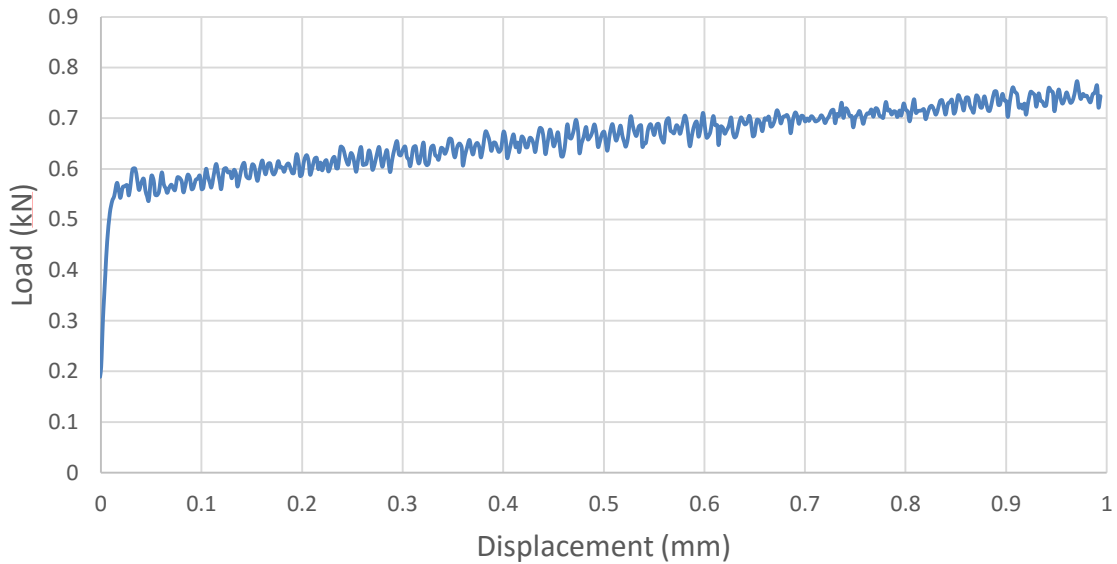**Figure 3.6: Shear hat sample before and after test**

Figure 3.7: Shear test data of extruded AZ80 in ED @400 ºC & 0.1/s

3.4 Anisotropic Material Model in DEFORM 3D

In this project, cylindrical pre-extruded Mg alloys were used. Rotational symmetry of mechanical properties was assumed for simplicity. An orthogonal coordinate system can be defined for a cylindrical body with rotational symmetry (Fig 3.8), with Z axis being the line of symmetry for rotation (longitudinal direction or extrusion direction), while X and Y axes (transverse direction) are perpendicular to each other and at the same time orthogonal to Z axis.

As rotational symmetry was assumed, flow stresses for compression and shear in X and Y directions are considered the same, thus the upsetting and shear tests were only conducted in one radial direction (TD).

In our case, it can be assumed that σ_{11} corresponds to Z direction, σ_{22} corresponds to Y direction, and σ_{33} corresponds to X direction. Using AZ80@400ºC and 0.01/s as example, the yield for ED and TD compressive flow stresses are determined to be 43.56MPa and 38MPa. The yield for shear stresses in TD is 13.3MPa, while the ED yield is 14.81MPa. The coefficients can be calculated using the equations in section 2.2. In addition, according to Hill's theory, "if there is rotational symmetry of the anisotropy in an element about the z axis, then F=G, N=G+2H".

19
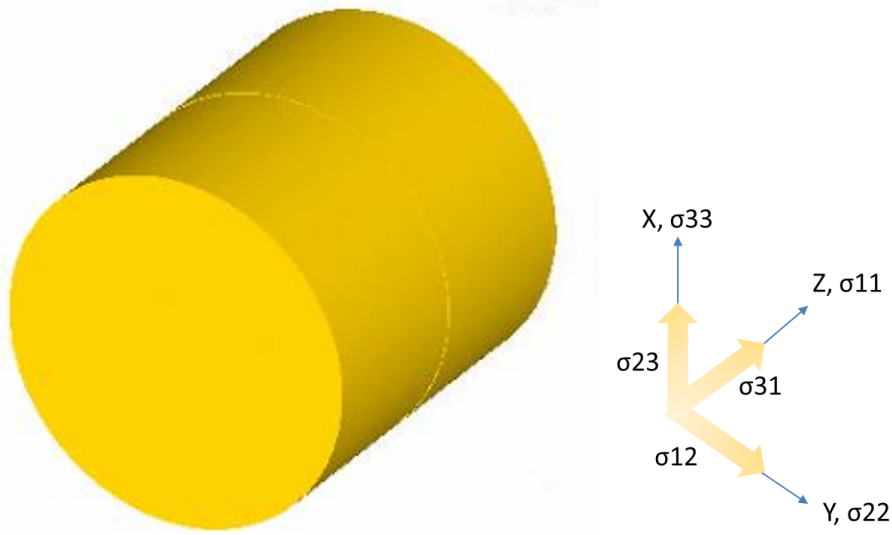
Figure 3.8 Orthogonal coordinate system for cylindrical billet

These anisotropic coefficients have to be calculated for each forging rate and temperature conditions and were assumed to be constants during the forging process. A complete material model of extruded AZ80 @400 ºC and 0.01/s is shown in Figure 3.9 below. Material models for other materials can also be found in the Appendix A.
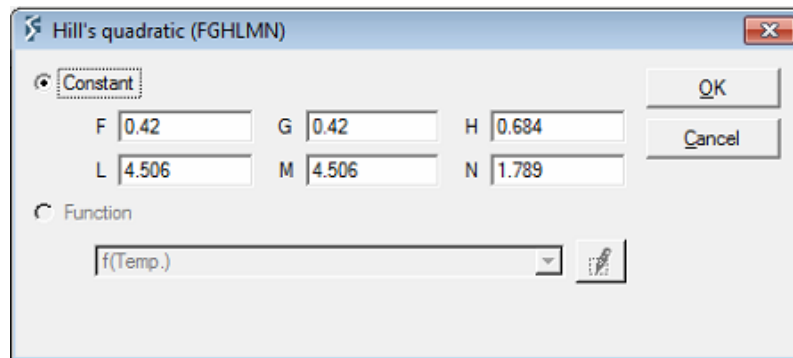
(a)
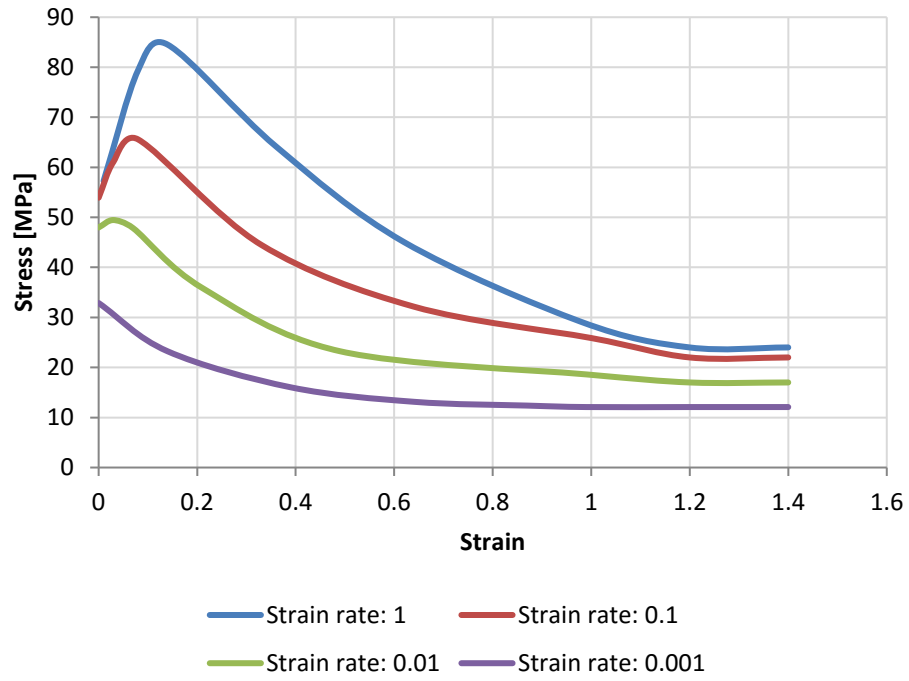
(b)

Figure 3.9: Complete material model for extruded AZ80 @400 ºC, 0.01/s,

(a) Anisotropic coefficients, (b) Flow stress

Chapter 4
Preliminary Forging Tests

4.1 Pancake Test

4.1.1 Overview

The pancake test is a forging process to axially compress a cylindrical billet between two flat dies (Figure 4.1). The material used in the test was extruded AZ31b from Hadco company with a diameter of 88.9mm and length of 133.35mm. The final height of the billet after compression was 13mm. The purpose of these pancakes were to calibrate the 500-ton hydraulic press load readings, to examine forging rate impact on load, and to compare experimental results with 2D numerical simulations.
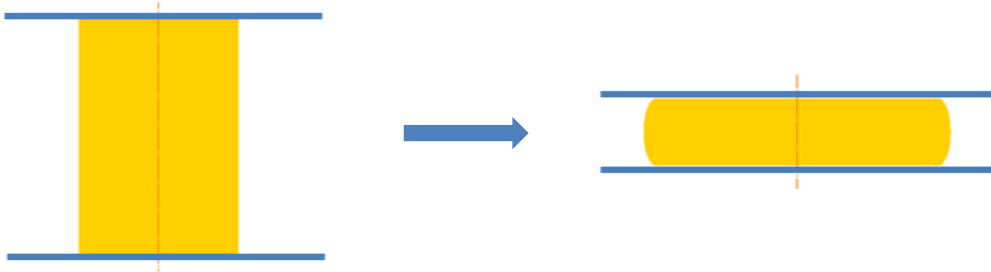
Figure 4.1: Illustration of pancake forging process

4.1.2 Experiments

Experiments were conducted by Lucian Blaga at CanmetMATERIALS in Hamilton under the direction of Bruce Williams and Jonathan McKinley. Extruded AZ31 billets with diameter of 88.9mm were cut to length of 133.35mm each. The graphite lubrication was sprayed evenly onto all surfaces of the specimen at room temperature. The billets were then heated in the oven for 3 hours to 400 ℃ before transferred onto the dies for experiment. The experiment was isothermal – dies were heated to the same temperature as the billet and maintained at that temperature during the forging process. Two forging rates were tested: 10mm/min (0.1667mm/s) and 200mm/min (3.33mm/s).

4.1.3 Numerical Simulation

An axisymmetric 2D model in DEFORM 2D was used to simulate the pancake forging process. The flat dies were simulated using rigid bodies with no deformation. Tooling temperature was set to 400 ℃ for the isothermal condition. No heat transfer was modelled in the simulation.

The 2D billet geometry had a radius of 44.45mm and a height of 133.35mm as shown in Figure 4.2. The material was assumed to be isotropic (flow stresses are the same in all directions), fully plastic, with E=44.8GPa, Poisson ratio=0.33 and density=1.77g/cm^3. Coulomb friction in DEFORM software was selected to calculate interfacial friction between tooling and material. An initial value of 0.3 was assumed based on the literature [44].

DEFORM 2D and 3D are both capable of auto-remeshing for large deformation process, which is ideal for forging simulations. Auto remeshing can be triggered by a number of options – maximum stroke increment in millimeters, maximum time increment in seconds, maximum step increment, or interference depth. In addition to these four keywords, remeshing is automatically initiated when the mesh is not usable (negative Jacobian).

The first three options are self-explanatory, "the interference depth criterion controls the initiation of remesh based on the interference between the slave object and master object" [45]. This is especially useful when sharp corners are involved in the die geometry. The user can also select to remesh the object globally or locally.

Auto remeshing can be very helpful, but it also limits the control the user has on the mesh. Once a bad element shape triggers the remeshing process, the object can no longer preserve the initial mesh. Thus the mesh optimization at the beginning of the simulation is not as useful as in other FE codes. Quadrilateral elements can be employed in 2D, but tetrahedron elements are the only option in 3D simulations. In this simulation, the number of elements was selected by the user at the beginning stage. The software then estimated the element size. This step can be reversed by defining the element size first. For this simulation, 1000 elements were used to mesh the 2D geometry with element size of 2mm (Figure 4.2 (a)).

Half of the billet was modelled in this simulation due to symmetry. The billet was placed at a distance to the edge of the dies to avoid mesh penetration at the sharp die corners, hence there was no need to use the four remesh capabilities in this simulation. However, auto remesh for bad element shape was active during the simulation, but was not triggered throughout the simulation (Figure 4.2 (b)).
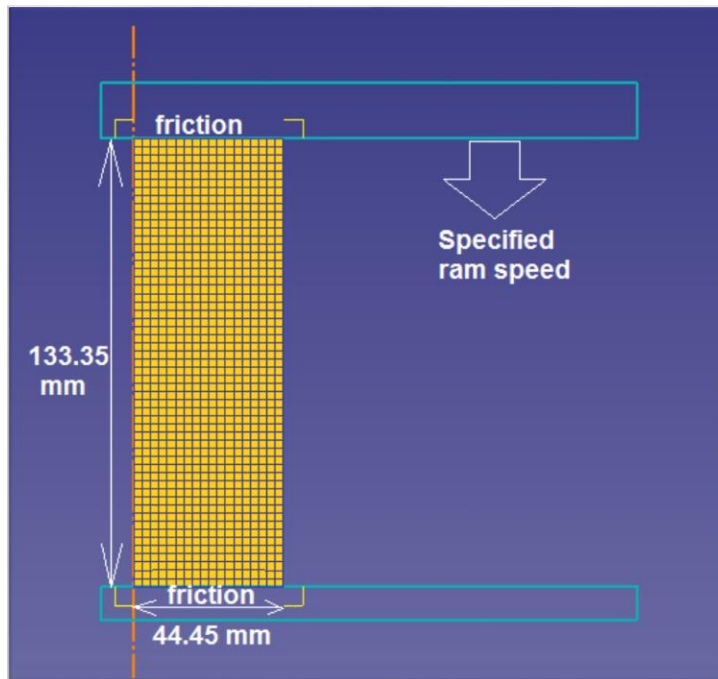
(a)
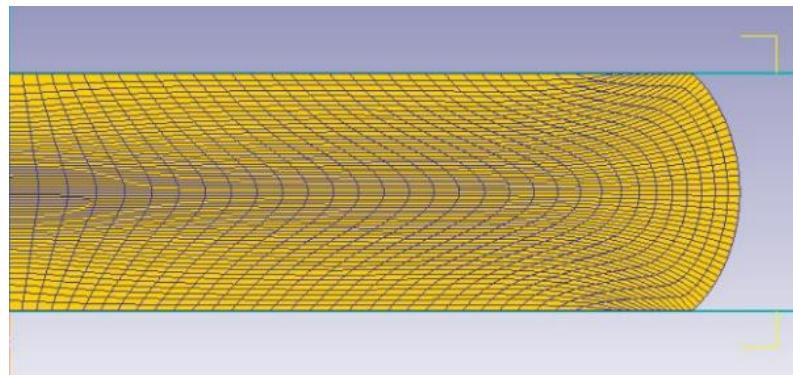
(b)

Figure 4.2 Mesh of the 2D cylindrical billet

(a) Mesh at beginning of simulation (b) Mesh at end of simulation

As material flow stress data was limited within the research group at the initial stage of the project, two simplified material models were employed based on literature values at 400 ℃ [2]:
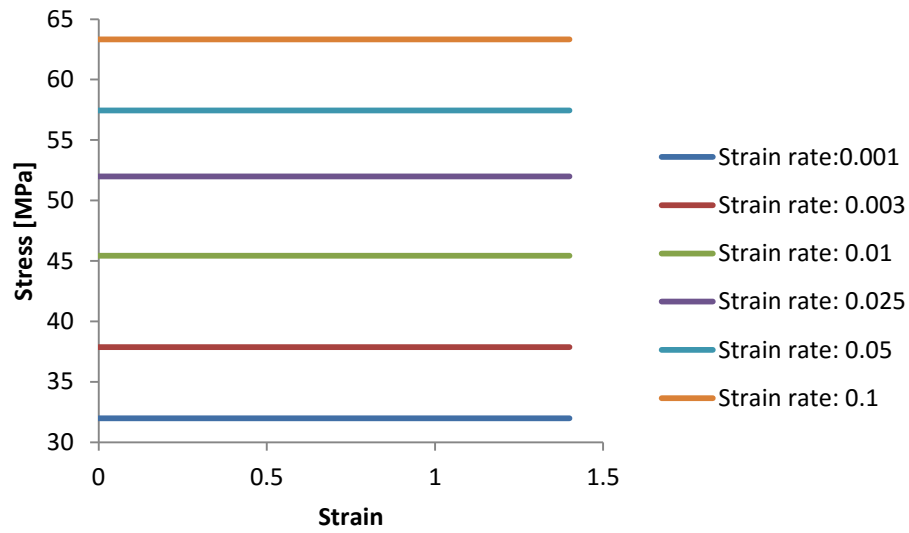
(a)
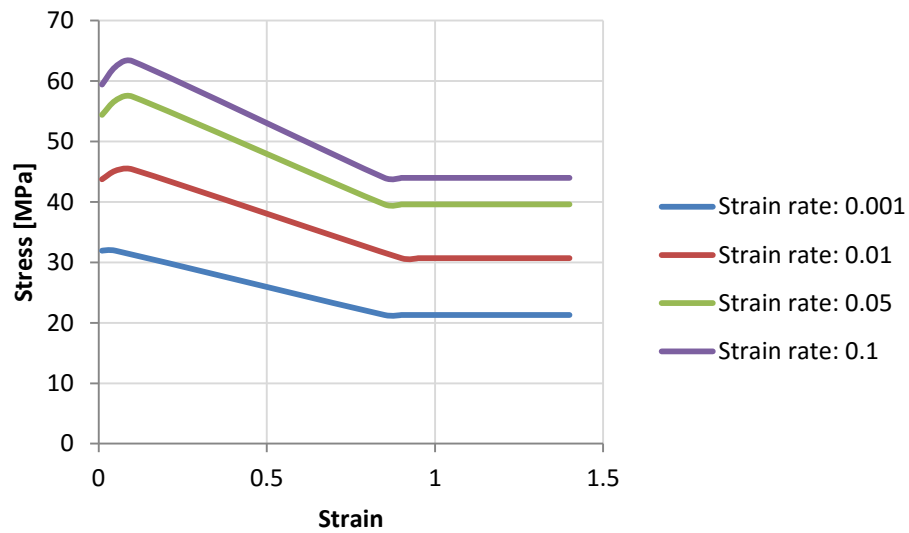
(b)

Figure 4.3: (a) Perfectly plastic material model (b) 4-point softening model

1. Perfectly plastic model

No hardening or softening was present after reaching the flow stress. One flow stress value represents the entire strain range for a given strain rate.

2. 4-point model

25

Four points were extracted from the effective flow stress curve, and a linear interpolation used between them. The four points were:

1. The start point of effective flow stress,
2. The peak of the effective flow stress curve,
3. The lowest value of the effective flow stress curve, and
4. Steady state value of the effect flow stress curve.

This model captures the major characteristics of the flow stress curve but has rather rough transitions between values which may result in numerical instability during FEM modelling.

4.1.4 Results

The Figure 4.4 shows load history for four experiments. The press does not have accurate load measurement, which likely is the reason for the difference in load for the tests that had the same forging conditions: Trial #22 and 28 or Trial #24 and 30.
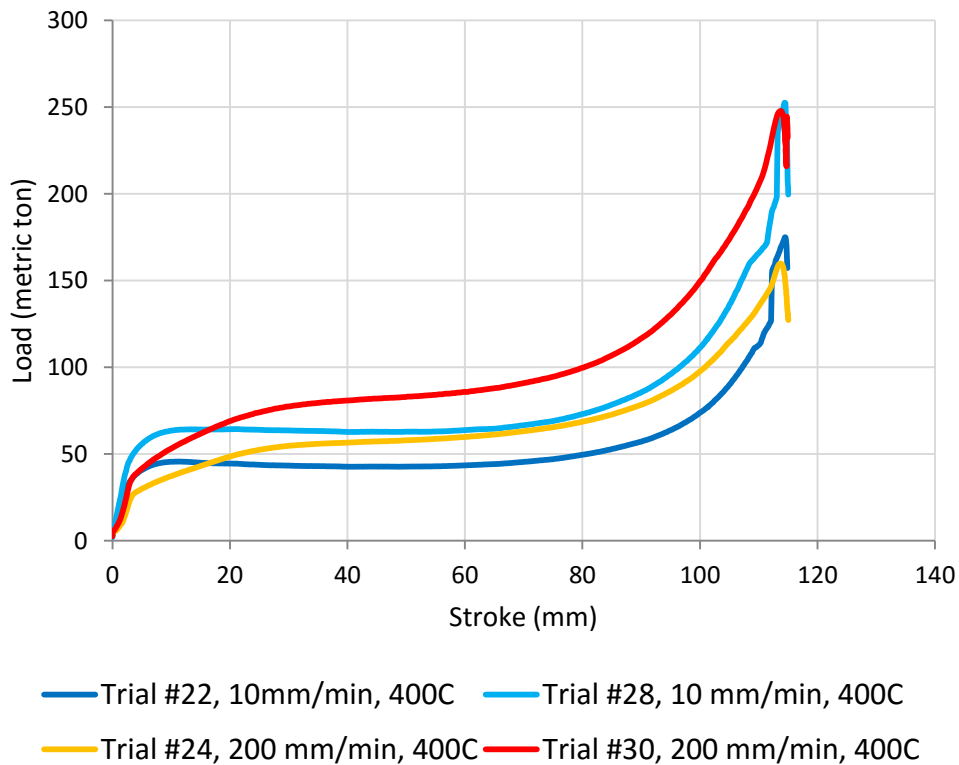
Figure 4.4: Load data of four experimental trials

Figure 4.5 and Figure 4.6 show the load predictions from simulations. The load increases with increasing coefficient of friction. The discontinuity in the 0.1667mm/s simulations was caused by the "limiting strain rate" variable in the workpiece properties definition in DEFORM software. The default value of this variable was 0.01, which worked fine for moderate to fast rate forgings (in this case 3.33mm/s) but was causing trouble at the slowest rate. According to DEFORM support (Chris Fischer, private communication, April 3, 2015), this value should be set to 1/100 or 1/1000 of the average strain rate the material experienced in simulation. By setting it to 0.0001, the discontinuity in load prediction was successfully removed in subsequent simulations.

Figure 4.5: Load prediction from numerical simulation for 0.167mm/s

Figure 4.6: Load prediction from numerical simulation for 3.33mm/s

4.2 Ring Compression Test

4.2.1 Overview
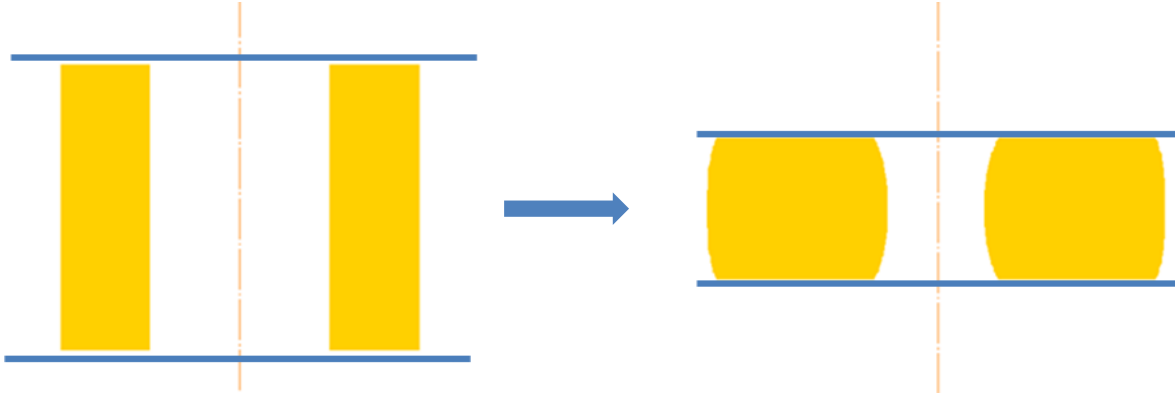
Figure 4.7: Schematic of ring compression test

One important factor that affects metal forming test and simulation result is interfacial friction between tooling and material. For high temperature forging processes, techniques to measure the coefficient of friction are limited.
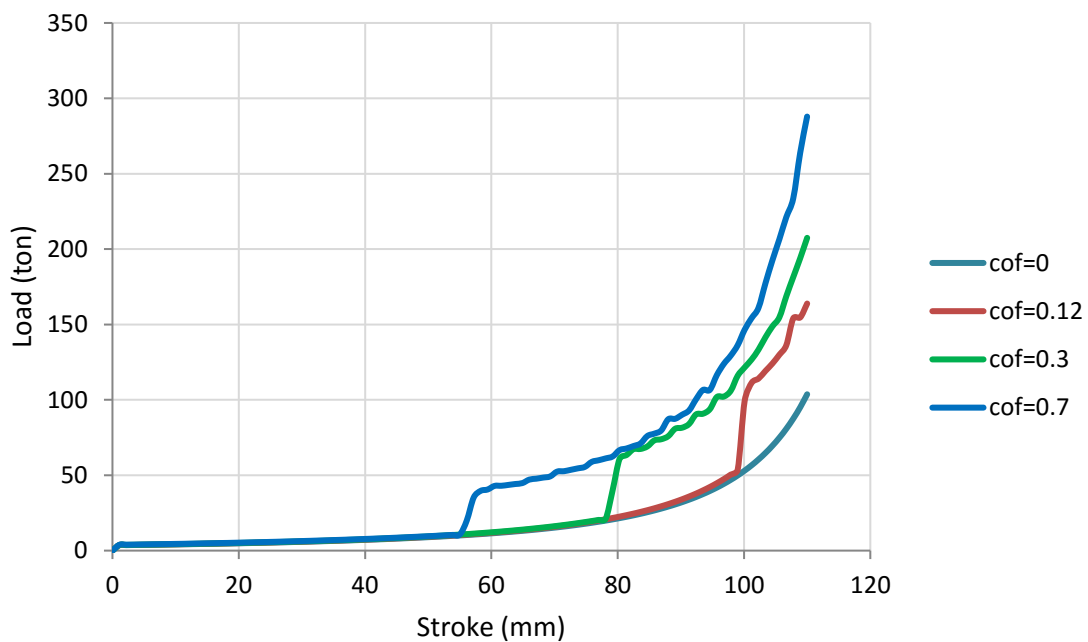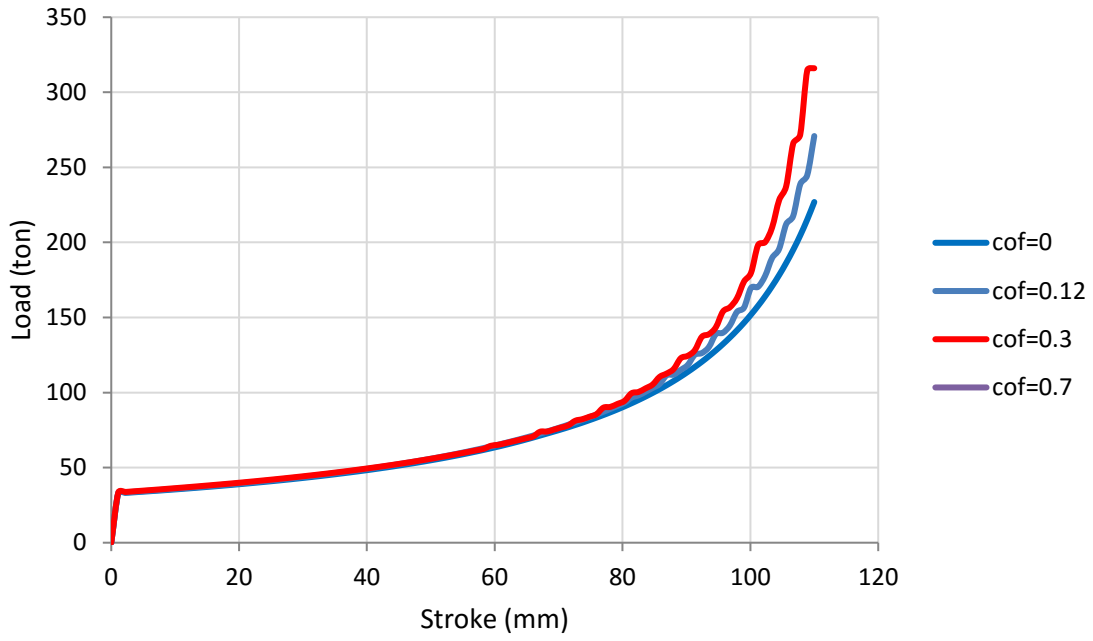
The ring compression test (Figure 4.7) was designed to measure the interfacial friction by Male and Cockroft [46]. As a ring-shaped specimen is compressed axially, the inner and outer radius behavior tends to fall into three categories [46]:

1.   "If interfacial friction were 0, the ring would deform in the same way as a solid disk, with each element flowing radially outward at a rate proportional to its distance from the center; that is, the internal diameter would increase.

2.   In the case of small but finite interfacial friction, the outside diameter of the ring is smaller than for the zero friction case.

3.   If friction exceeds a critical value, only part of the ring flows outward and the remaining part flows to the center, decreasing the inside diameter."

Thus the measurement of internal diameter of a compressed ring is a sensitive indication of interfacial friction, as the final inner diameter increases when friction is low and decreases when friction is larger.

A friction calibration curve correlates reduction in height and reduction of internal diameter to interfacial friction factor for a specific material. In order to estimate the fiction for our materials, the calibration curve needs to be generated through FE simulation.
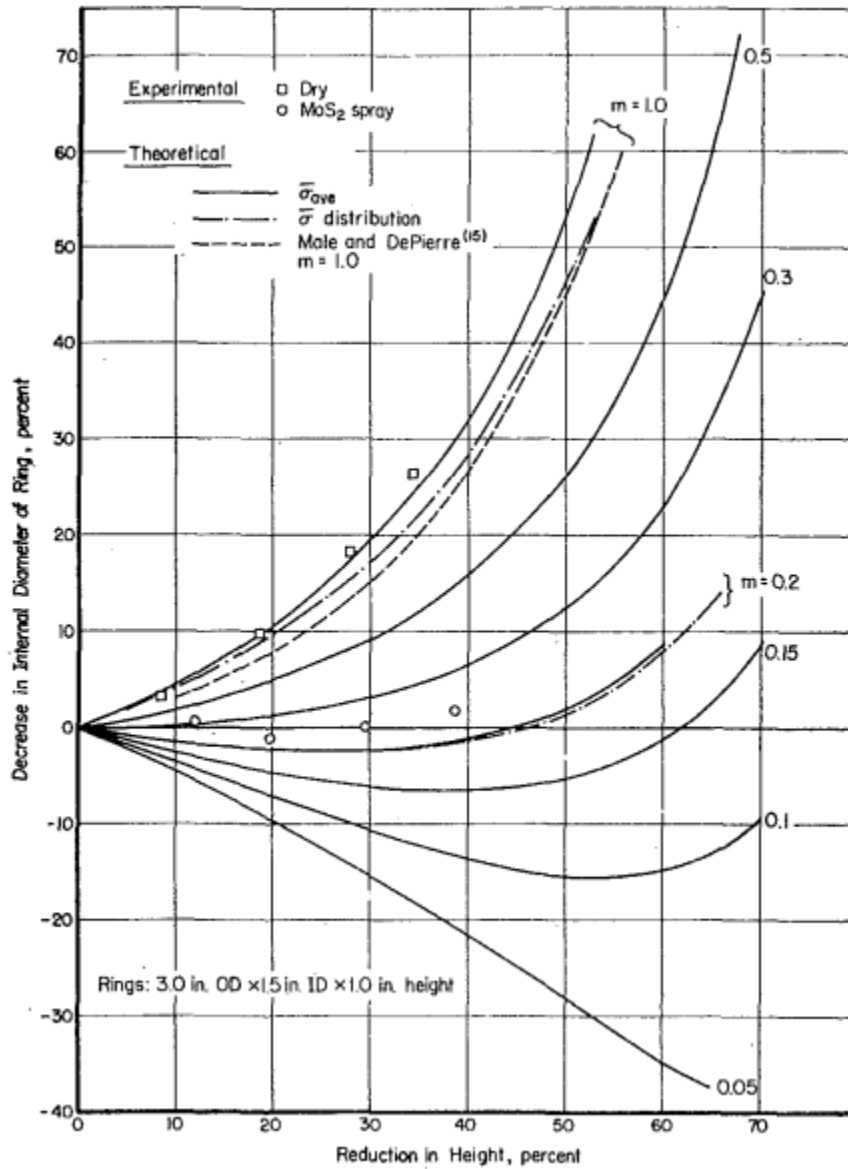
Figure 4.8: A typical friction calibration curve [47]

In the DEFORM software, interfacial friction can be modelled using Coulomb friction, with a coefficient μ. Coulomb friction was used in all simulations in this thesis. The calibration curves were generated for different μ values using numerical simulation.

4.2.2 Experiment

Specimens with the following ratio of lengths, 6:3:2 (outer dimeter: inner diameter: height), were selected based on literature suggestions [48] for the ring compression test. Cylindrical extruded AZ31 materials with an outer diameter of 88.9mm were available. They were machined to an inner diameter of 44.45mm and height of 29.64mm to match the 6:3:2 ratio (Figure 4.9).

Figure 4.9: Ring billet with thermocouple

Figure 4.10: 500-ton hydraulic forging press (dies closed)

Two common lubrications for hot metal forming process were tested: graphite and boron nitride. The lubrications were sprayed onto both inner and outer surfaces of the rings as well as the dies from spray cans at room temperature.

All tests were isothermal. Dies were heated to the designated temperature and maintained at the temperature during the forming process, 400 ℃ in this case. The interfacial friction at forging temperature was of interest, however, the lubrica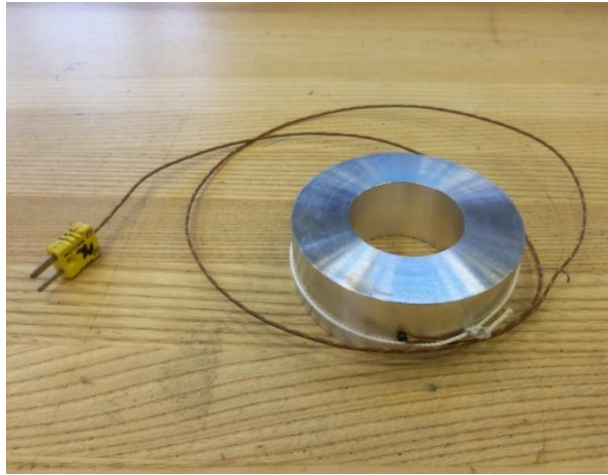tion does not adhere to the material when applied at the forging temperature. Thus the specimens were lubricated at room temperature then heated up in the oven for 3 hours to 400 ℃ before transferring onto flat forging dies on the 500-ton hydraulic press (Figure 4.10) to perform the compression test.

Two rates were used for each lubricant: 10mm/min (0.1667mm/s) and 400mm/min (6.6667mm/s). Two replicates were used for each condition for a total of 8 specimens. Results will be presented with the simulations.

4.2.3 Numerical Simulation

An axisymmetric 2D model in DEFORM 2D was used to simulate the ring compression test (Fig 4.11). The geometry of the model matched the experiments. The material was assumed to be isotropic (flow stresses are the same in all directions), fully plastic, with E=44.8GPa, Poisson ratio=0.33 and density=1.77g/cm^3.
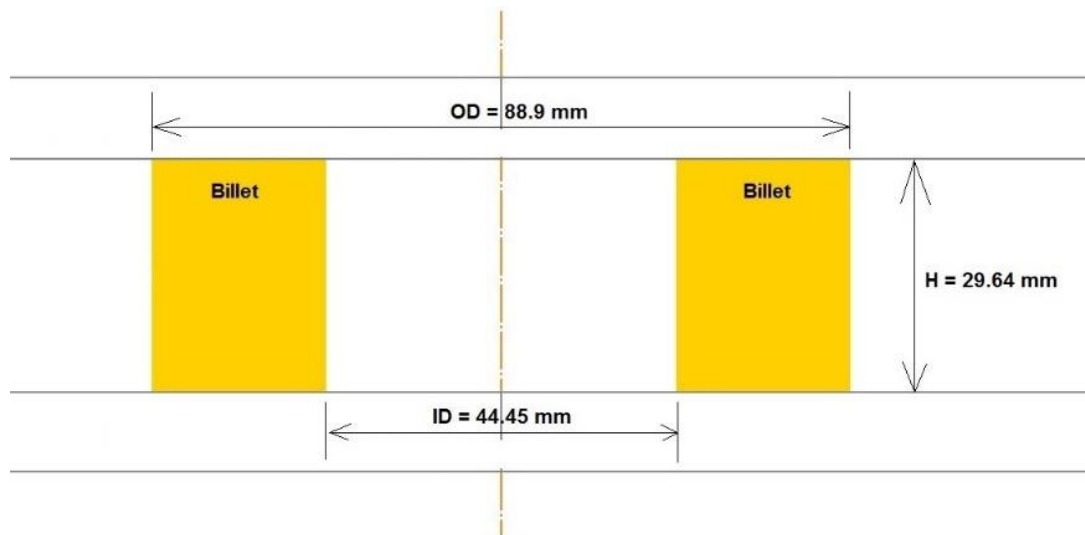
Figure 4.11: Schematic of ring compression simulation

Material true stress - true strain curves were generated using literature values [2] for strain rates of 0.001, 0.003, 0.01, 0.025, 0.05 or 0.1. The flow stresses generated were then converted to effective (plastic) strain vs. true stress and entered into the software as tabulated data. Figure 4.12 shows the literature curves and the resulting data in DEFORM.
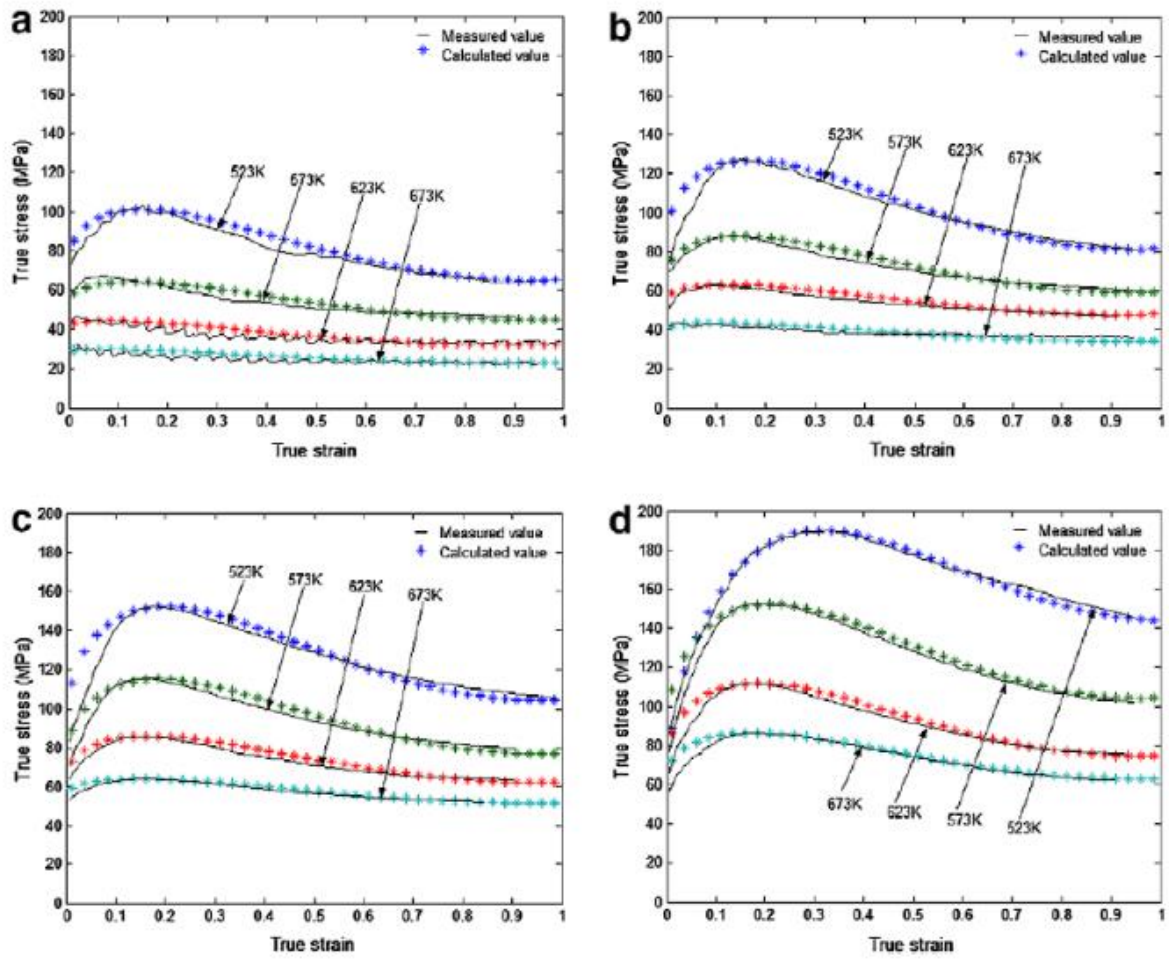
(a) $\dot{\varepsilon} = 0.001\ \mathrm{s}^{-1}$, (b) $\dot{\varepsilon} = 0.01\ \mathrm{s}^{-1}$, (c) $\dot{\varepsilon} = 0.1\ \mathrm{s}^{-1}$, (d) $\dot{\varepsilon} = 1\ \mathrm{s}^{-1}$

Figure 4.12: AZ31 material data [2]
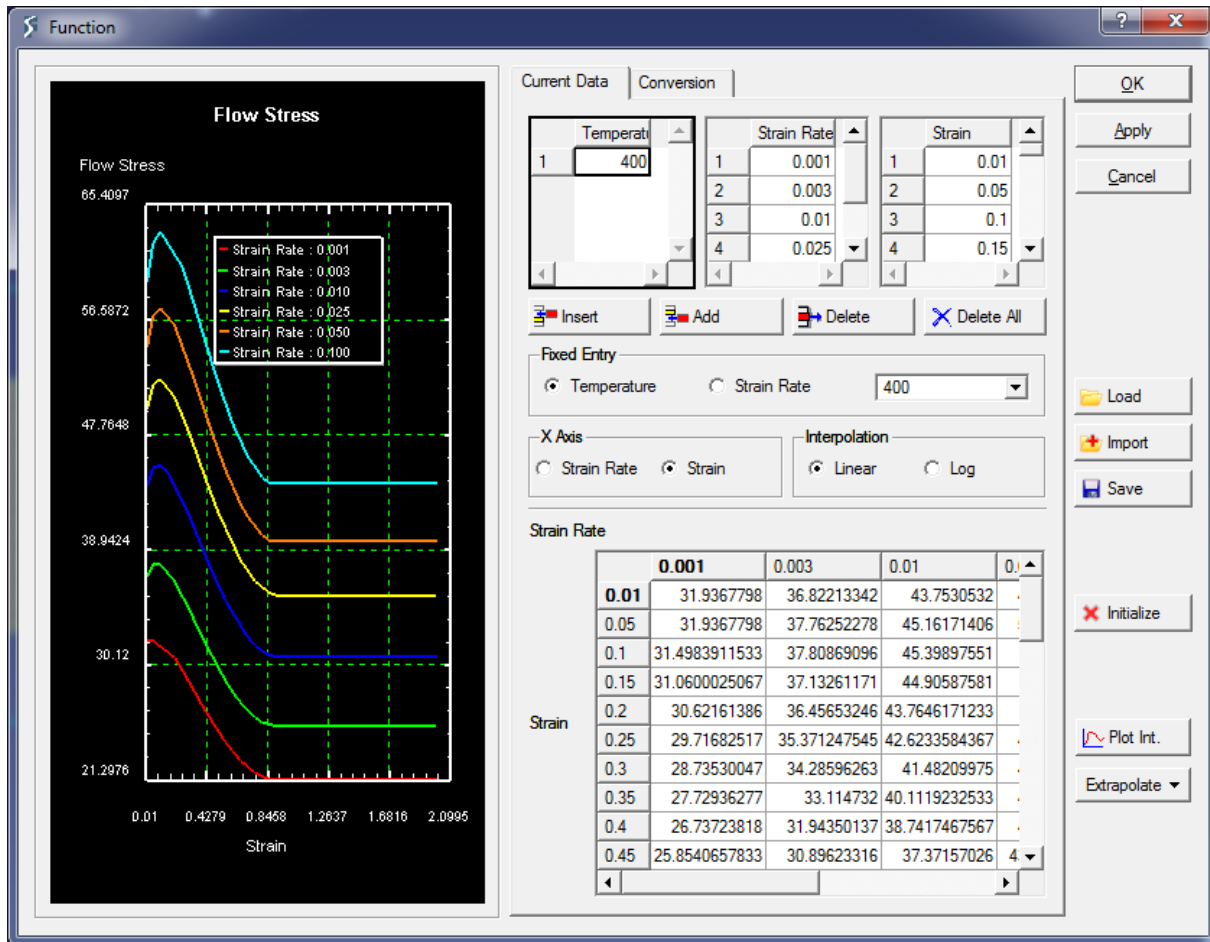
Figure 4.13: Material flow stress definition in DEFORM 2D

The upper and lower platens were modelled using two rigid flat dies, where the lower die was fixed in space and the upper die travels downwards at the constant given velocity until the displacement reaches half of the original ring height (14.82mm).

Two thousand quadrilateral elements (Figure 4.14) were used to mesh the ring geometry. Element size ratio of 3 was used such that the smallest element had length of 0.5mm and the largest had 1.5mm. Auto remeshing was enabled for distorted elements.

The Coulomb coefficient of friction μ in the simulations were varied from 0 to 1 in increments of 0.1.
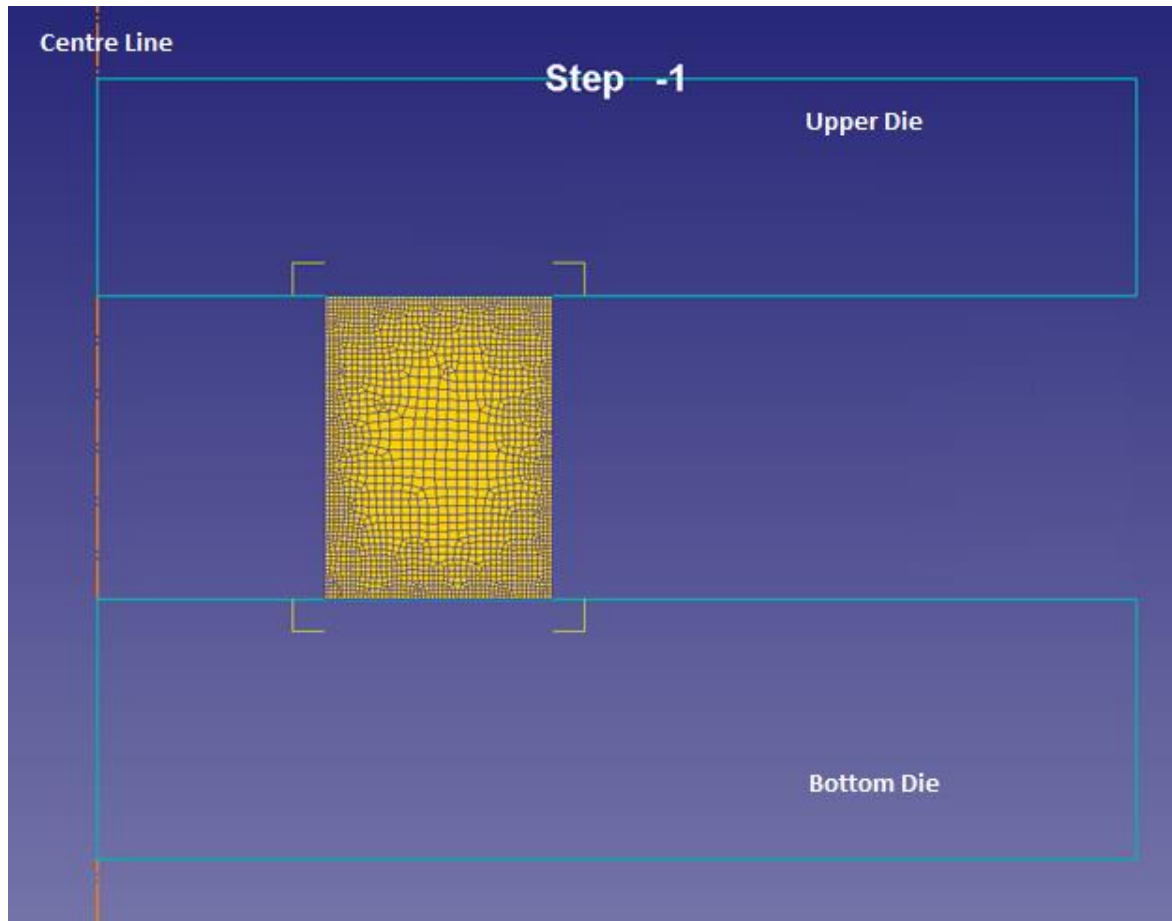
Figure 4.14: Mesh of the ring billet in 2D simulation

4.2.4 Results

The simulation results of inner diameter at half height of the ring were recorded and processed using the following equation:

$$\% \text{ decrease in inner diameter} = \frac{\textbf{Original Inner diameter} - \textbf{Deformed Inner diameter}}{\textbf{Original Inner diameter}} * \textbf{100}\% \qquad (9)$$

The height of the ring at each simulation step was also recorded and processed:

$$\% \text{ reduction in height} = \frac{\textbf{Original Height} - \textbf{Deformed Height}}{\textbf{Original Height}} * \textbf{100}\% \qquad (10)$$

One of the experimental results is shown in Figure 4.15. The inner circles of the deformed rings were not perfectly round, possibly due to material anisotropy and uneven temperature distribution in the forging dies. Image processing software, Image-Pro Plus Version 6.3, was employed to measure the

35

circumference of the internal circles for average radius calculations with the help of Yuquan Ding from the materials lab. The average internal diameters were then calculated and processed using Equation 9 before plotting on the calibration diagram.

Figure 4.15: Compressed ring using graphite as lubrication with 10mm/min

Judging from the limited number of friction curves on the calibration diagram, the graphite lubrication has a coefficient of friction roughly between 0.15 and 0.2 for both forging rates (Figure 4.16 (a) and (b)). The boron-nitride lubrication results in a coefficient of friction slightly higher than graphite, close to 0.2 for 3 tests and in between 0.2 and 0.3 for one trial. It appears that graphite causes lower friction hence was used for subsequent testing. Simulations were performed using a coefficient of 0.2 based on the ring test result.
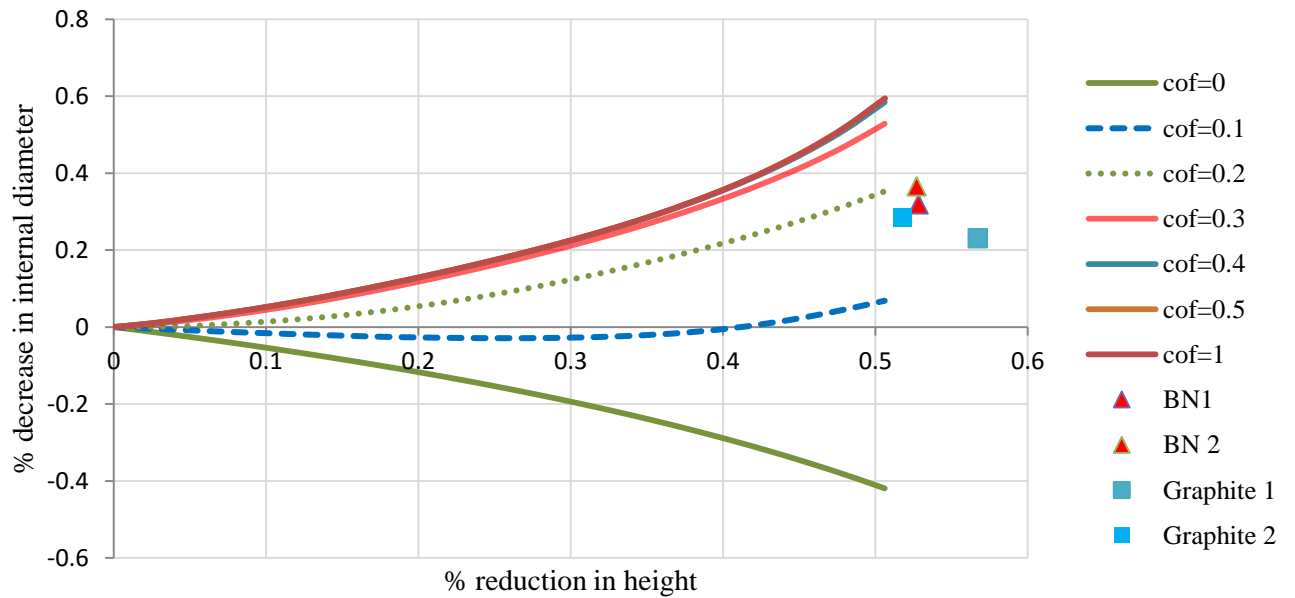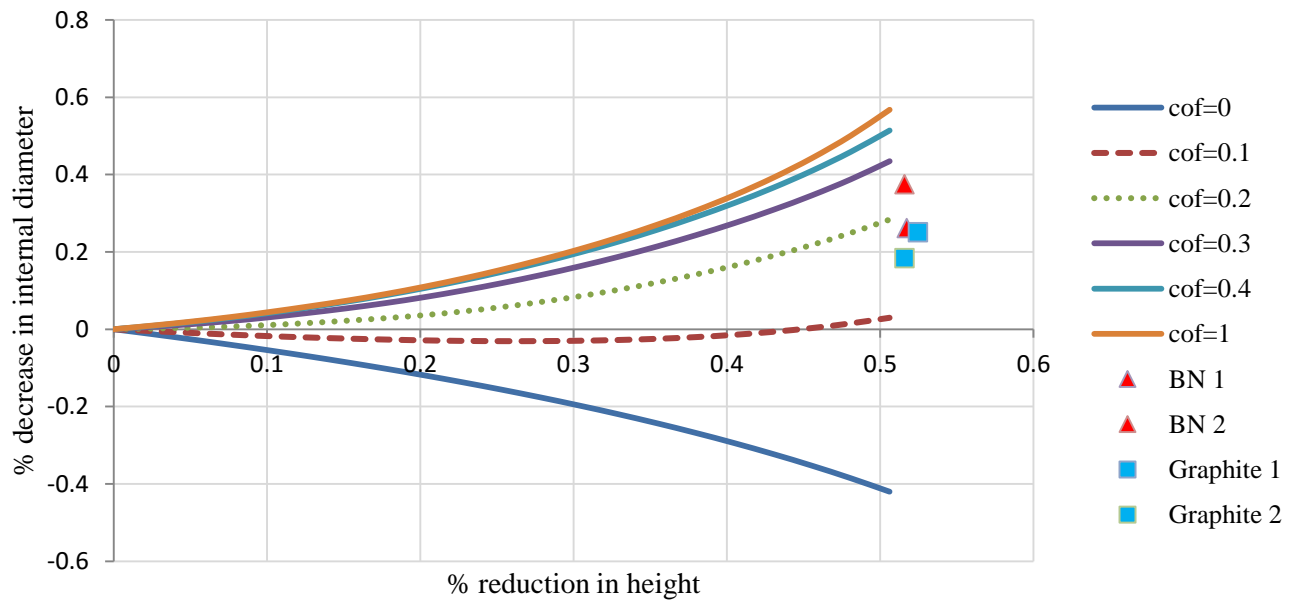
Figure 4.16: Coefficient of friction calibration curve (a) 10mm/min (b) 400mm/min

4.3 Flatbread Test

4.3.1 Overview
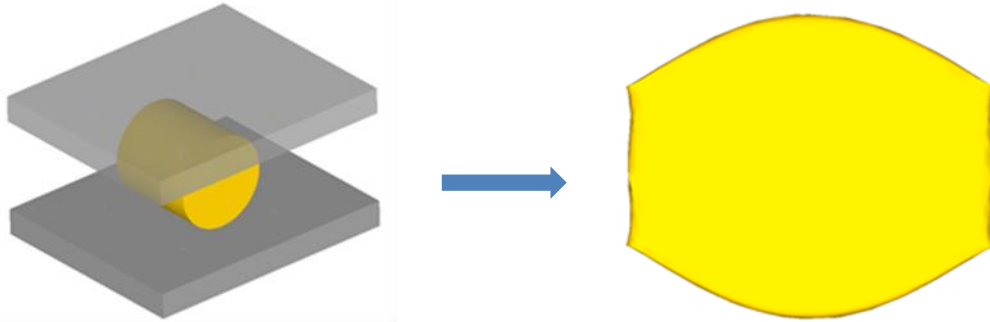
Figure 4.17: Schematic of flatbread forging

A so-called flatbread specimen was used to investigate the effect of forging in the transverse material direction, Fig. 4.17. Left over extruded AZ31b materials from a previous project at Canmet was used in this test.

The flow stress in the extrusion direction for AZ31b was the only data available early in the project. However, preliminary testing of pancake and ring specimens suggested that the material was anisotropic. Hill's coefficients were found in the literature [49] for AZ80. A hybrid model consisting of flow stress of AZ31b extrusion and literature value of AZ80 Hill's coefficients was used as an initial attempt to explore the use of the anisotropic model.

The flatbread test compresses a cylindrical billet radially using two flat dies. This not only promotes more complicated material flow, but also mimics the billet orientation in real life control-arm forging process.

4.3.2 Experiment

The material used in this test was AZ31b extrusion with diameter of 63.5mm and length of 65mm. The specimens were lubricated at room temperature with graphite using spray cans then heated up in the oven to 400 ºC for 3 hours. The dies were heated to 400 ºC before and during the forging process. Three forging rates were tested: 3.9mm/min (trial 13a), 39mm/min (trial 14a) and 390mm/min (trial 15a). All experiments were performed at CanmetMATERIALS, by Lucian Blaga, under the direction of Bruce Williams and Jonathan McKinley.

4.3.3 Numerical Simulation

A 3D model was necessary to simulate the flatbread forging test. The billet with a diameter of 63.5mm and length of 65mm was positioned with its longitudinal axis aligned with the global Z axis. The X and Y directions in the simulation represent the radial directions of the billet. Two rigid flat dies were used, with the lower die fixed. The upper die had velocities of 3.9mm/min, 39mm/min, and 390mm/min.

The isotropic material model was not adequate to replicate the behavior of the tested materials, since the shape of the deformed specimen was not accurately predicted. An anisotropic material model had to be employed. The simplest anisotropic model included in Deform is the Hills's model. This required the flow stress curve as well as Hill's anisotropic coefficients, which are obtained from the compression and shear flow stresses.

The flow curves used in this model were generated by the forging group. AZ31b extrusion flow stresses at true strain rates of 0.001/s, 0.01/s, 0.1/s and 1/s at 400 ºC were converted to effective stresses at the corresponding rate, then supplied to the material database in DEFORM as tabulated data (Appendix A). AZ80 Hill's 6 anisotropic coefficients were taken from the literature [49] for a different material (AZ80) in a 'hybrid' model, as a first attempt to investigate the significance of anisotropy modelling. This hybrid model cannot be expected to produce realistic results, but was used to explore the importance of anisotropy in the simulation, and its effect on material flow. The material was assumed to be fully plastic with E=44.8GPa, Poisson ratio=0.33 and density=1.77g/cm^3. Interfacial coefficient of friction was set to 0.2 according to the previous ring test results.

The mesh of the billet is shown in Figure 4.18. Fifteen thousand tetrahedron elements were used to mesh the initial geometry with element sizes ranging from 2mm to 4mm (Figure 4.18). One hundred simulation steps were defined with step increment of 0.6mm/step. The simulation finished within 20 minutes on a desktop computer (Intel Core i7 4790 @ 3.6GHz, 32GB RAM).
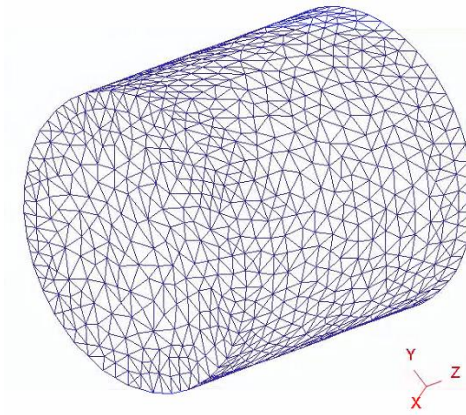
Figure 4.18: Mesh of billet in 3D simulation

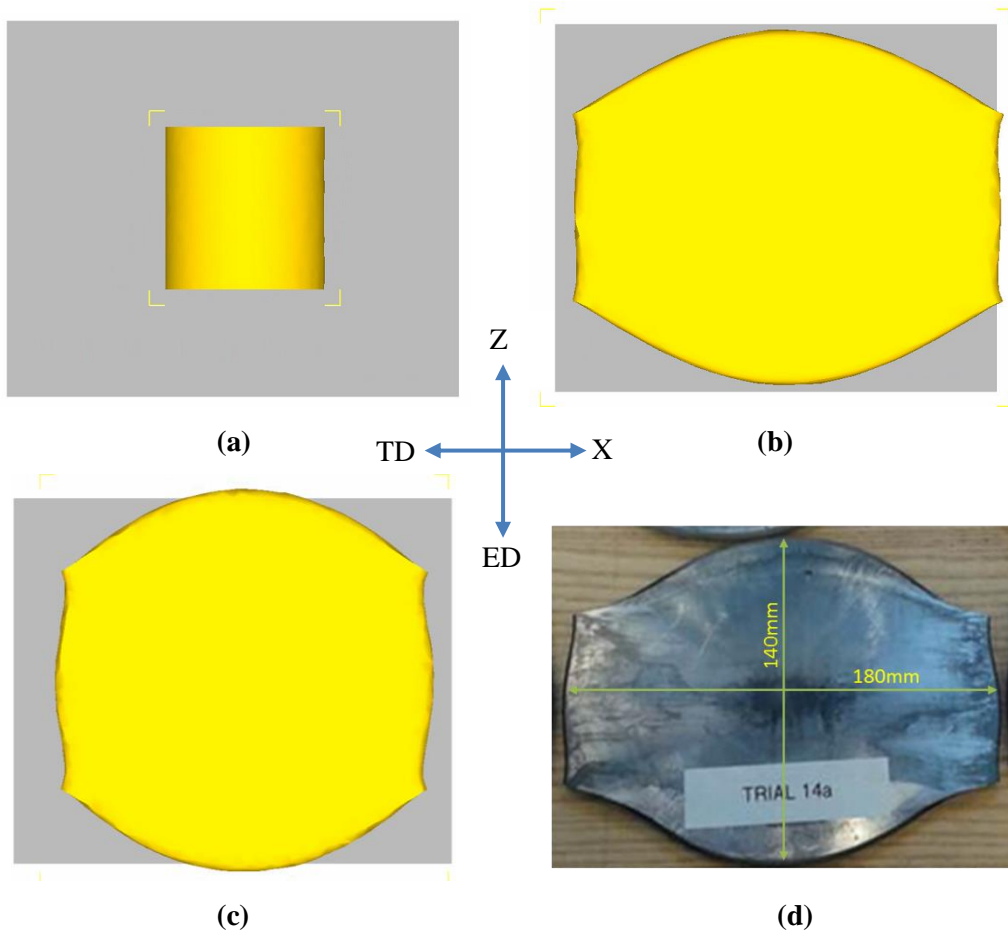## 4.3.4 Results

(a)

(b)

(c)

(d)

Figure 4.19: (a) Initial billet orientation (b) Anisotropic material simulation

**(c) Isotropic material simulation (d) Test result**

Figure 4.19(a) shows the initial billet orientation on the die, with its longitudinal axis aligned with the Z axis. Figure 4.19(b) reveals the anisotropic material simulation result. Figure 4.19(c) presents the same simulation using isotropic material model. Figure 4.19(d) shows one of the experimental result. Initially, when the experimental result came out, it was intuitively assumed that the billet was oriented horizontally (from left to right in Figure 4.19(b)). The simulation proved this to be a mistake. By comparing the final geometry, it was clearly seen that the billet was placed along the Z axis (vertical direction).

The difference between isotropic and anisotropic simulations are also easily identifiable. The isotropic material expanded uniformly into all directions forming a generally circular shape. The anisotropic material flowed more in the transverse direction than the longitudinal direction. In addition, the amount of material flow in the longitudinal direction was less than that in the isotropic simulation. The anisotropic result was no doubly closer to the test result even though this was a hybrid model that was not intended to fully replicate the actual material behavior. The discrepancy in dimensions of major and minor axes indicated that improvements of the material model were necessary.

Surface cracks were identified on the ED end surfaces of the forgings (Figure 4.20 (a)). According to the simulations (Figure 4.20 (b)), the maximum damage value on the flatbread was located at the same location of the cracks and the value was just above 0.5. This was the critical damage value reported in [36] for AZ31. It appeared from this that the damage criterion was able to predict surface failures reasonably well.
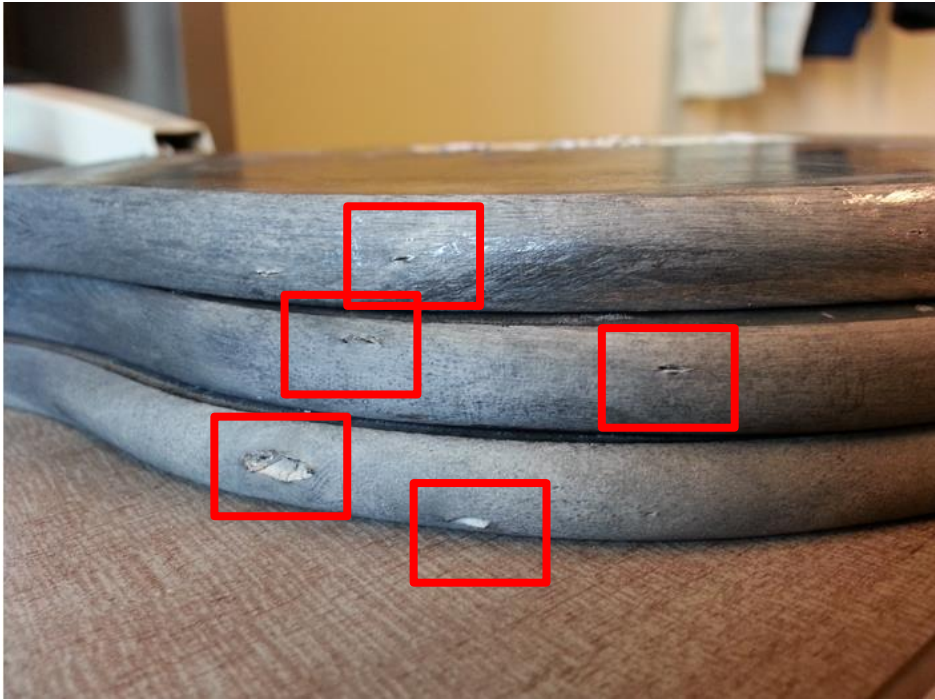
(a)
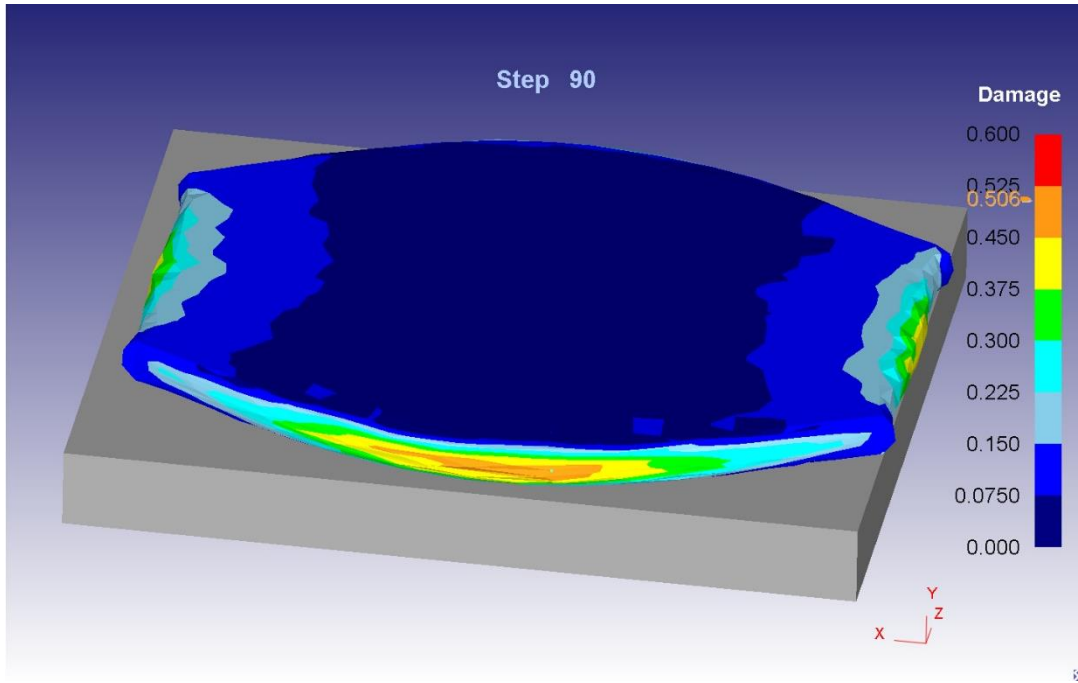
(b)

Figure 4.20: (a) Surfaces cracks on flatbread forgings (b) Damage distribution in simulation

Chapter 5

Small-Scale Forging Specimen (110-Ton Press)

5.1 Overview

A small scale forging test that could be used to validate simulation was required. One key parameter in the forging process is load. The 500-ton hydraulic press that was used in preliminary testing was not equipped with load cells for accurate load reading, but instead used the pressure in the hydraulic lines to calculate force. Consequently, the force recorded by the system could be a combination of the resistance from the material, the force required to move the bolster, and the inertial force of the large bolster (Bruce Williams, private communication, February 24, 2015). At high speeds, the inertial force of the bolster might become significant and lead to significant errors. For example, an inconsistent trend was seen in the pancake forging results below (Figure 5.1), with the intermediate rate experiment showing the highest load.
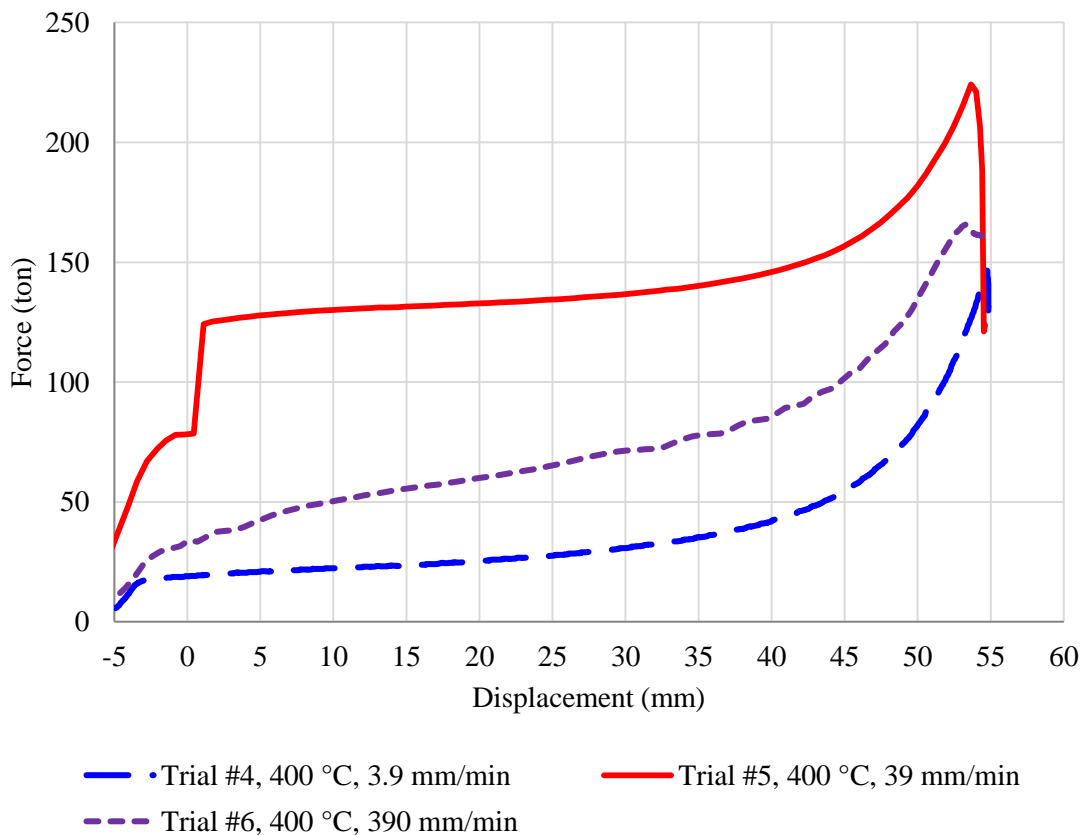

Figure 5.1: Pancake forging load vs. displacement

Fortunately, an Interlaken SP225 press at CANMET with 110-ton load capacity was equipped with load cells and LVDTs (linear variable displacement transducer) for accurate load and displacement monitoring. A test specimen on this press to validate geometric and load predictions in numerical simulation was required. It was decided to make one side of the specimen flat in order to save die manufacturing cost. Apart from shape and load predictions, minimum forging thickness of magnesium alloys, variation in strain and damage on the specimen, and test sample accommodation were to be considered in the design. The maximum forging load limit of 110 tons was also considered.

The test samples to be extracted from this forging included tensile and cubic samples. The tensile sample had a dimension of 80mm x 12mm x 6mm. The cubic sample had a side length of 6mm.

5.2 Geometry Design

5.2.1 Axisymmetric Design

The first attempt on 110-ton forging specimen design was inspired by a few successful Mg alloy forgings from the literature. Skubisz et al. [50] used the geometry in Figure5.2 to test forgeability of both cast and wrought AZ31 and AZ61 in warm closed-die forging conditions. The web and rib features of this geometry provided adequate assessment of material flow and die filling information during forming. The central upper cavity offered additional information about die filling at the centre. Defects were found at the bottom and on the inner rib surface. However, this flashless design was not possible without a high-precision closed-die forging system, which was beyond the expectation for this specimen.

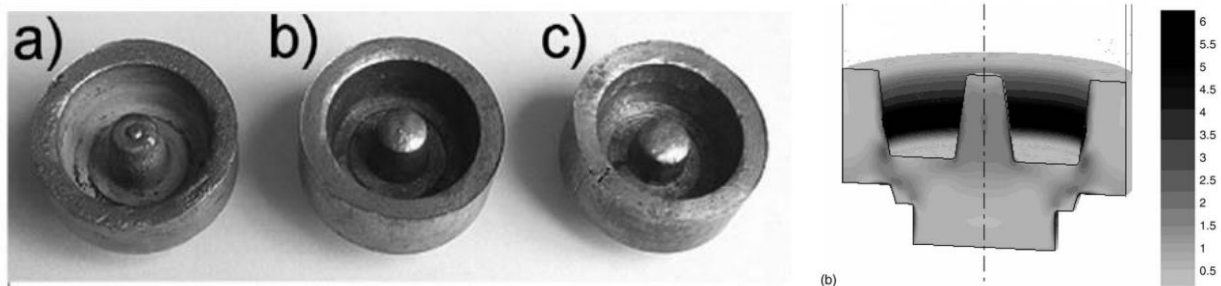
Figure 5.2: Axisymmetric sample design [50]

Another axisymmetric specimen design was proposed by Jeon et al. [51] that had both forward and backward extrusion (Figure 5.3). The top (backward) extrusion part was particularly of interest as it

consisted of features including rib, web and flash. The existence of flash indicated an open-die forging process.
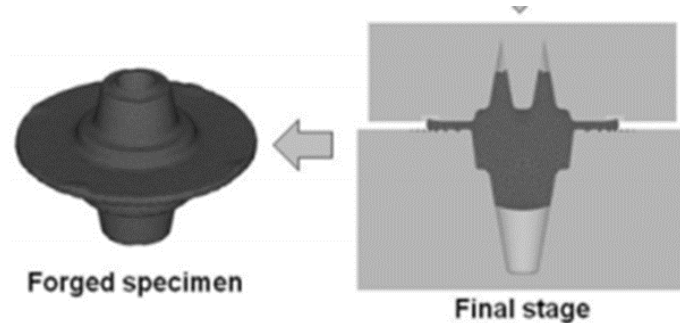

Figure 5.3: Forward/backward extrusion sample design [51]

A similar geometry for small-scale test was initially developed for this research based on this backward extrusion idea (Figure 5.4 (a)). The dimensions of the design were shown in Figure 5.4 (b) with a rib thickness of 3mm, which was the smallest forgeable thickness found from the literature. One goal of this geometry was to test the height of such a thin rib after forging. A billet with a diameter of 24mm and length of 30mm, with as cast AZ80 properties at 400 ℃ was used in the simulation. The effective strain distribution at final forging step was plotted in Figure 5.4 (c). The final forging load was less than 30 tons using an average strain rate of 0.001/s in simulation.

Although this axisymmetric specimen satisfied almost all the test needs, it had to be abandoned since no test samples were possible due to the curvature of the rib and the thin web.

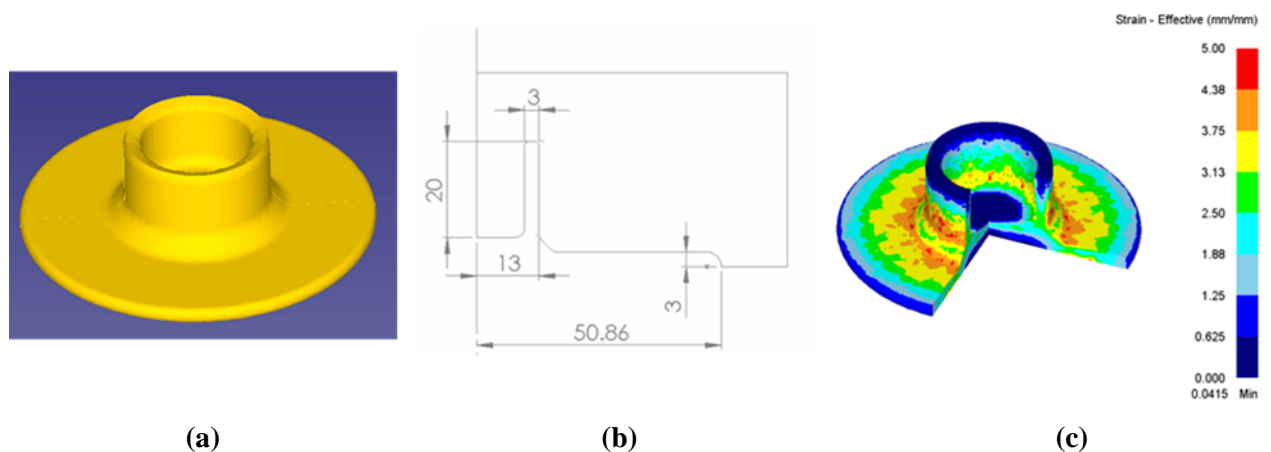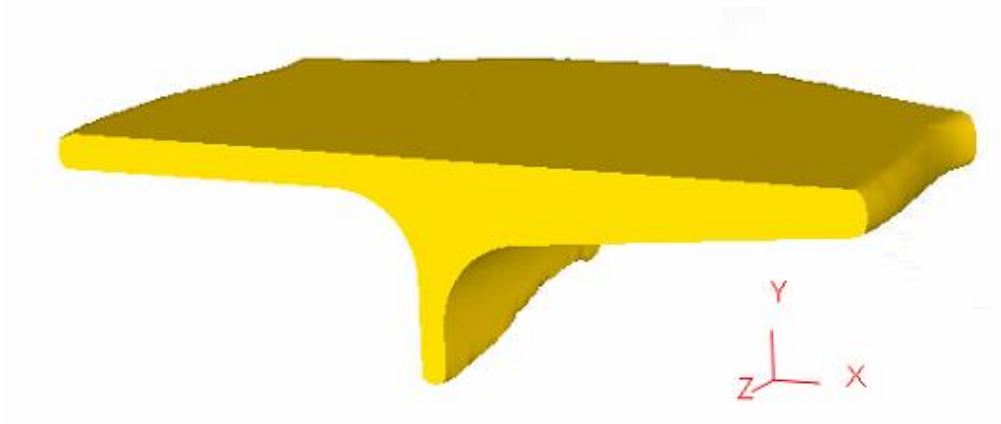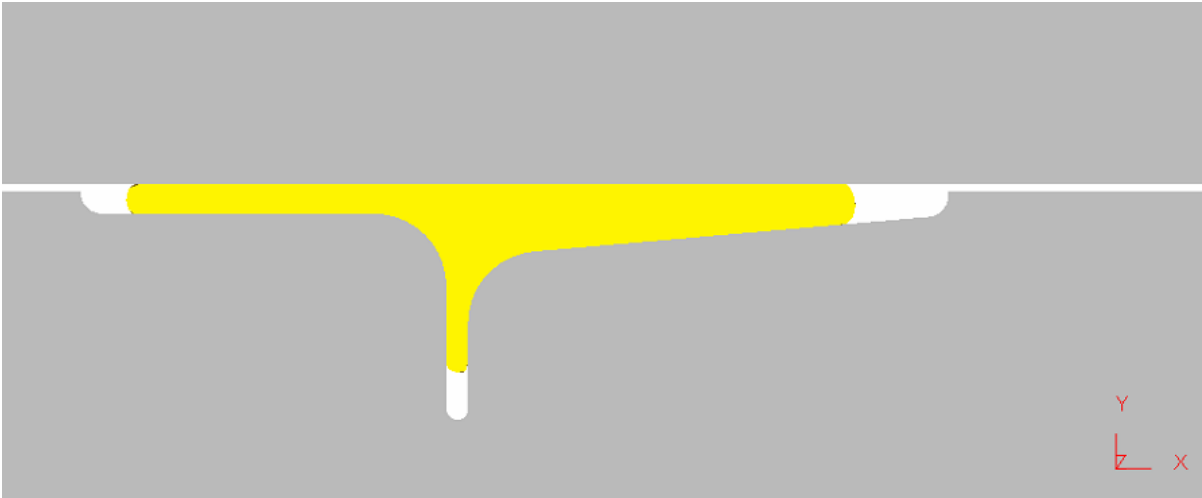(a)   (b)   (c)

Figure 5.4: Axisymmetric 110-ton forging sample design

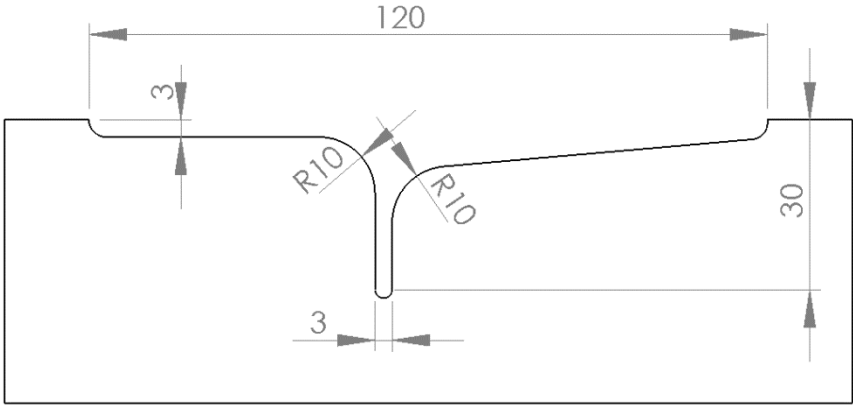**(a) Isometric view (b) Dimensions (c) Effective strain plot**

45

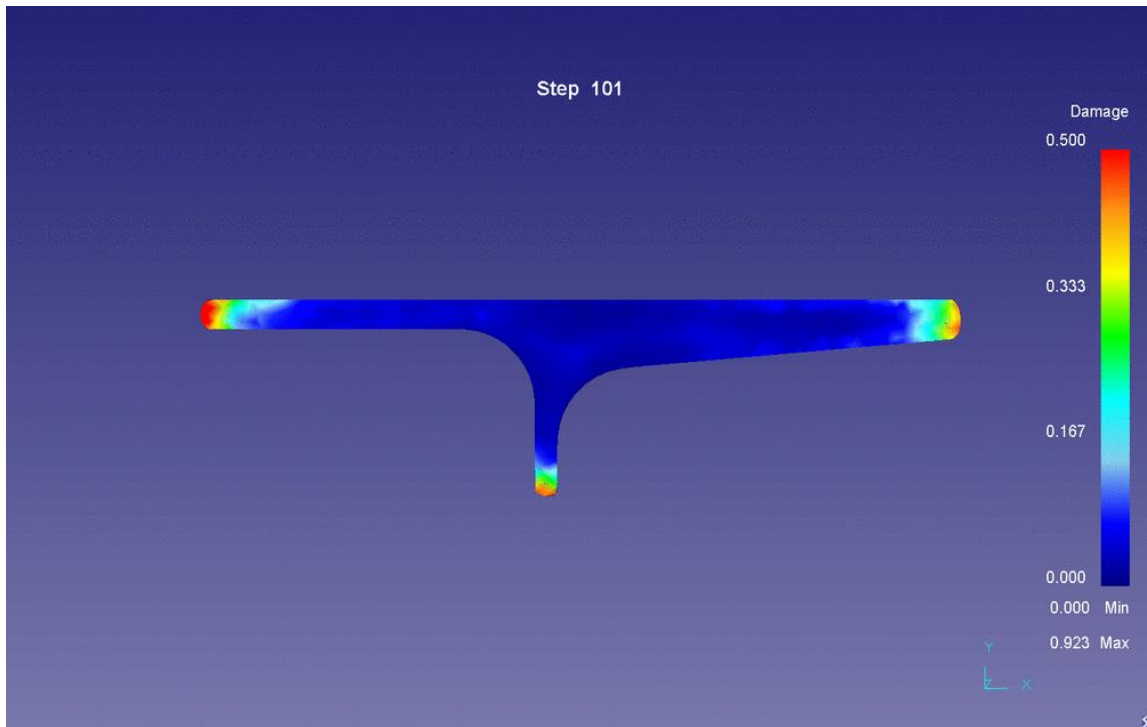## 5.2.2 T-shape Design with Slope

(a)

(b)

(c)

(d)

Figure 5.5: T-shape design with slope feature (half model due to symmetry)
(a) Isometric view (b) Front view (c) Die dimensions (d) Damage distribution

A new design (Figure 5.5 (a) and (b)) was proposed based on Gontarz and Dziubinska's work [23] to forge a flat part with ribs. Gontarz and Dziubinska used a closed-die system with 4 pieces of tooling to produce the geometry to ensure 100% die filling. For our purposes, complete die filling might not necessarily be favorable. Underfill in the die cavity can provide information on material flow and how well the simulation replicates unconstrained material behavior. It is therefore more attractive for simulation validation.

The T-shape was designed such that the web and rib share a common thickness of 3mm (Figure 5.5 (c)). The inner corner radius was a suggested value of 10mm from the literature [52] to promote material flow into the deep and narrow rib region. The depth of the rib was designed such that only the middle section of the rib tip was to contact the die when fully closed. By doing so, the majority of the rib would not be constrained by the die and would be able to flow freely to provide for geometric comparisons between the simulation and experiments. A slope was added to the right side of the rib with the intention to introduce gradual change in strain and damage. Such a design could also easily

47

accommodate a few tensile test samples and cubic compression samples. However, the simulation results in Figure 5.5(d) showed that damage only occurred on the edges of the specimen, instead of in the slope region. An effective strain plot (Figure 5.6) also indicated a rather uniform strain distribution along the slope.
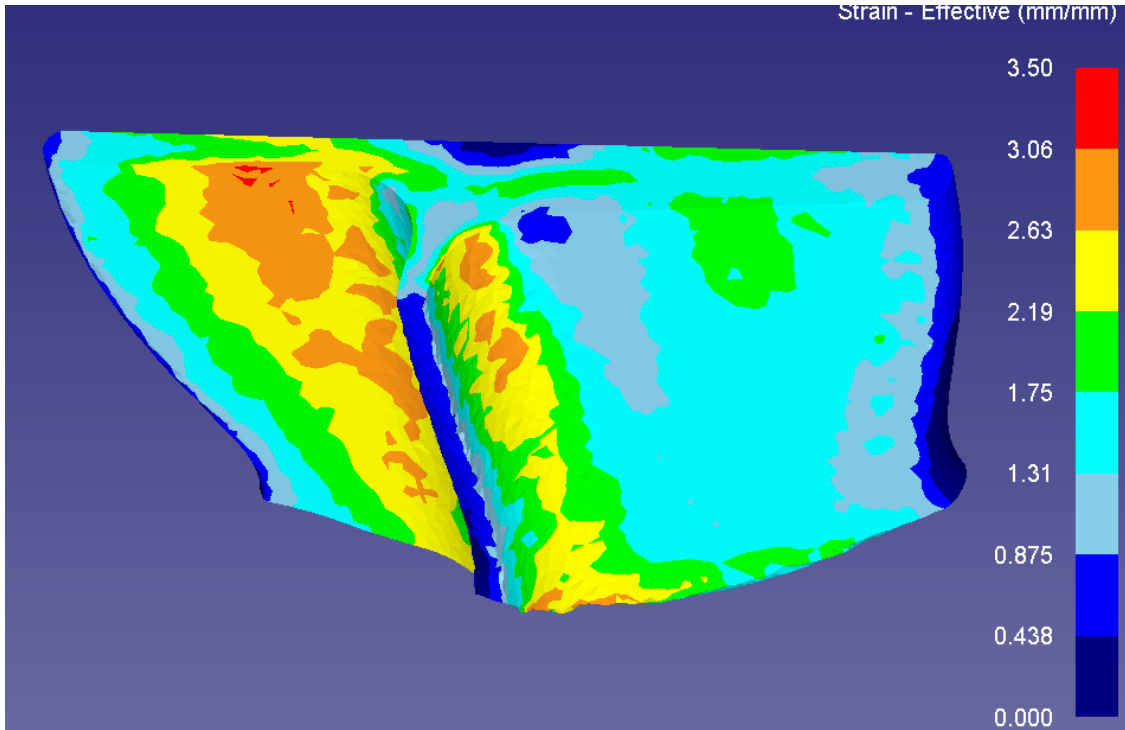
Figure 5.6: Effective strain plot of sloped sample

5.2.3 T-shape Design with Step

The slope was replaced by a step design which could accommodate even more test samples and was also able to generate a higher variation in effective strain, Figure 5.7. The initial billet used in the simulation had a diameter of 18mm and a length of 60mm. The max load using as cast AZ80 flow stress at 400 °C was 110 tons for 0.001/s strain rate. This was not an acceptable load case considering that 0.001/s was the slowest rate in the test matrix and lower temperatures would dramatically increase load in the deformation process, exceeding the capacity of the press.

A smaller billet size of ø20mm x L45mm was selected after a few simulation iterations to ensure load readings for all test materials and conditions were under the 110-ton limit and the final forging geometry was long enough (L>70mm) to allow for tensile samples.

(a)

(b)

Figure 5.7: T-shaped design with step feature (a) Isometric view (b) Cross-section view
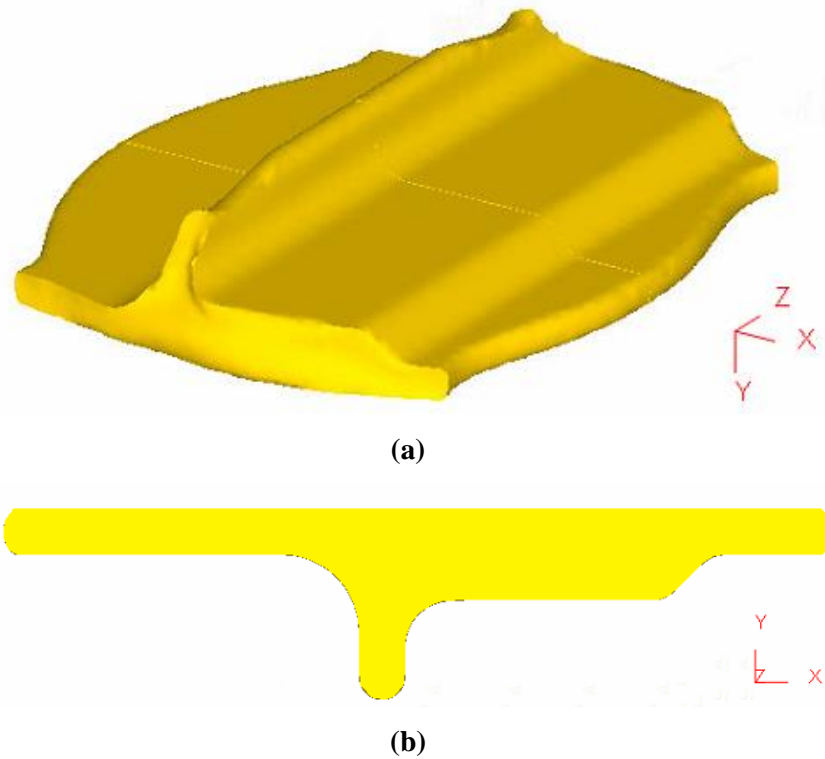
5.3 Tooling Design

This specimen geometry required only one die and one flat platen. The die was originally recessed (Figure 5.8(a)) with a lip of 3mm on the sides such that the flat platen contacts the die upper surface directly when fully closed. McKinley suggested (Jonathan McKinley, private communication, November 3, 2015) to use a proud die (Figure 5.8(b)) instead of recessed to have the ability to vary the thickness of the specimen if necessary. Proud dies could also prevent direct impact at high velocity and hence prolong tooling life. The final die was proud with a die stopper of 3mm thickness to ensure a correct web thickness. Jonathan McKinley worked on the external geometry and mounting features to make sure this die would fit on the 110-ton press.

Both the die and platen on the 110-ton press were equipped with thermocouples for temperature monitoring. Thermal insulation was used between the die and the press to prevent excessive heat loss.
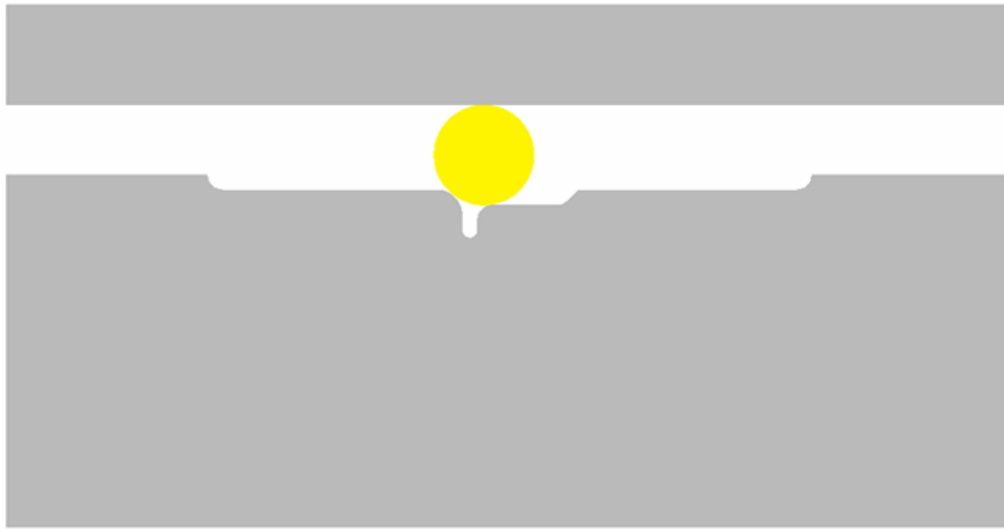
(a)
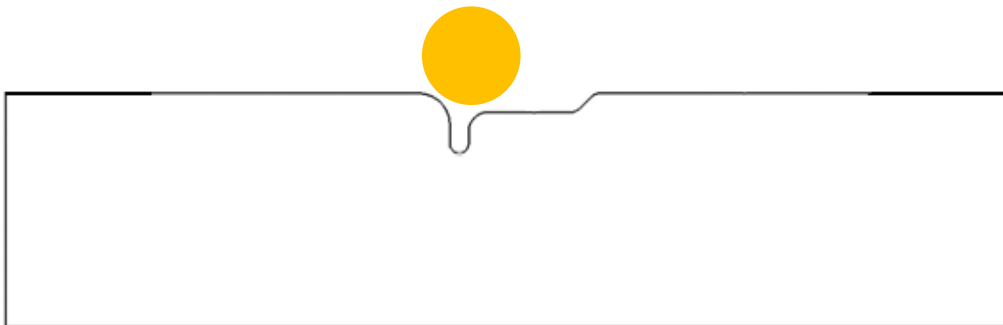
(b)

Figure 5.8 (a) Recessed die design (b) Proud die design

5.4 Experiments

Three extruded materials were tested in these experiments – AZ31, AZ80 and ZK60. The billets, with a diameter of 20mm and length of 45mm, were machined from larger 63.5mm diameter extruded rods. These billets were taken from a 40mm diameter ring in the 63.5mm rod (Figure 5.9) to be consistent with the Gleeble billet machining location.
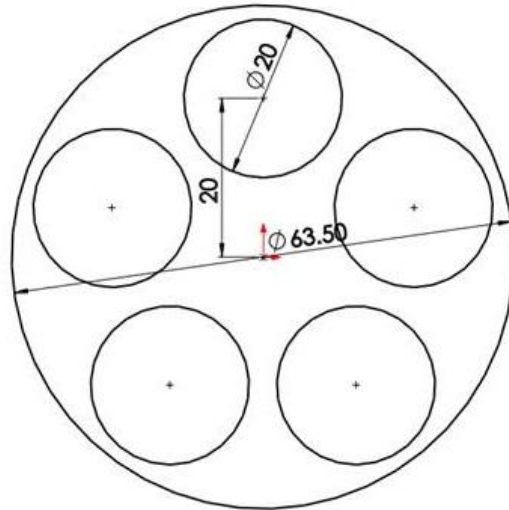
Figure 5.9: Billet location on bar stock

The test temperatures for these materials were selected based on previous Gleeble forging results and suggestions from the forging group: 400 $^{\circ}$C for AZ80, 450 $^{\circ}$C for ZK60 and 500 $^{\circ}$C for AZ31.

Forging rates were calculated based on average strain rates within the billet at the final forging step in the simulation. A 0.001/s average strain rate translated to 0.004mm/s die speed and 1/s average strain rate corresponded to 4mm/s. The upper limit of the 110-ton press was on the order of 40mm/s and a decision was made to try out this faster rate to test material behavior, although it was not possible to obtain material data at this rate for comparison with simulations due to limits of the Gleeble.

The total die travel for this test was less than 20mm. A die speed of 0.004mm/s would have taken more than 80 minutes to finish, which was not practical. A speed of 0.04mm/s would need 500 seconds (<10 minutes), 0.4mm/s required 50 seconds, 4mm/s needed 5 seconds, and 40mm/s could finish within 1 second.

The faster four rates – 0.04, 0.4, 4 and 40mm/s were selected for all three materials, Table 1.

Table 1: Small scale specimen test matrix

		0.04mm/s	0.4mm/s	4mm/s	40mm/s
AZ80	400 $^{\circ}$C				
ZK60	450 $^{\circ}$C				
AZ31	500 $^{\circ}$C				

Before forging, both the dies and materials were sprayed with graphite lubrication at room temperature. Then the heaters were turned on to heat up the die and platen to the designated temperature. The billets were placed in an oven for 3 hours to ensure uniform temperature distribution before being transferred onto the 110-ton press for forging. The billets were placed along the rib cavity and against the left shoulder of the die (Figure 5.8(b)). Results will be discussed along with the simulations.

5.5 Numerical Simulation

A 3D model was employed for this simulation in DEFORM 3D (Figure 5.10). The billet was modelled using fully plastic material, while the dies were modelled using rigid elements with no deformation.

A billet with the aforementioned dimensions was created with its longitudinal axis aligned with the global Z axis in the simulation and placed on the lower die. The upper platen traveled down towards the lower die at the constant given velocity and stopped at a height such that the web thickness was 3mm. Contact between the billet and lower die was initiated at the beginning of the simulation, while the contact between the billet and upper platen developed as the platen traveled down. Coulomb coefficient of friction was set to 0.2 between all contacting surfaces.

The anisotropic material model required a flow stress curve and 6 Hill's coefficients. The flow stress defined in the material model was the effective stress-strain curve converted from the true stress–strain curve from Gleeble testing.

The Hill's anisotropic coefficients were assumed to be constant during constant velocity forging in an isothermal process. Four sets of coefficients were required in the simulations, one set for each forging rate, as four different rates were tested in this experiment for each material.
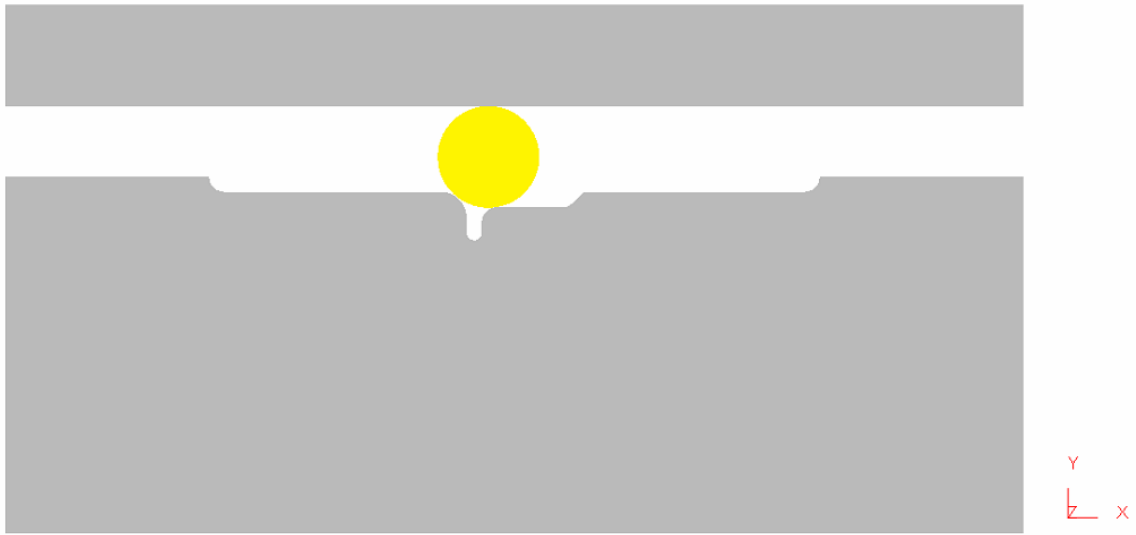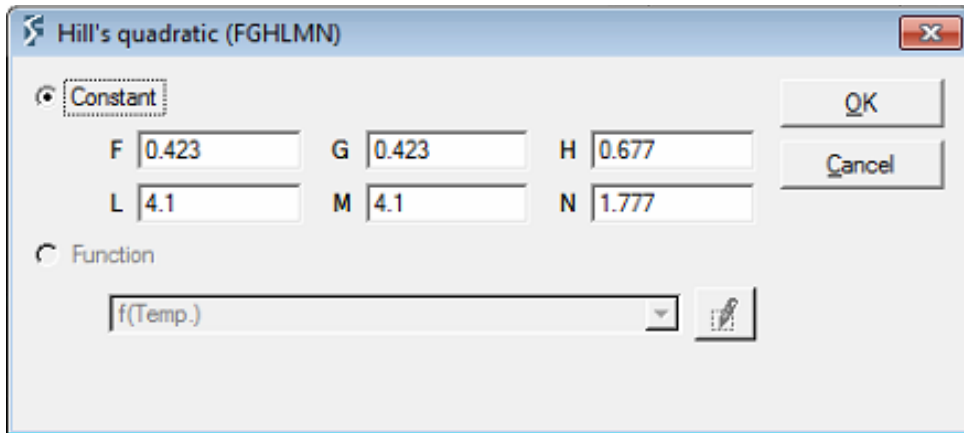
Figure 5.10: 3D model of 110-ton forging

The figure below (Figure 5.11) shows a complete material model in simulation of extruded ZK60 for forging rate of 0.4mm/s and temperature of 450ºC.

(a)
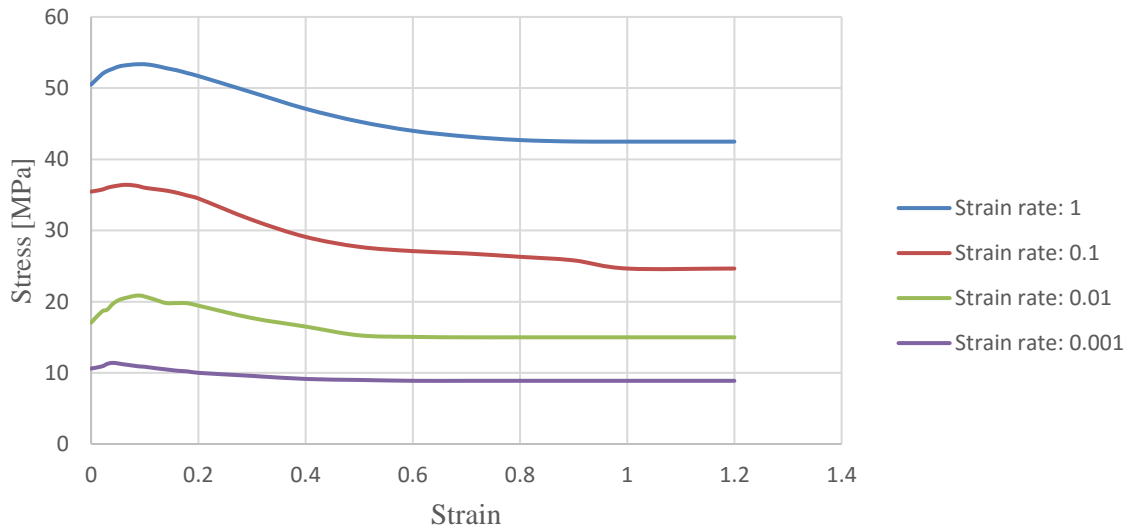
(b)

Figure 5.11: Material model for extruded ZK60 @450° C & 0.4mm/s

(a) Hill's coefficients (b) Flow stress

Figure 5.12: Mesh of billet

Only half of the billet length was modelled in simulation due to symmetry. Fifty thousand tetrahedron elements, with a size from 0.4 to 0.8mm, were used to mesh the billet (Figure 5.12). Simulations with 100,000 and 150,000 elements were also ran for mesh sensitivity study. The geometrical results from the higher mesh density did not differ much from the 50,000-element mesh – the difference was

54

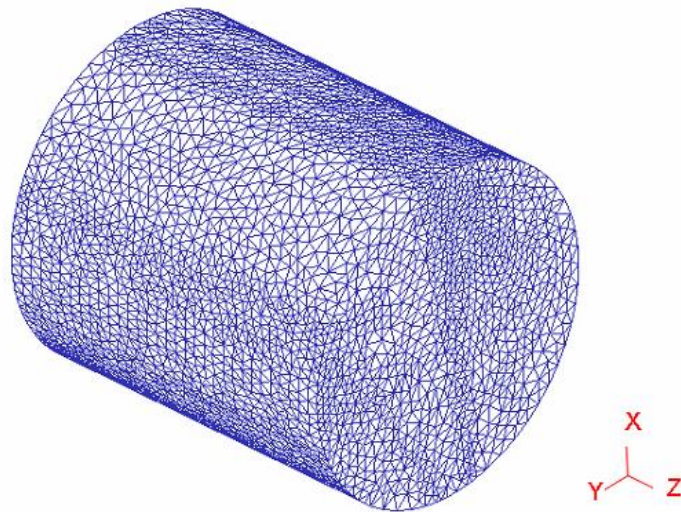within a few percent. Similar trend was found for load predictions. Apart from that, the higher mesh density resulted in two to three times longer total run time of the simulations. Thus, 50,000 elements were used for all subsequent simulations as a compromise between simulation time and accuracy. Since the die was not flat, remeshing was enabled when the interference depth was beyond 30% of the element size. Two hundred simulation steps were defined for a total die travel of 13.9mm with step increment of 0.07mm/step. The total simulation time for each condition was around 1 hour.

5.6 Results & Comparisons

Four forging rates (0.04mm/s, 0.4mm/s, 4mm/s and 40mm/s) were tested for each extruded material. Only the slower three were simulated due to the lack of material flow stress data at the highest forging rate. Only extruded ZK60 forgings will be discussed here; other results can be found in Appendix B. Figure 5.13 below shows the top view of all specimens. All the forgings share similar dimensions with a few millimeters variation.
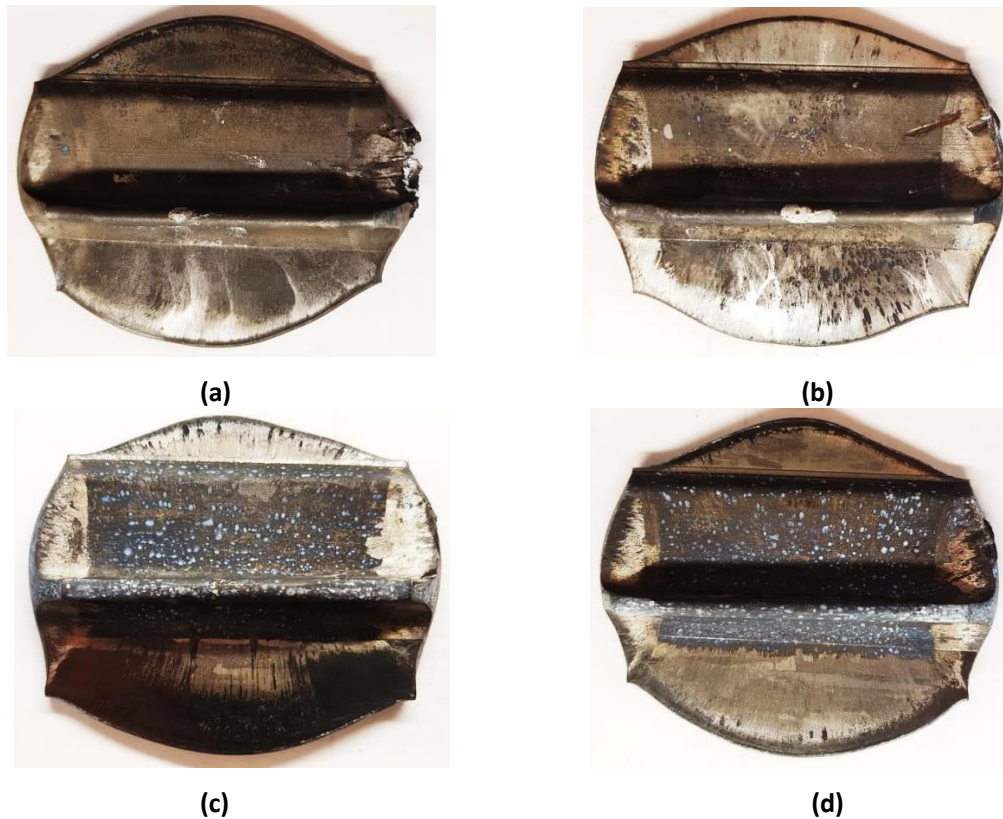

(a)

(b)

(c)

(d)

Figure 5.13: 110-ton forging results of extruded ZK60

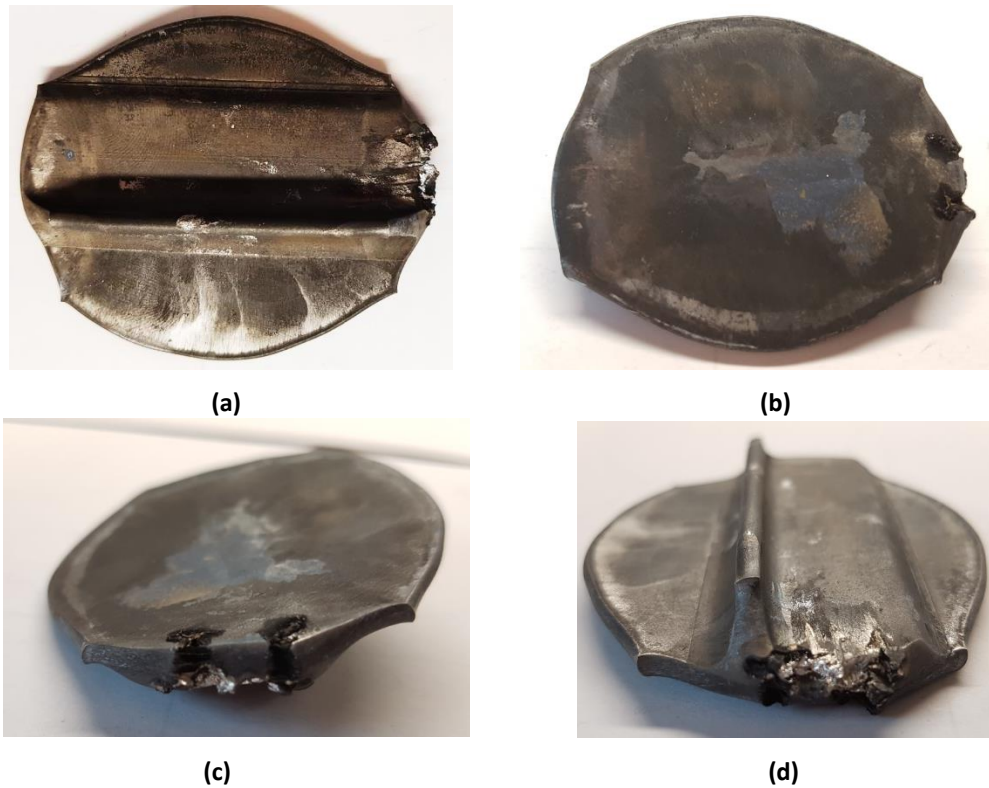**(a) Trial 10 – 0.04mm/s (b) Trial 11 – 0.4mm/s (c) Trial 12 – 4mm/s (d) Trial 13 – 40mm/s**

Figure 5.14: Cracked surface on extruded ZK60 forging Trial 10

(a) Top view (b) Bottom view (c) & (d) Side view

Among the forging trials for all materials, only SF10 (ZK60, 0.04mm/s, 450 ℃) showed cracking at one end of the specimen. A closer view is shown in Figure 5.14. According to simulation, the Cockroft & Latham damage values at that region range from 0.12 to 0.3 (Figure 5.15 (a)). The damage values increase as the forging rate increases, which suggests that local failure is more likely to happen for faster rate forgings. However, this specimen was tested at the slowest rate. This anomalous result suggests that there may have been a defect in this specimen. A repeat of test SF10 is in progress to verify this assumption. Aside from this specimen, the fact that the faster two rates did not show any visible material failure suggests that the critical damage value for ZK60 at 450 ℃ should be above 0.44 (Figure 5.15 (b)).
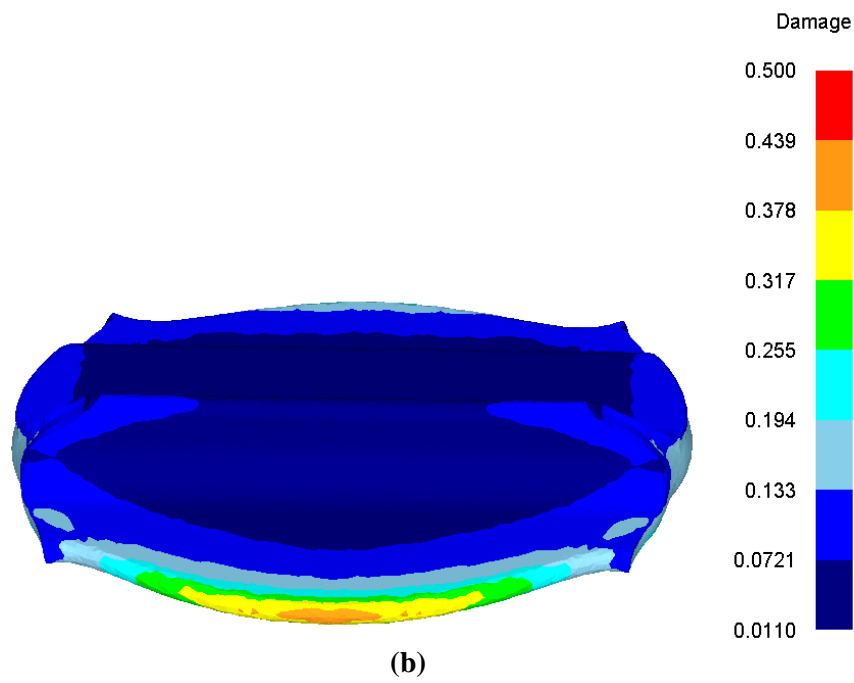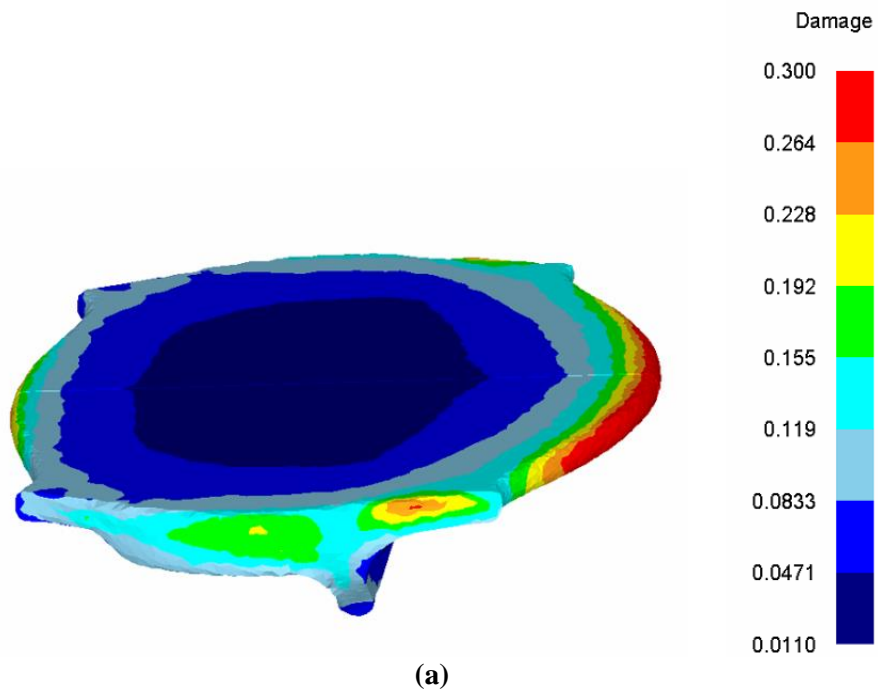
(a)

(b)

Figure 5.15: Damage value distribution for extruded ZK60 @ 450 ºC & 0.04mm/s

(a) Side view (b) Front view

The sample geometry was designed so that a number of features can be measured and compared between tests and simulations (Figure 5.16). Feature 1 is the distance between the upper left and right tips. Feature 2 is the maximum width of the specimen. Feature 3 is the measurement between lower left and right corners. Feature 4 is the maximum height of the sample. Feature 5 measures the height between the lower and upper corners.
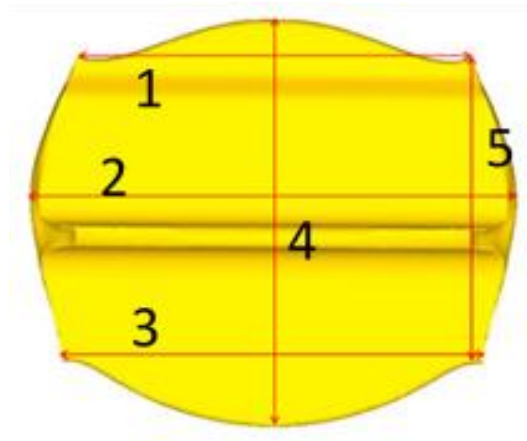
Figure 5.16: Feature numbers of 110-ton sample

The simulation results are not explicitly listed here but superimposed onto the specimen pictures for visual comparison (Figure 5.17). Complete results are available on the project Sharepoint site [53]. Both the samples and simulation results are to scale in order to highlight differences in dimensions. The percentage difference between simulation and experimental values were calculated using

$$\% \text{ difference} = \frac{\text{Simu} - \text{Exp}}{\text{Exp}} \text{ x } 100\% \tag{11}$$

A positive difference suggests over-prediction in simulation result and a negative value represents under-prediction.

As can be seen from Table 2, the largest difference was for SF10, with feature 1 under-predicted by 12.12% and feature 5 over-predicted by 13.79%. This is likely a result of the cracked surface which affected overall material flow. Despite the difference in dimensions, the curvature of the bottom edge was well-captured.

Table 2: Feature dimensions for ZK60 trials in millimeters

ZK60	1	2	3	4	5
Trial 10 - 0.04mm/s					
Aniso	52.75	70.41	60.83	54.90	41.93
Exp	60.03	69.46	57.8	57.89	36.85
% diff	-12.12	1.37	5.24	-5.16	13.79

ZK60	1	2	3	4	5
Trial 11 - 0.4mm/s					
Aniso	53.9	67.65	56.29	50.54	37.5
Exp	56.37	65.95	55.45	53.78	39.08
% diff	-4.38	2.58	1.51	-6.03	-4.04

ZK60	1	2	3	4	5
Trial 12 - 4mm/s					
Aniso	55.22	67.88	56.87	50.41	38.41
Exp	55.17	65.39	57.92	54.15	38.27
% diff	0.09	3.81	-1.81	-6.91	0.37

Both SF11 and SF12 simulations agreed well with experiments. The maximum difference for both were below 7% and happened to be feature 4, max height. The rest of the dimensions were almost exactly the same between simulations and tests. The material flow on the sides was extremely complicated, with in-plane flow as seen in the pictures and out-of-plane motion to form the rib. With that said, the curvature of the outlines and overall shape of the specimens were successfully captured. This proves the reliability of the simulation method using the anisotropic material model.

The 110-ton forgings were not only for geometric comparisons, but also to validate the forging load predictions using the load cell on the 110-ton press. Below are plots of Load-Displacement curves for 3 forging rates (Figure 5.18). The green curves are load predictions from anisotropic material simulations. The red curves are from isotropic material simulations. The dashed-lines are experimental results. The isotropic material simulations predict higher loads.

It is clear from the plots (Figure 5.18 (a), (b) and (c)) that for all three forging rates, the experimental load agrees well with both simulation predictions at the early stage of the forging process where no

large deformation happens. As the die displacement increases and material starts to fill the rib cavity, the experimental load tends to follow the isotropic prediction. At the end of the process, the load curve falls in between the isotropic and anisotropic simulations. The final forging load seems to match the anisotropic simulation better. This is expected given that this model most closely models material behavior, and also gave the best shape predictions.

An attempt was made to correlate the under-prediction of specimen area and the forging load. The area could not be measured directly from the DEFORM software; an estimation using major axis (Feature 2) x minor axis (Feature 4) was used. Area under-predictions of 3.9%, 3.6%, and 3.4% were found for Trial 10, 11, and 12 respectively. The forging load differences between experiments and anisotropic simulations were calculated to be -1%, +7%, +20% for Trial 10, 11, and 12 respectively. No obvious relations between area and load were found. The discrepancy in load prediction need to be further investigated in the future.
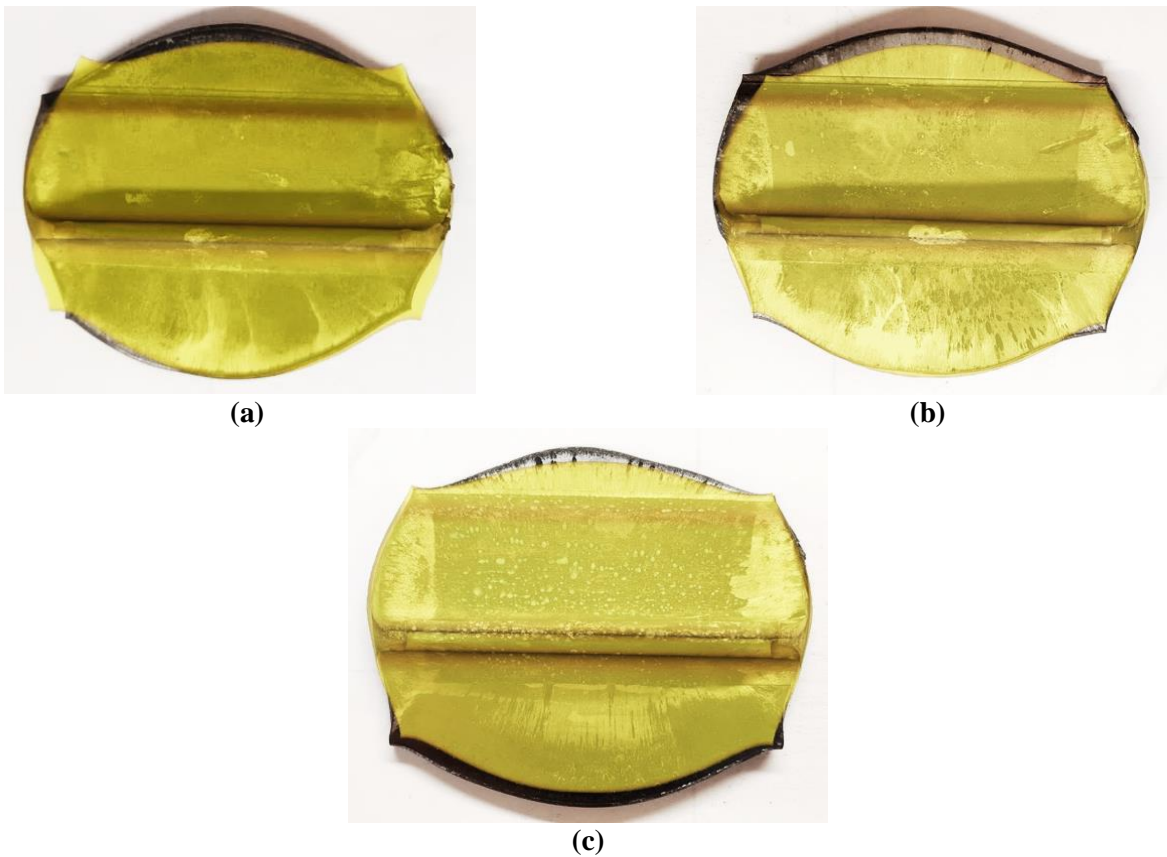

(a)

(b)

(c)

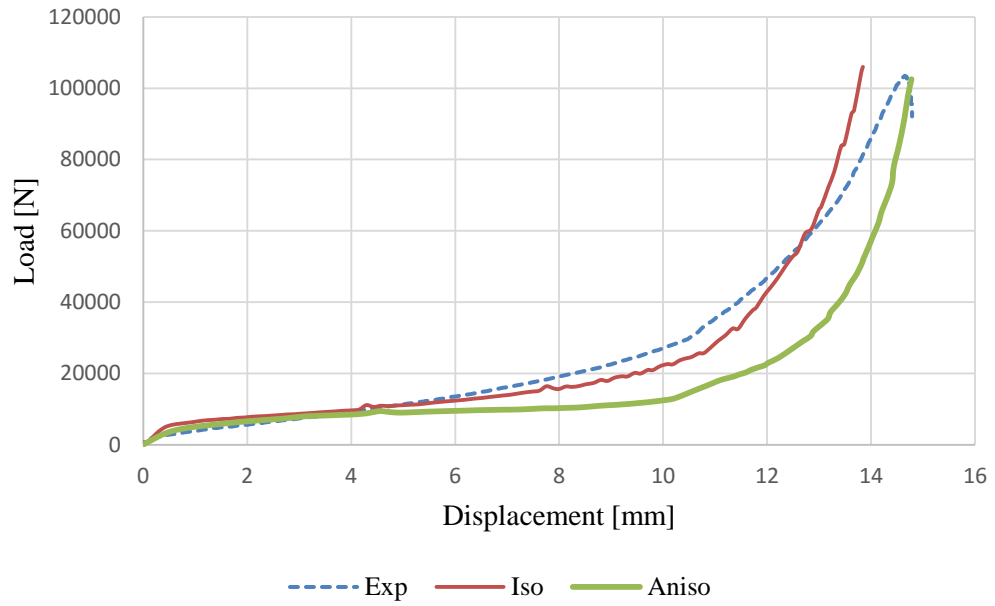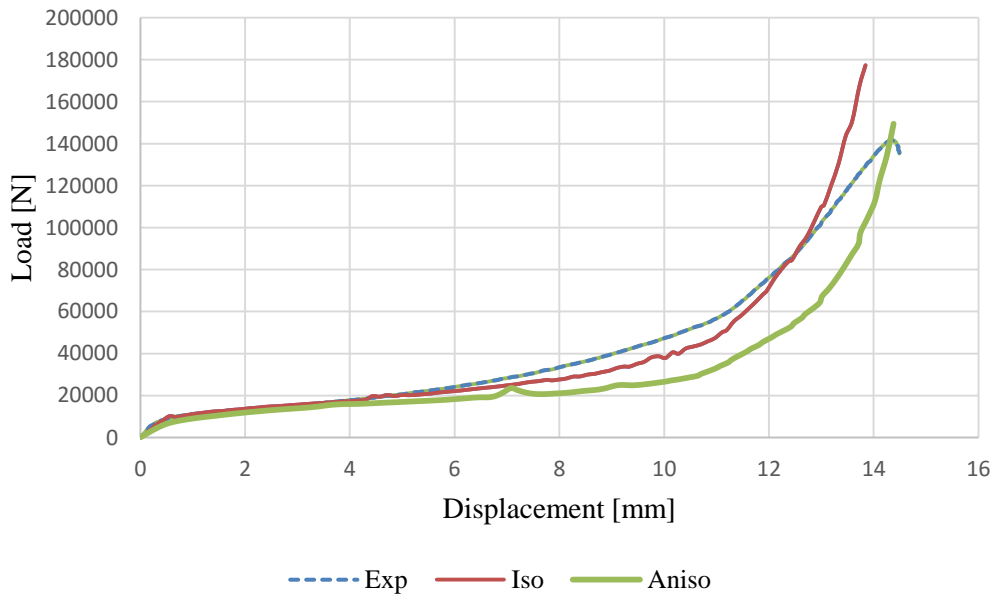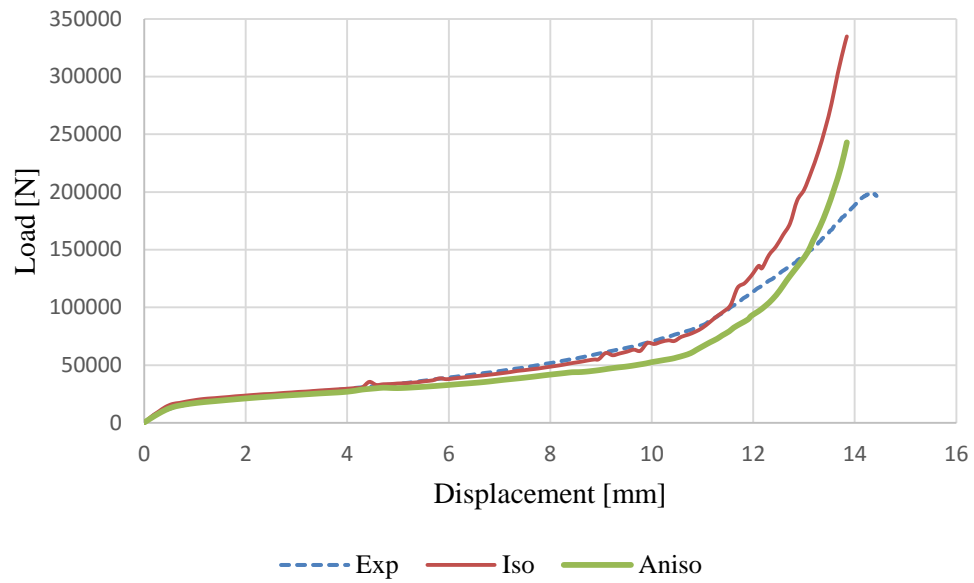**Figure 5.17: Comparison of simulation and test results**

(a) Trial10 - 0.04mm/s (b) Trial11 - 0.4mm/s (c) Trial 12 - 4mm/s

(a)

(b)

(c)

Figure 5.18: Load-Displacement curve for extruded ZK60

**(a) 0.04mm/s (b) 0.4mm/s (c) 4mm/s**

Chapter 6

I-beam Specimen Forging (500-Ton Press)

6.1 Overview

The specimen for the 500-ton press was intended to fill the gap between small scale Gleeble forging and the final control-arm. This required a representative geometry to capture the possible features on the final design. At the same time, it should be relatively easy to forge in experimental trials. Three important features were identified on the benchmark component (Alex Strong, private communication, 2015): the ball-joint retainer, the 'boomerang' shape of the control arm, and the I-beam cross-section.

Strong (Alex Strong, private communication, 2015) did preliminary work to evaluate the ball-joint retainer design. The boomerang shape of the control-arm could be achieved using an additional bending process before forging. The main focus of the 500-ton forging sample design fell on the I-beam geometry selection. Forging tooling design was another challenge and had a huge impact on the I-beam geometry in return. Test sample accommodation was also a factor in design. The samples to be enclosed included tensile samples, cubic samples, and rotating-bending samples (Figure 6.1).

A fully anisotropic material model was used in 3D simulation based on previous experience of 110-ton forging simulation. As mentioned in the previous chapter, the load reading of 500-ton hydraulic press was not accurate, thus a quantitative load comparison was not possible. Geometric comparisons between experiment and simulation were conducted.
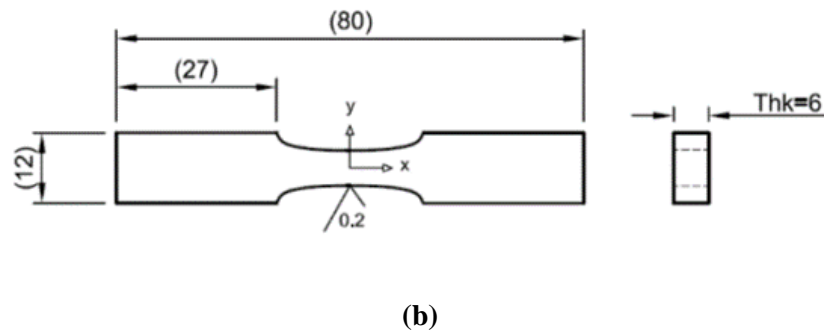

(a)

(b)
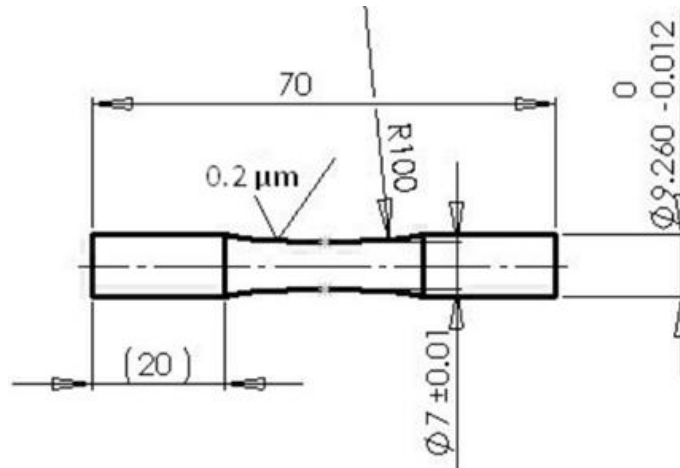
Figure 6.1: Dimensions of test samples in millimeter

(a) Rotating-bending sample (b) Tensile sample

6.2 Geometry and Tooling Design

6.2.1 Design 1.0
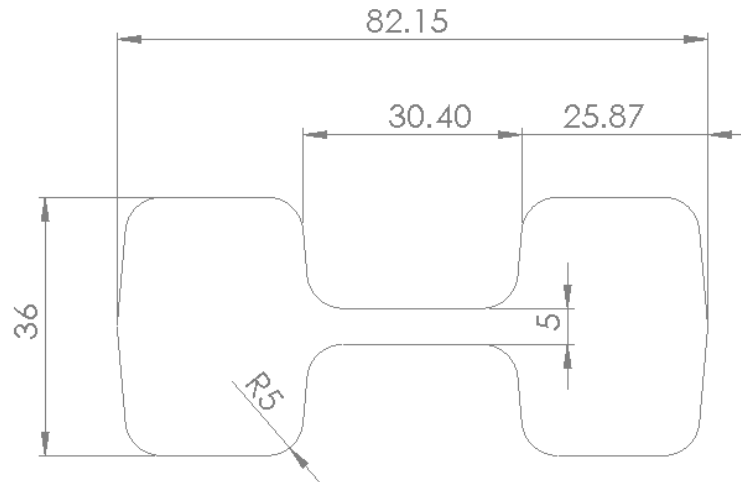
Figure 6.2: I-beam Design 1.0

The first design attempt (Figure 6.2) was mainly based on the cast-Al benchmark component cross-section geometry. Certain dimensions were modified to achieve the 20% mass reduction goal in the project proposal. However, this cross-section geometry lost 23% in bending stiffness (Alex Strong, private communication, 2015) when compared to the benchmark component.

Five degrees of draft angle was applied to all vertical surfaces to allow easier material ejection from the dies. All corners of the design shared a radius of 5mm.

The amount of flash and the flash-land geometry are critical in tooling design for a successful product. Assuming the length of the design to be 70mm - which was enough to accommodate the tensile sample (60mm) and at the same time a good balance to save material, the billet forged from Mg alloy would weigh 230g. Using Figure 6.3 from literature [41] yields:

Flashland thickness = 1.7mm

Flashland width = 8mm

w/t ratio = 4.7

According to literature [54], the the typical width to thickness ratio for the flashland was 2 to 5. A higher ratio would cause large stresses on the die and could reduce die life significantly. In our case, the ratio was 4.7, within the recommended window. Below (Figure 6.4) is a 2D tooling design using the above dimensions.
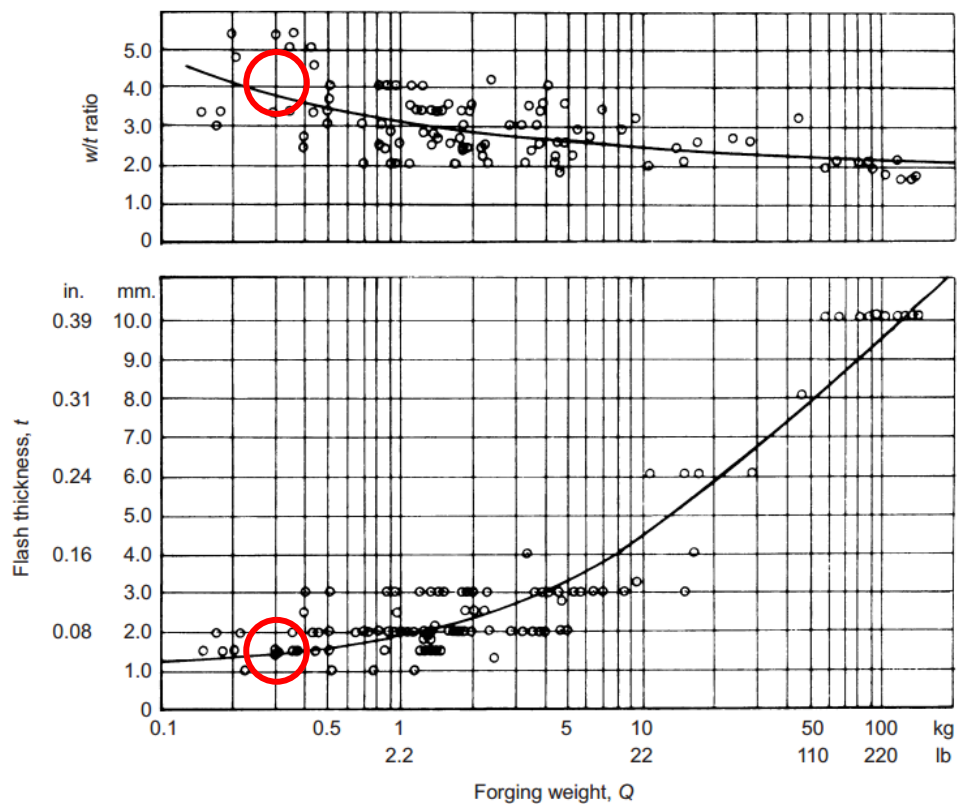

Figure 6.3: Flashland thickness and width design chart for carbon and alloy steel forgings [41]
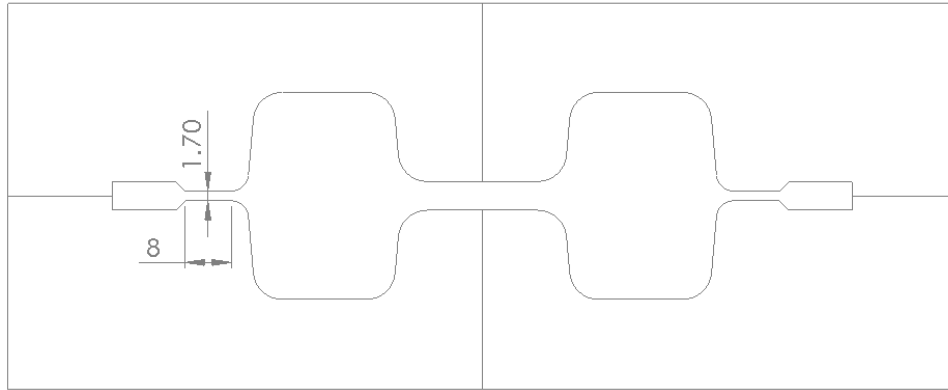
Figure 6.4: Tooling design for Design 1.0

6.2.2 Design 2.0
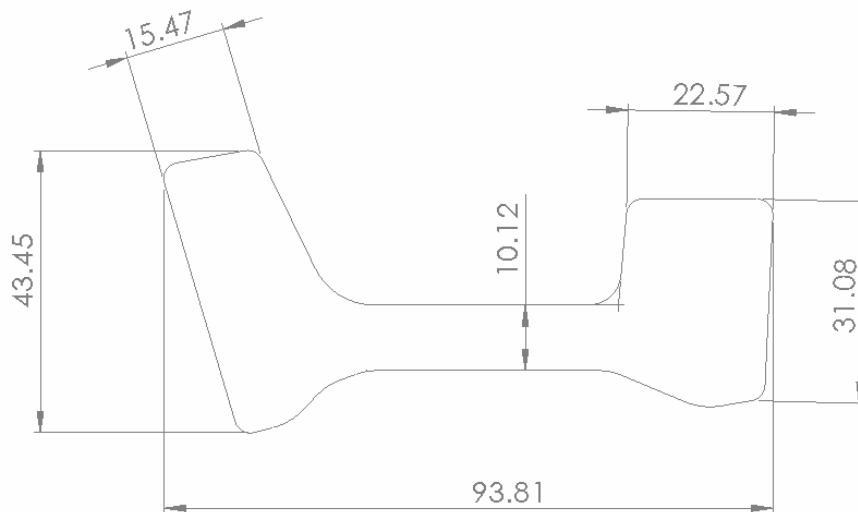
Figure 6.5: Design 2.0

Design 2.0 (Figure 6.5) was proposed based on the control arm structural optimization results made available later by Alex Strong (Figure 6.6 (a) and (b)).

From the optimization result, one distinctive cross-section in each arm of the component was selected as a potential specimen geometry, in this case Section 1 (Figure 6.6(c)) and Section 2 (Figure 6.6(d)). Section 1 had smooth curvatures and large radii along its contours. Although not symmetric about its horizontal axis, the geometry was mostly flat and did not seem to be challenging to forge. Section 2 however, was far more interesting with an I-beam section. It can be decomposed into three parts: left

66

shot rib, middle thin web, and right tall rib. The external corners of the ribs were sharp and abrupt. Both ribs were not vertical but at a slight angle to the web, which could cause difficulty in the forging process. The variation in rib size could help study material flow for different tooling geometries. Hence, section 2 was selected as the potential specimen geometry. A simplified shape was created based on the dimensions of section 2 with added features for easier forging – draft angles, fillets, and a straightened web (Figure 6.7 (a) and (b)).

(a)

(b)

(c)

(d)
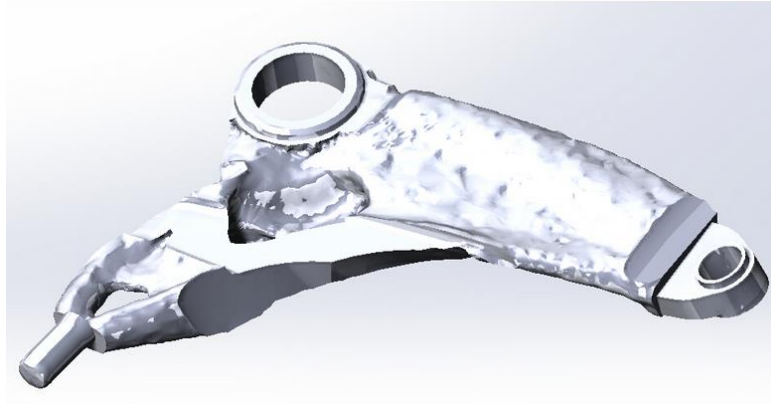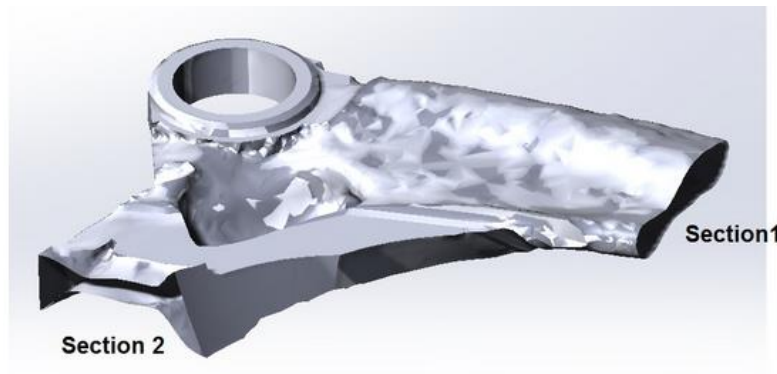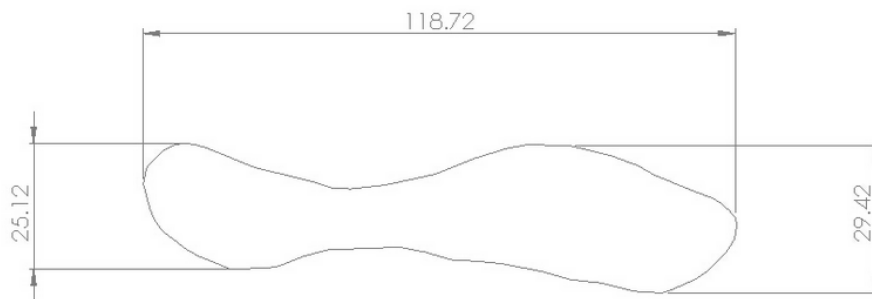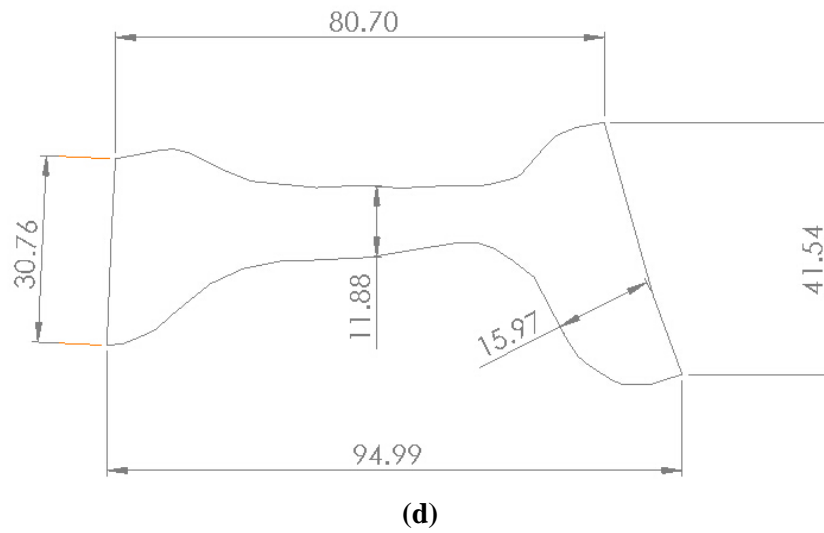
Figure 6.6: (a) Structural optimization result (b) Cross-section locations

(c) Section 1 dimensions (d) Section 2 dimensions

(a)

(b)
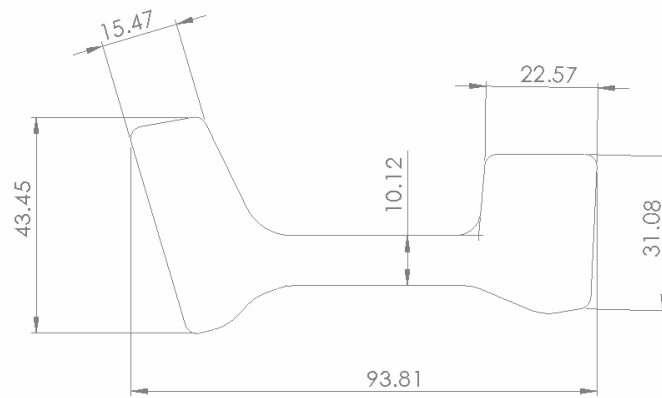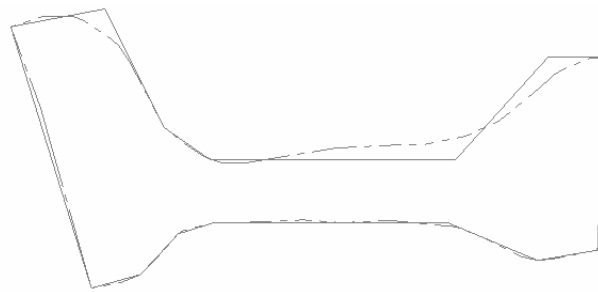
Figure 6.7: (a) Simplified cross-section geometry (b) Simplified geometry dimensions

As mentioned earlier, the most difficult part in tooling design for this geometry was caused by the angled ribs. As shown in Figure 6.8 below, the parting line of the upper and lower dies had to be on the very top of the forged specimen, in order to extract the product from the dies after forming [55]. Figure 6.9 shows an initial die design attempt in 2D.
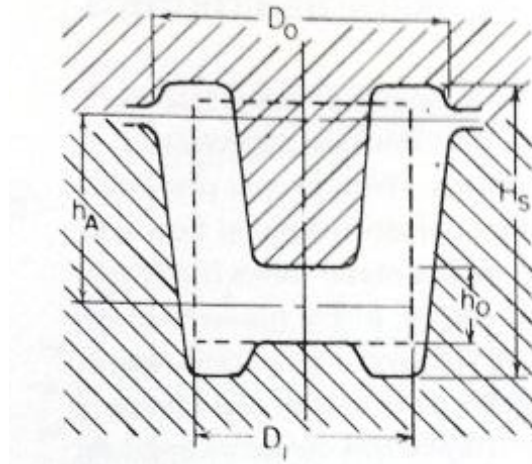
Figure 6.8: Parting-line location for geometry with inclined rib [55]
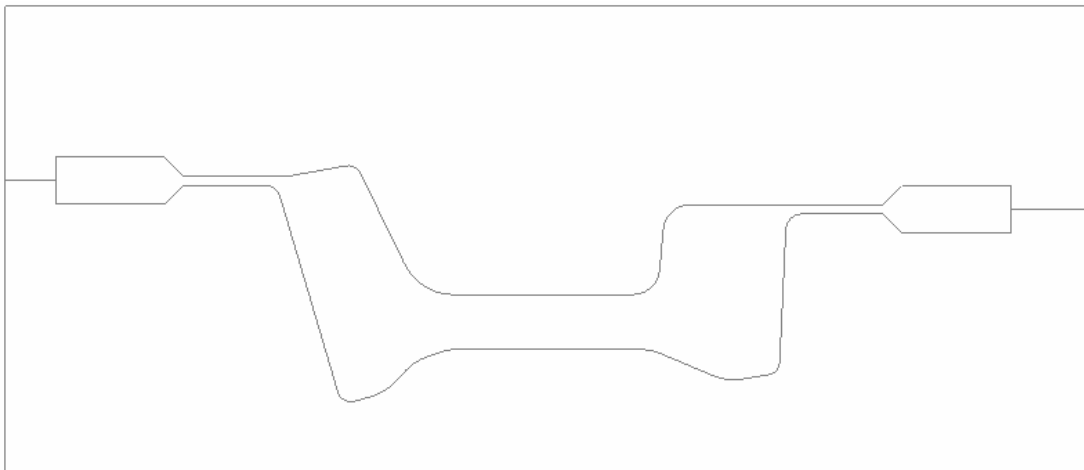
Figure 6.9: Initial die design in 2D
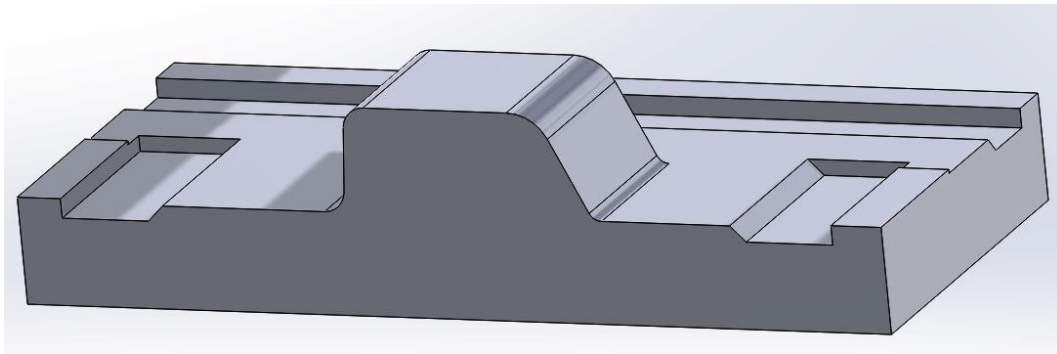
(a)
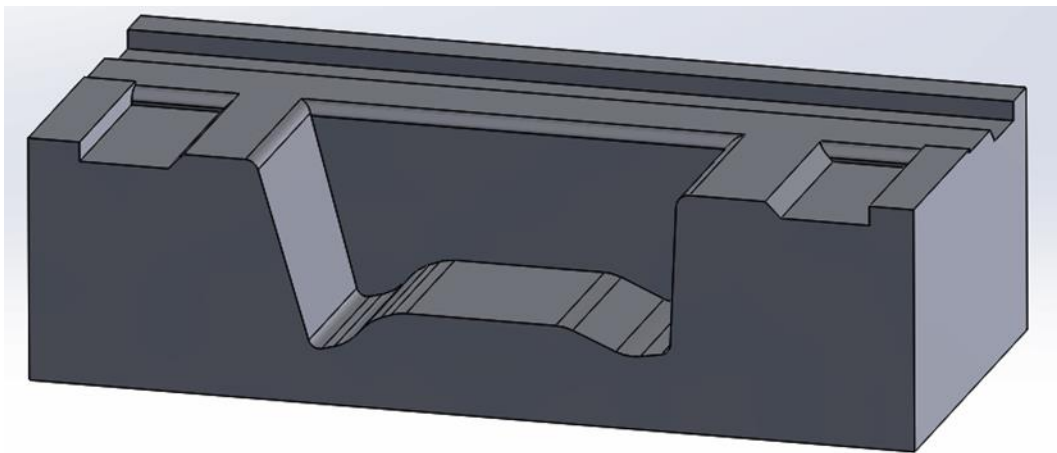
(b)

Figure 6.10: (a) 3D upper die design (b) 3D lower die design (sectioned from plane of symmetry)

The top parting line for the 2D die design solved one issue but brought another for 3D die design. In order to achieve the top parting line, the upper die must have a protruding male part to extend into the female lower die (Figure 6.10 (a) and (b), all 3D dies are sectioned from plane of symmetry for illustration purpose). This was not a problem in 2D, but in 3D, due to the draft angle on the lower die side wall (Figure 6.11 (a) and (b)), a vertical flash would form in addition to the horizontal flash (Figure 6.11 (c)). Flash in two directions would increase trimming cost and processing time dramatically, and should be avoided whenever possible.
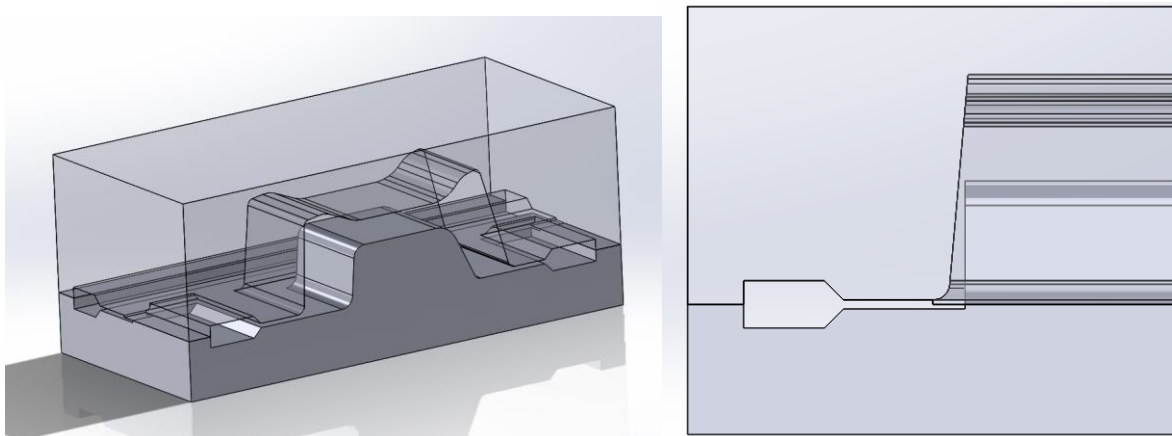
(a)

(b)
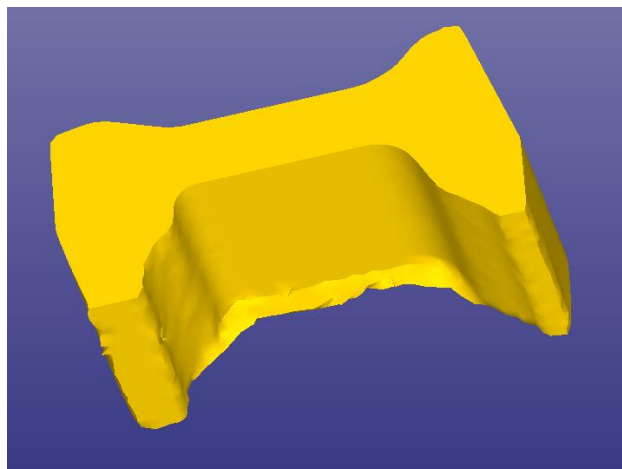
(c)

Figure 6.11: (a) Isometric view of 3D die design (b) Side view of 3D die design

(c) Forged sample with vertical flash

It was possible to remove the vertical flash, but at the cost of die complexity. Figure 6.12 (a), (b), (c), and (d) below show a viable design by implementing a much more complicated 3D parting line design. Figure 6.13 shows a finished forging specimen using these dies.

In summary, Design 2.0 added a variation in rib geometry for material flow testing, but also required a more complicated parting-line design. The gain in rib diversity did not justify the increased die complexity and manufacturing cost.
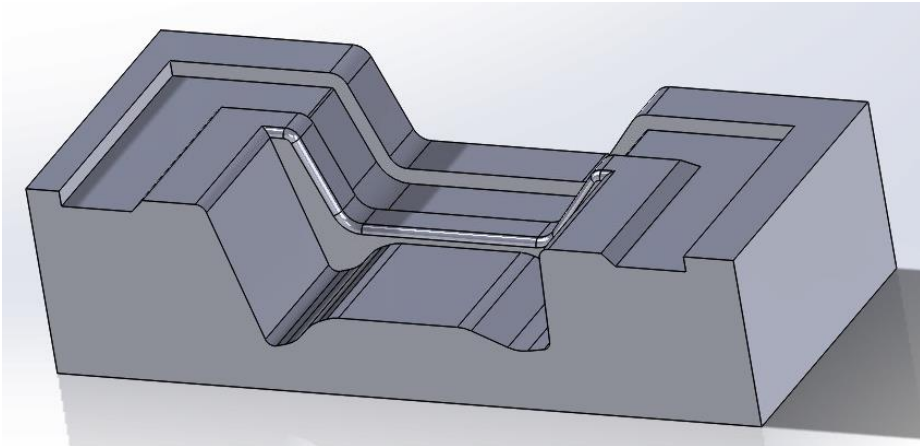
(a)
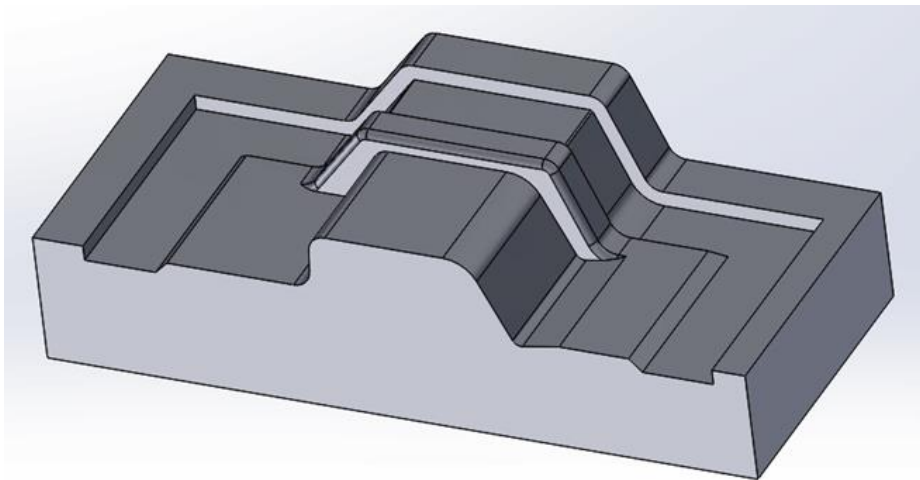
(b)
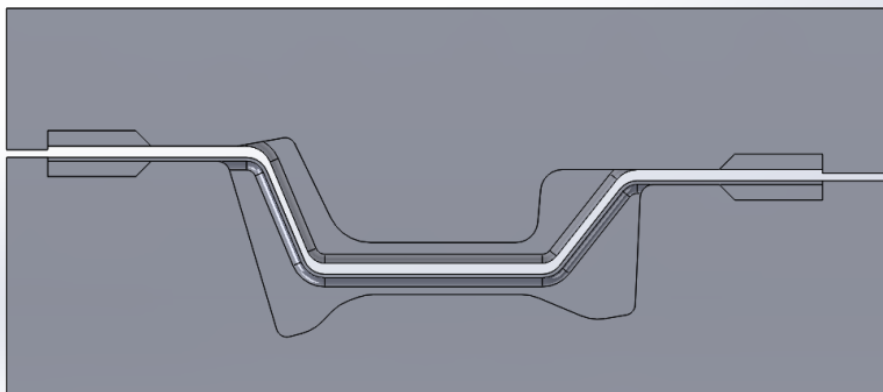
(c)
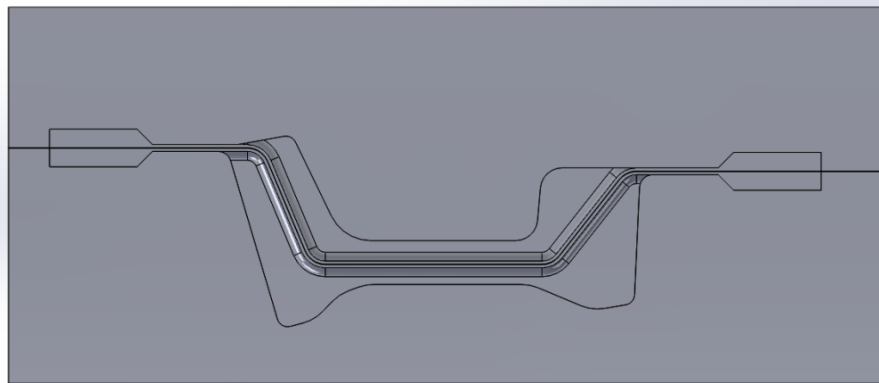
(d)

Figure 6.12: (a) Lower die design (b) Upper die design

(c) Dies mating each other to show flash geometry (d) Dies fully closed
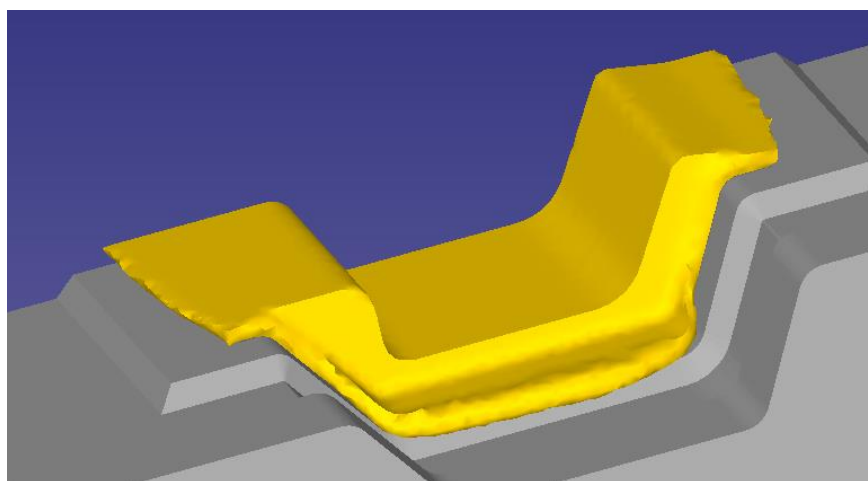
Figure 6.13: Forging sample using complex die design

6.2.3 Design 3.0

(a)   **(b)**
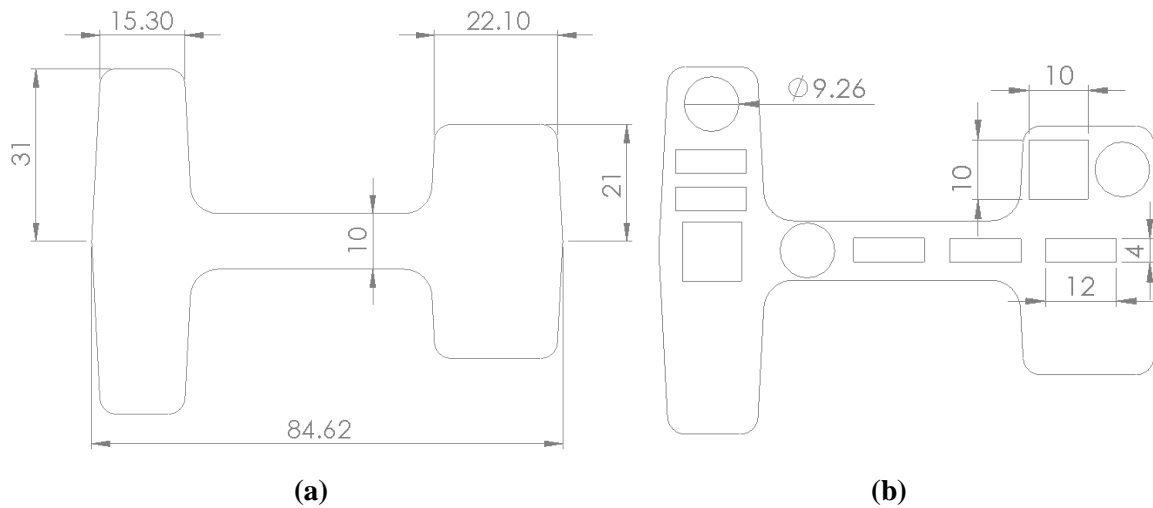
Figure 6.14: (a) Design 3.0 with dimensions (b) Potential sample locations on Design 3.0

Design 2.0 was believed to be the closest geometry to the first optimized control-arm cross-section. The angled ribs were a special feature, but required excessive effort to manufacture. The final design for the intermediate sample was based on the Design 2.0 with reasonable simplifications for easier production and tooling design (Figure 6.14(a)). The angles on both ribs were removed, which allowed the parting line to be located at the centre. The ribs were made symmetric about the centre line so that the upper and lower dies shared the same geometry. Five degrees of draft angle were added to all vertical surfaces to allow easier material extraction after forging, although 3 degrees was standard for Mg alloys [42].

By making these modifications, a more conventional I-beam geometry was achieved, while allowing all three types of test samples to be housed in numerous locations (Figure 6.14 (b)). The thin and tall ribs to the left would be much more difficult to fill completely during forging than the wide and short ribs to the right. This design enabled the researchers to examine material flow for different geometries and could provide valuable insight into control arm geometry design.

The final die design below (Figure 6.15 (a) and (b)) featured a proud flashland design instead of recessed, to allow adjustment of flash thickness and some control of die fill. Detailed die drawings can be found in the Appendix C. A complete die assembly model can be found in Figure 6.16.
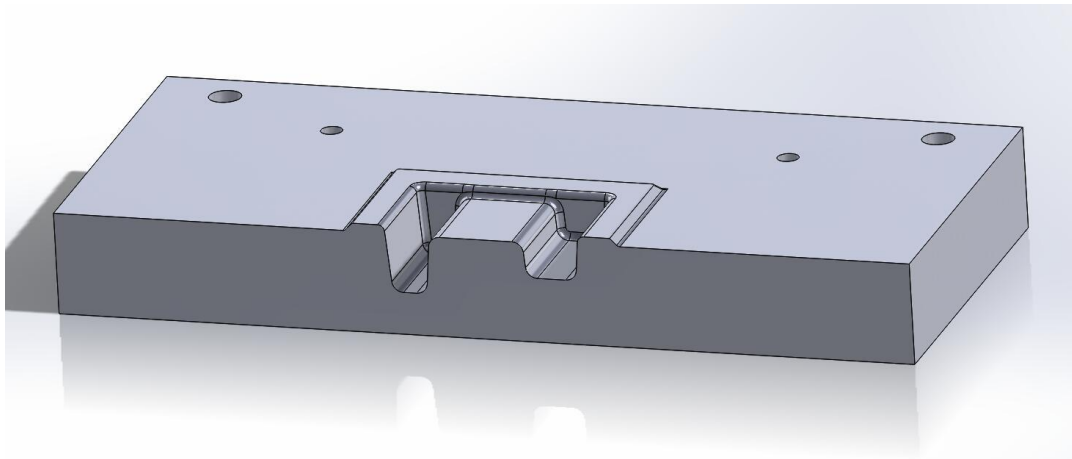
(a)
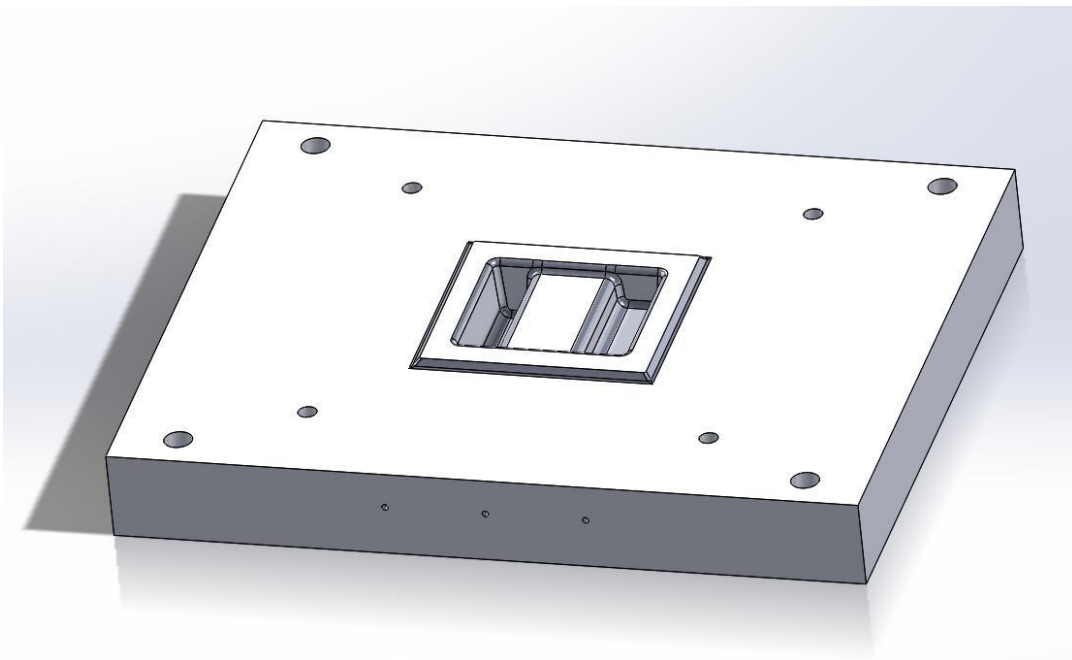
(b)

Figure 6.15: (a) Half of lower die (b) Complete model of lower die
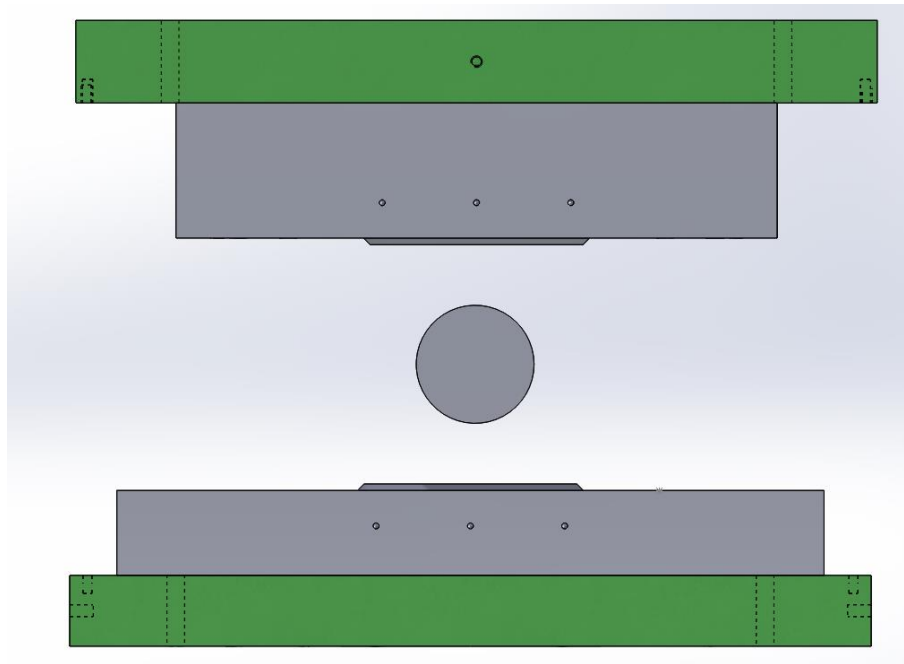
Figure 6.16: Full assembly of dies and heaters on 500-ton press

6.3 Experiments

All experiments were carried out at CanmetMATERIALS in Hamilton, by Lucian Blaga under the direction of Bruce Williams and Jonathan McKinley. The materials used in this experiment included extruded AZ31, extruded AZ80 and extruded ZK60. The forging temperature for AZ31 was 500 ℃, AZ80 was at 400 ℃, and ZK60 was at 450 ℃. The billets used in this experiment had a diameter of 63.5mm and length of 70mm. A preform geometry design was conducted with 23 design iterations to minimize damage value during forging. However, the preform had to be abandoned due to extra die cost. The final cylindrical billet dimensions were selected based on simulation die filling and to avoid machining of the raw Ø63.5mm bars in stock to save time.

The dies and billets were both lubricated with graphite at room temperature. The billets were then heated up in the oven for 3 hours to the forging temperature. The dies were heated by the heater plates under the dies and maintained at the forging temperature during the experiments to ensure isothermal forging. At the beginning of the test, the billet was transferred from the oven onto the lower die, then pushed against the guiding tool to ensure correct positioning (Figure 6.17) to the absolute center of the die opening.

Three forging rates were used: 0.067mm/s, 0.667mm/s and 6.667mm/s. The slowest 0.067mm/s test required 15 minutes to complete, the 0.667mm/s test needed 90 seconds, and the fastest finished in around 10 seconds. These rates were based on simulation average strain rates in the final forging step, to match the average strain rates in the 110-ton tests. The 0.067mm/s corresponded to an average strain rate of 0.01/s, 0.667mm/s referred to 0.1/s, and 6.667mm/s translated to 1/s.

Both dies were equipped with thermocouples. The heater plates beneath each die had thermocouples installed as well. The temperature readings of the dies were used to monitor the thermal conditions during testing. Thermocouples were also welded onto some of the test billets (Figure 6.18).
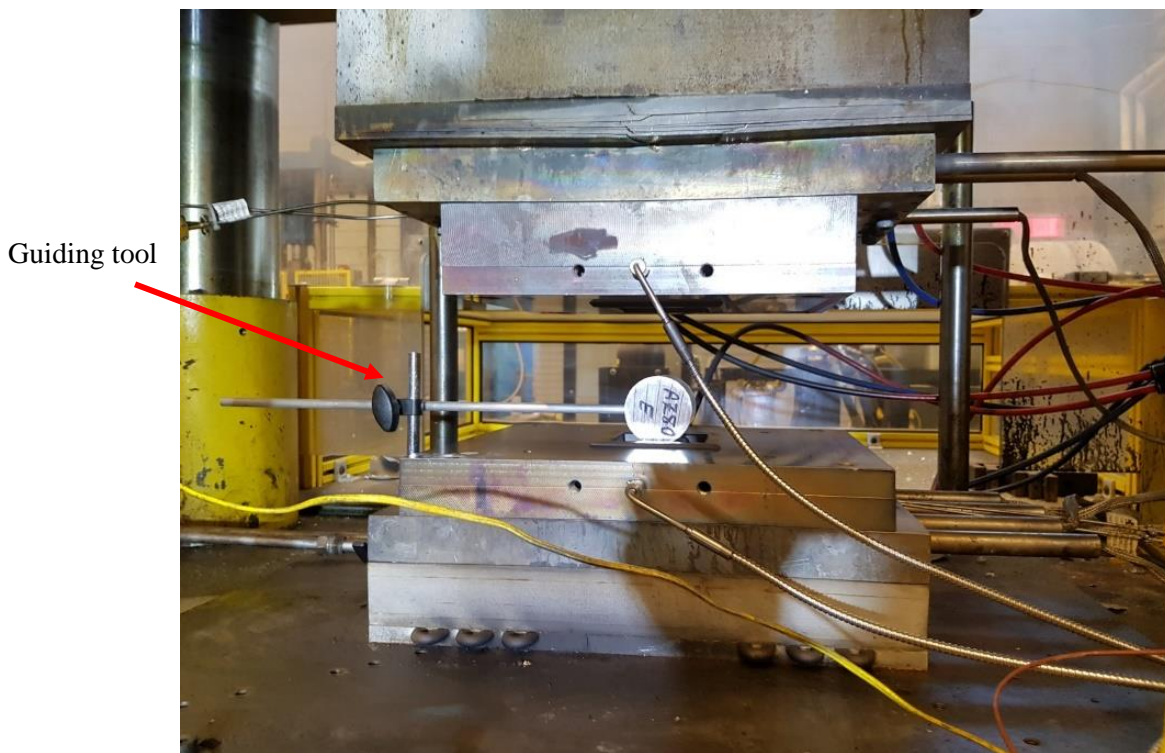
Figure 6.17: Test setup on 500-ton press at CanmatMATERIALS

Figure 6.18: Billet with thermocouple

6.4 Numerical Simulation

A 3D model was used in the simulation to capture material anisotropy and deformation. A billet with the aforementioned dimensions was created in the pre-processor. The longitudinal axis of the billet was aligned with the global Z axis. The global X and Y axes were in the transverse plane.

The lower die in this simulation was fixed in space, while the upper die was assigned a constant downward velocity – 0.067mm/s, 0.667mm/s, or 6.667mm/s. The upper die was stopped when the flash thickness reached 1.7mm.

Only half of the billet was modelled due to symmetry (Figure 6.19), and was meshed with 72,000 tetrahedron elements (Figure 6.20). The elements had a size ratio of 3 and the length varied from 0.6mm to 1.8mm. Mesh sensitivity study was carried out to balance simulation accuracy and total run time. In addition to the 72,000-element mesh, 100,000 elements and 150,000 elements were used. The 100,000 and 150,000-element meshes resulted in slight differences in the final geometry by only a fraction of a millimeter and took more than 3 times to solve. Thus, 72,000 elements were used for all subsequent I-beam forging simulations. In all simulations, the interference remeshing trigger was set

to 0.7 of element size. One hundred simulation steps were defined with a step increment of 0.53mm/step.

The billet was positioned in the absolute center on the lower die opening: an equal distance to the left and right flashlands, mid-way in the Z direction (Figure 6.19 (c)). Contact was generated between the billet and the lower die at the beginning of the simulation. Contact between the billet and upper die develops as the upper die engages the billet. The interfacial coefficient of friction was set at 0.2 for all contacting surfaces.

The anisotropic material model in this simulation was the same as for the 110-ton simulation for each extruded material. The effective flow stress was provided as tabulated data in the material definition. Hill's coefficients were defined for each forging rate. One entire simulation took 2.5 hours to finish.
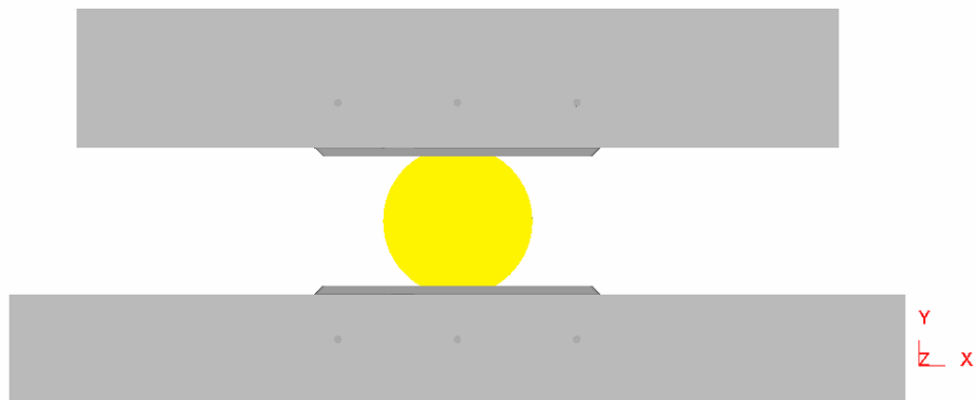
(a)
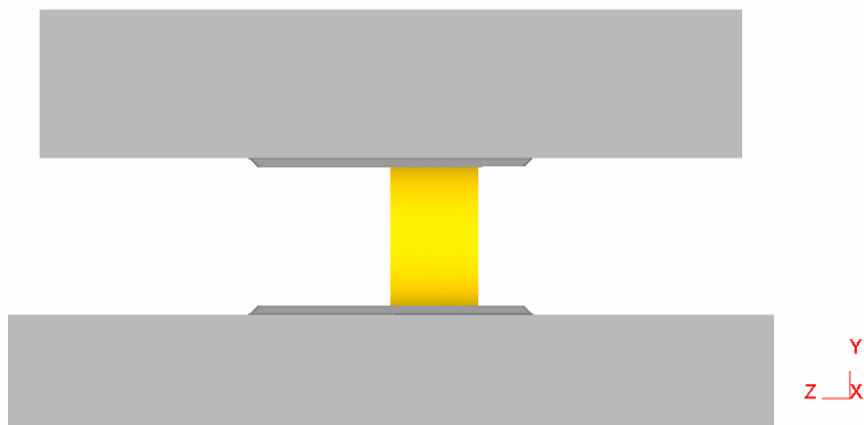
(b)
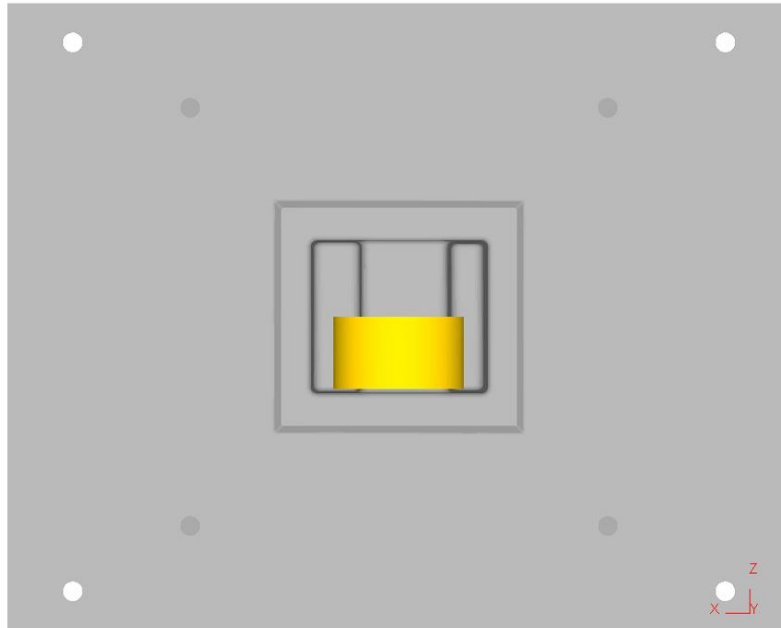
(c)

Figure 6.19: Complete simulation model (a) Front view (b) Side view (c) Top view
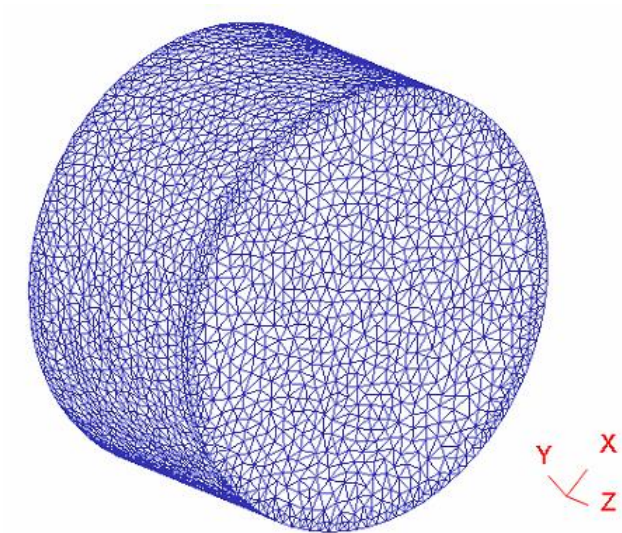
Figure 6.20: Mesh of billet

6.5 Results
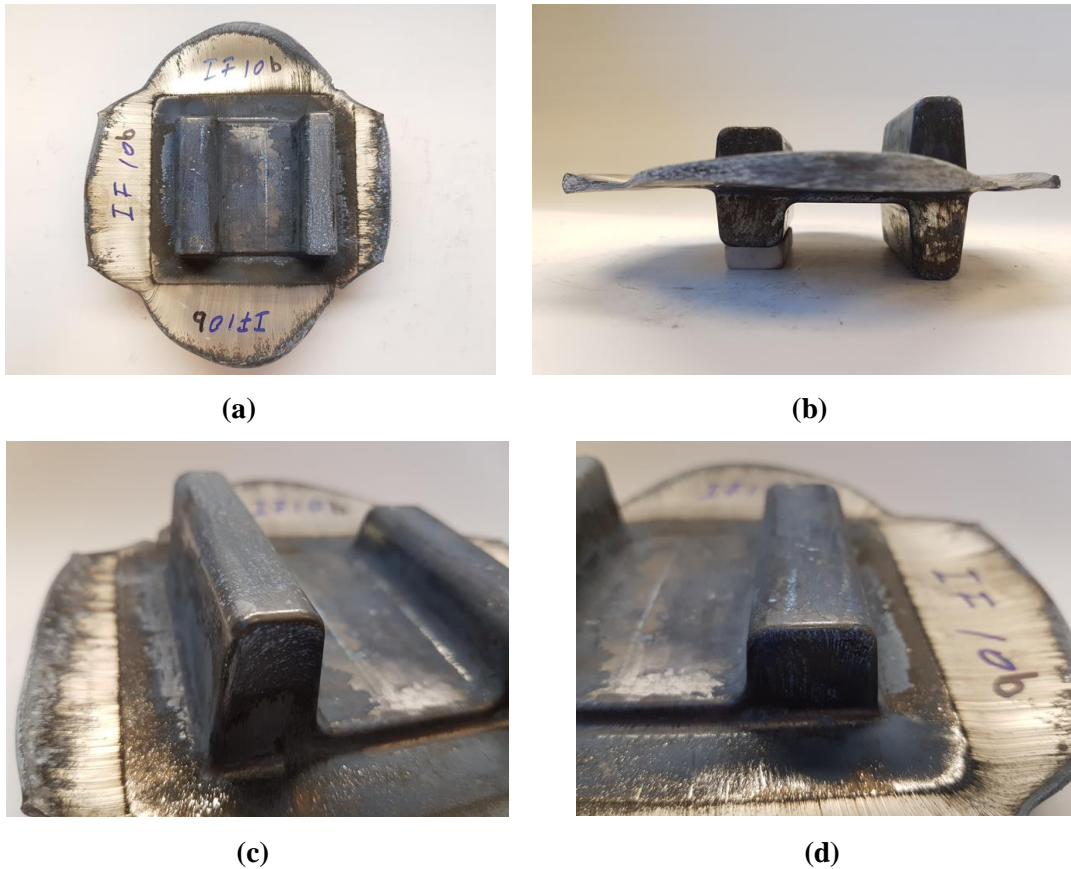
Figure 6.21: (a) Top view of Trial 10b (b) Side view of Trial 10b

(c) Close view of thin/tall rib (d) Close view of wide/short rib

The overall outcome of these 500-ton forgings met expectations. None of the test materials cracked for any forging conditions; this was not surprising as the geometry was designed to stay below the critical damage value. Some had minor underfills at the thin and tall rib corners, and some were more difficult to remove from the dies after forging.

The ZK60 forgings will be discussed here. The results for other materials can be found in Appendix D. Extruded ZK60 was forged at 450 ℃ using 3 displacement rates – 0.06mm/s, 0.6mm/s, 6mm/s. Figure 6.21 (a) and (b) are top and side views of specimen Trial 10b, which was forged at 0.06mm/s. The dark surface finish on the I-beam was due to the residual graphite lubrication. The flash region was able to retain the material's original appearance, as it was formed by material internal to the billet. The I-beam geometry is clearly seen in the side view.

Figure 6.21 (c) and (d) take a closer look at the two ribs. The wide-short rib was designed to fill with ease, and was shown to be so. On the other side, the thin-tall rib was much harder to form. Some minor underfills were spotted on a few other specimens. These extruded ZK60 forgings however, appeared to be free from defects. The 2mm corners at the tip of the rib were completely filled, as was the top rib surface.

Five degrees of draft was applied to all vertical surfaces for easier sample ejection after forging, but this did not seem to be enough for certain materials. AZ80 and ZK60 alloys were forged at relatively low temperatures comparing to AZ31's 500 °C. It took some effort to extract these materials from the dies, but it was not impossible. On the other hand, AZ31 at 500 °C was too soft to be pried out directly after forging, and hence had to be extracted after cooling to room temperature.

In these forging experiments, although the press was calibrated to stop at the same displacement, the actual forging thickness varied for all tests. This does not affect the final forging geometry significantly, however it must be considered when comparing the test results to the simulations. Trial 10b, 11b and 12b had an average flash thickness of 1.41mm, 1.42mm and 1.44mm respectively. The simulations were run to the same flash thickness for each specimen.

A geometric comparison of simulation and experimental results is shown in Figure 6.22. The simulation results (in yellow) are superimposed onto the sample photos for direct visual comparison. Figure 6.22(a) shows results for IF10b, ZK60@450 °C and 0.06mm/s. Figure 6.22(b) shows result for IF11b, ZK60@450 °C and 0.6mm/s. Figure 6.22(c) shows results for IF12b, ZK60@450 °C and 6mm/s. In all simulations and tests, the I-beam was formed completely, thus the comparison here focuses on the flash geometry. The best simulation was for the rate of 0.06mm/s in Figure 6.22(a). Both the outline and the curvatures of the edges were captured fairly well. For all specimens, the ED flash had a more pronounced convex curve while the TD flash was rather flat. The region between the ED and TD flashes at the four corners were also well-modelled. The simulation was able to predict material flow behaviour differently in the extrusion and transverse directions.

Simulation results for IF11b and IF12b were not as good as IF10b. The shape of the edges were close and the flash geometries for the ED were not far off. The corners where the flashes join were well-captured. However, the simulation under-predicted material flow in TD. One possible reason for the discrepancy is heat generation during the forging process with the faster rates. The internal

temperature could increase rapidly due to the work being done on the billet, which could lead to easier material flow.

(a)

(b)
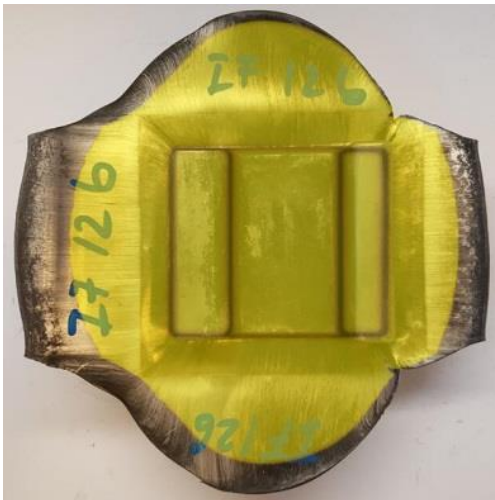
(c)
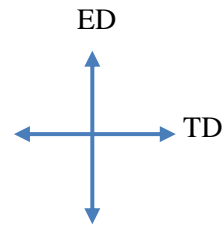
Figure 6.22: (a) Trial 10b (b) Trial 11b (c) Trial 12b

In all of the 500-ton forging trials, no surface crack was observed. For ZK60 at 450 ℃ and 0.06mm/s, the damage value distribution from simulation is given below in Figure 6.23. Figure 6.23 shows that the I-beam portion of the forging suffered damage below 0.125, and the maximum damage occurred at the tip of the flash, which had a value less than 0.44. Based on previous experience with the small-

scale (110-ton) forgings, the critical value for ZK60 for the same forging condition was likely above 0.44, which was higher than the maximum predicted damage. The fact that no surface failure was observed supports this critical value.

(a)

(b)
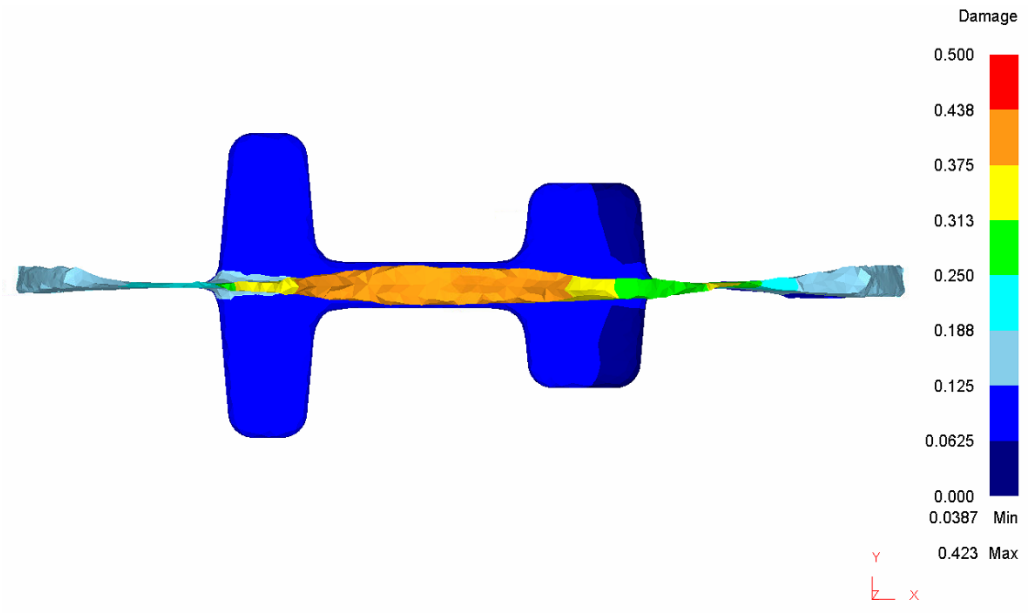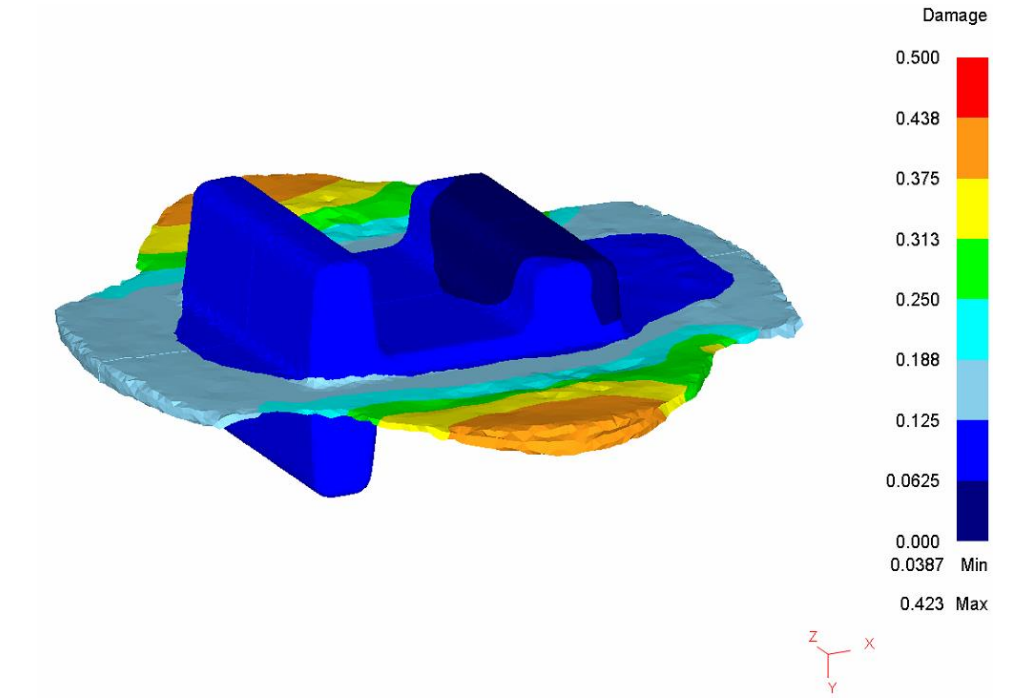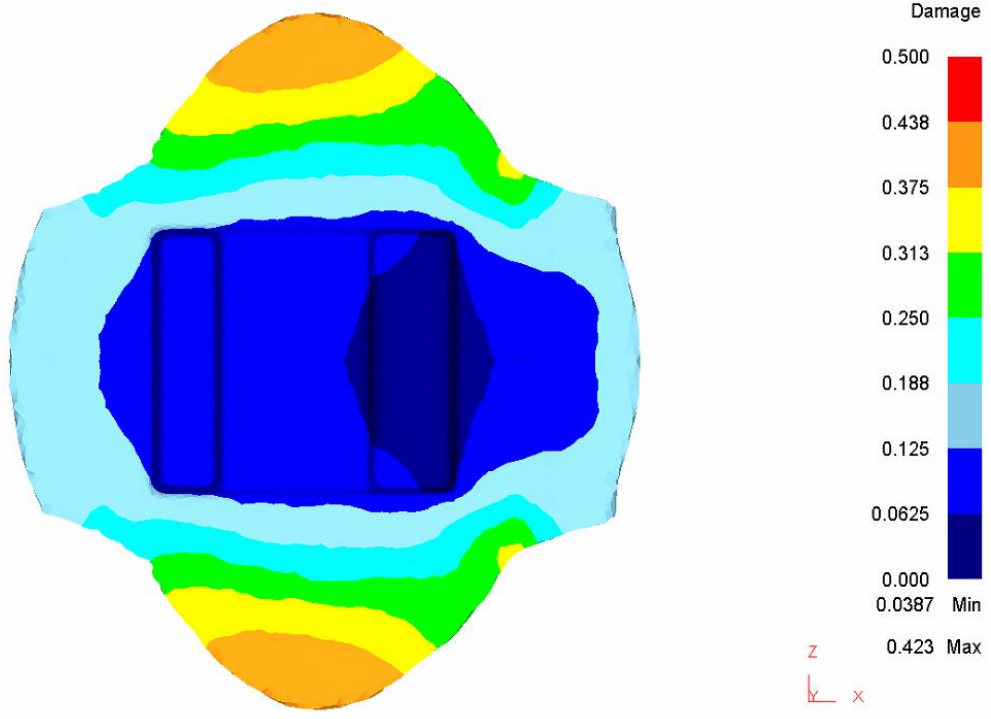
(c)

Figure 6.23: Damage prediction from simulation (a) Isometric view (b) Side view (c) Top view

Chapter 7

Conclusions and Recommendations

7.1 Conclusions

In this work, an attempt was made to design a simplified test specimen with the help of finite element simulation. In order to fine tune the forging parameters and validate the simulations, a number of simpler and lower-resolution forging tests had to be conducted.

The forging design started in 2D with axisymmetric forging simulations. A simple isotropic perfectly-plastic model and a four-point softening model were used to represent the material and to investigate frictional effects on the forging load for pancake tests. It appeared that the load in simulation increased with increasing coefficient of friction, but the actual interfacial coefficient still need to be determined.

The ring compression test was introduced to help further understand the interfacial friction for different lubrications in the forging process. Graphite lubrication resulted in a coefficient of friction of 0.2 based on the calibration curve and this value was used in all subsequent simulations. Flatbread tests were then conducted to investigate material flow in a more complicated forging condition. The simulation helped clarify the initial billet orientation. At this point, the necessity of using an anisotropic material model in 3D simulations in order to fully capture material behavior was clear.

In addition to the compressive tests, shear tests were performed to calculate Hill's anisotropic coefficients to be used in 3D simulations to model material anisotropy. The shear samples were based on the literature and tests were conducted for each forging rate and temperature.

The 110-ton press forgings were added to the plan as they were considered necessary for simulation validation, especially because that press was equipped with load-cells for accurate load measurements. A number of sample geometries were considered and a T-shaped specimen with a step feature was selected based on considerations of material flow and the need to extract test samples. Both geometry and load results from simulations and tests were compared and the simulation method proved its reliability.

The final component of this work was the simplified sample design based on the knowledge acquired from the previous small-scale forgings and the production of an optimized a-arm by Strong [56]. The forging process parameters were selected based on previous experience. A cross-section geometry was based on the latest structural optimization result from Alex Strong and altered to adapt to the forging process. Accommodation of material characterization test specimens and a symmetric parting line was considered in the design of this specimen. The final specimen design was small enough to save material and minimize complexity and at the same time representative of the actual control arm geometry. It was able to test material forgeability and help fine-tune forging process parameters at the same time.

7.2 Recommendations

7.2.1 Numerical Simulation

1. Coulomb friction was used in all simulations. This may not be the best option for high pressure scenarios like forging. Another option in the software is friction factor m. Switching to friction factor m might have an impact on load prediction. In order to determine m for the current lubrication, the calibration curves need to be generated for the ring compression test, ideally with latest material data for each candidate material. With the measurements from the rings, the factor m can be easily determined.

2. Heat transfer was not included in the simulations in this work; the isothermal assumption was used for simplicity. In the actual tests, due to heat generation in the forming process and heat loss to the surrounding environment, an isothermal condition may not be accurate. Billet temperature may vary during the test, and could be modelled and compared with experimental data.

3. Even if heat transfer is considered in the simulation process, there is another limitation of the material model. The Hill's anisotropic model is not temperature sensitive, i.e., the coefficients do not change with temperature. Other models or user routines could be used to take into account these thermal effects.

4. The shear and compressive tests for anisotropic coefficients were conducted without repeats, which can lead to unreliable data and could be the cause of the discrepancy in some of the simulations. Now that these tests had been proven to work, more repeats should be conducted

for future tests.

5. In all the present simulations, the die velocities were set to be constant from the beginning to the end of the test. It is not so in the actual experiments. In fact, the press had to start from zero velocity and accelerate following a polynomial curve, and then slow down at the end of the process. DEFORM software has the capability to define the die velocity as a function of time. This is likely to have some effect on the forging load prediction.

6. The critical damage values for all materials were obtained from the literature. It would be prudent to generate these data for the present materials within the group using the proposed method in [34] or [35].

7.2.2 Forging Design

1. Some specimens were extremely difficult to extract from the dies immediately after forging. Ejection pins must be used for the final control arm die design. Five degrees of draft angle on vertical surfaces would be enough for dies with these push-up pins. Five millimeter corner radius has proven to be formable for the candidate materials.

2. The simplified forging sample was forged in one stage, i.e., no preform step was used. In industry, it is not rare to see parts produced in 3 or more steps with 1 or 2 preforming steps. Proper preforming can make material flow into narrow and tall cavities much easier and dramatically reduce the one-time forging load. The final component will definitely need preforming steps. The preforms can be designed with the help of FE simulation (DEFORM). The damage values can be used as an indication of failure in the preforming stage. The goal of the preform design is to minimize damage and promote material flow into the critical regions.

3. In order to achieve the boomerang shape of the control arm, the initial billet should go through a bending step, then the preform stages in the blocker dies, followed by the final forming step and trimming process.

4. Precision forging is another possible solution to avoid preform steps at a cost of special forging equipment.

Bibliography

[1]   Optimum Design of Fatigue-Critical Automotive Components Made of Magnesium Alloys",
        Automotive Partnerships Canada, 2014

[2]   J. Liu, Z. Cui, and C. Li, "Modelling of flow stress characterizing dynamic recrystallization
        for magnesium alloy AZ31B," Computational Materials Science, vol. 41, pp.375-382, 2008.

[3]   *DEFORM v11.1 system documentation*, Scientific Forming Technologies Corporation,
        Columbus, Ohio, 2016, pp. 173.

[4]   *DEFORM v11.1 system documentation*, Scientific Forming Technologies Corporation,
        Columbus, Ohio, 2016, pp. 175.

[5]   D. Kobold, G. Gantar, and T. Pepelnjak, "Finite element analysis of magnesium AZ80
        wrought alloy anisotropic behavior during warm forging," *Mechanika*, vol. 18(3), pp. 251-
        258, 2012.

[6]   R. Hill, "A theory of the yielding and plastic flow of anisotropic metals," Proceedings of The
        Royal Society of London. London: The Royal Society, 1948, pp.281-297.

[7]   D.W.A. Rees, *Basic Engineering Plasticity*, Elsevier, pp. 339-367, 2006.

[8]   Y. Bai and B. Dodd, Ed., *Adiabatic shear localization: occurrence, theories, and
        applications.* Waltham, MA: Elsevier Ltd, 2012.

[9]   L.W. Meyer and E. Staskewitsch, "Adiabatic shear failure under biaxial dynamic
        compression/shear loading," *Mechanics of Materials*, vol. 17(2), pp.203-214, 1994.

[10]   E. El-Magd and M. Abouridouane, "High speed forming of the light-weight wrought alloys,"
        in 1st International Conference on High Speed Forming, Dortmund, Germany, 2004.

[11]   J. Peirs, P. Verleysen, J. Degrieck, and F. Coghe, "The use of hat-shaped specimens to study
        the high strain rate shear behavior of Ti-6Al-4V," *International Journal of Impact
        Engineering*, vol. 37, pp.703-714, 2010.

[12]   E. El-Magd and M. Abouridouane, "Characterization, modelling and simulation of
        deformation and fracture behavior of the light-weight wrought alloys under high strain rate
        loading," *International Journal of Impact Engineering*, vol. 32, pp.741-758, 2006.

[13]   T. Pepelnjak, V. Magoc, and B. Barisic, "Analysis of shear hat test in digital environment,"
        Metalurgija – Sisak then Zagreb, vol. 51(2), pp. 153-156, 2012.

[14]   J. Peirs, P. Verleysen, and J. Degrieck, "The use of hat-shaped specimens for dynamic shear
        testing," *Foundations of Civil and Environmental Engineering*, No. 11, 2008.

[15] J. Yoon and S. Lee, "Warm forging of magnesium AZ80 alloy for the control arm in an automobile," *Journal of Automobile Engineering*, vol. 229(13), pp.1732-1738, 2015.

[16] A. Gontarz, Z. Pater, and K. Drozdowski, "Hammer forging process of lever drop forging from AZ31 magnesium alloy," *Metalurgija*, vol. 52, pp.359-362, 2013.

[17] W.J. Kim, H.W. Lee, J.P. Park, M.G. Kim, and U.S. Yoon, "Forging of Mg-3Al-1Zn-1Ca alloy prepared by high-frequency electromagnetic casting," Materials and Design, vol. 30, pp.4120-4125, 2009.

[18] F. Ju and Z. Xia, "Modeling and simulation of Mg AZ80 alloy forging behavior," Magnesium Technologies, 2008.

[19] B. Viehweger, A. Karabet, M. During, and L. Schaeffer, "Forging of Mg-alloys AZ31 and AZ80," Werkstofftech, vol.36, No.5, 2005.

[20] D. Shan, W. Xu, X. Han, and X. Huang, "Study on isothermal precision forging process of rare earth intensifying magnesium alloy," Materials Science and Engineering B, vol. 177, pp.1698-1702, 2012.

[21] Y. Zhang, S. Jiang, Y. Zhao, and D. Shan, "Isothermal precision forging of aluminum alloy ring seats with different preforms using FEM and experimental investigation," *International Journal of Advanced Manufacturing Technology*, vol. 72, pp.1693-1703, 2014.

[22] K.P. Rap, Y.V.R.K. Prasad, and K. Suresh, "Materials modeling and simulation of isothermal forging of rolled AZ31B magnesium alloy: anisotropy of flow," *Materials and Design*, vol. 32, pp.2545-2553, 2011.

[23] A. Gontarz and A. Dziubinska, "Forming of flat parts with ribs from magnesium alloy," *Aircraft Engineering and Aerospace Technology: An International Journal*, vol. 86/4, pp.356-360, 2014.

[24] P. Skubisz, J. Sinczak, and S. Bednarek, "Forgeability of Mg-Al-Zn magnesium alloys in hot and warm closed die foring," Journal of Materials Processing Technology, vol. 177, pp.210-213, 2006.

[25] C. Yang and G. Ngaile, "Preform design for forging and extrusion processes based on geometrical resemblance," Proceedings of The Institution of Mechanical Engineers, vol. 224, Part B: Journal of Engineering Manufacture, 2010.

[26] T. Takemasu, V. Vazquez, B. Painter, and T. Altan, "Investigation of metal flow and preform optimization in flashless forging of a connecting rod," *Journal of Materials Processing Technology*, vol. 59, pp.95-105, 1996.

[27] Y. Shao, B. Lu, H. Ou, F. Ren and J. Chen, "Evolutionary forging preform design optimization using strain-based criterion," *International Journal of Advanced Manufacturing Technology*, vol. 71, pp.69-80, 2014.

[28] H.S. Valberg, *Applied Metal Forming Including FEM Analysis*. New York: Cambridge University Press, p.134, 2010.

[29] T. Pepelnjak, R. Werkhovern, D. Kobold, and K. Kuzman, "Analysis of Warm Magnesium Forging in Digital Environment," *Journal for Technology of Plasticity*, vol. 35, 2010.

[30] P. Christiansen, J. H. Hattel, and N. Bay, " Modelling of damage during hot forging of ingots," in Fifth International Conference on Steelsim, Ostrave, Czech Republic, 2013.

[31] A.V. Rao, N. Ramakrishnan, and R.K. Kumar, "A comparative evaluation of the theoretical failure criteria for workability in cold forging," Journal of Materials Processing Technology, vol. 142, pp.29-42, 2003.

[32] H. Kakimoto and T. Arikawa, "Prediction of surface crack in hot forging by numerical simulation." in *Eleventh International Conference on Technology of Plasticity*, Nagoya, Japan, 2014, pp. 19-24.

[33] A. Gontarz, Z. Pater, K. Drozdowski, A. Tofil, and J. Tomczak, "FEM analysis of the forging process of hub part from AZ80 magnesium alloy," in *Tenth World Congress on Computational Mechanics*, Sao Paulo, Brazil, 2012.

[34] S.W. Kim, and Y.S. Lee, "Comparative study on failure prediction in warm forming processes of Mg alloys sheet by the FEM and ductile fracture criteria," *ASM International 2013 Metallurgical and Materials Transactions B*, vol. 45B, p.415, 2014.

[35] Y. Xue, Z.M. Zhang, and Y.J. Wu, "Study on critical damage factor and the constitutive model including dynamic recrystallization softening of AZ80 magnesium alloy," *Science of Sintering*, vol. 45, pp.199-208, 2013.

[36] H.S. Valberg, *Applied Metal Forming Including FEM Analysis*. New York: Cambridge University Press, p.275, 2010.

[37] B.L. Jenkins, S.I. Oh, and T. Altan, "Investigation of defect formation in a 3-station closed die forging operation," *Annals of CIRP*, vol. 38, 1989.

[38] European Aluminium Association, "Design of Forgings," pp. 14, 1994.

[39] A.M. Sabroff, F.W. Boulger, and H.J. Henning, *Forging Materials and Practices*. New York: Reinhold Book Corporation, p.67, 1968.

[40] H.S. Valberg, *Applied Metal Forming Including FEM Analysis*. New York: Cambridge University Press, p.281, 2010.

[41] G.E. Dieter, H.A. Kuhn, and S.L. Semiatin, EDs., *Handbook of Workability and Process Design*. Ohio: ASM International, p.212, 2003.

[42] G.E. Dieter, H.A. Kuhn, and S.L. Semiatin, EDs., *Handbook of Workability and Process Design*. Ohio: ASM International, p.162, 2003.

[43] J. Luan, C. Sun, X. Li, and Q. Zhang, "Constitutive model for AZ31 magnesium alloy based on isothermal compression test," Materials Science and Technology, vol. 30, no. 2, 2014.

[44] Friction and Friction Coefficients. *The Engineering Tool Box* [Online]. Available: http://www.engineeringtoolbox.com/friction-coefficients-d_778.html [July 18, 2016]

[45] *DEFORM v11.1 system documentation*, Scientific Forming Technologies Corporation, Columbus, Ohio, 2016, pp. 378.

[46] G.E. Dieter, H.A. Kuhn, and S.L. Semiatin, EDs., *Handbook of Workability and Process Design*. Ohio: ASM International, p.64, 2003.

[47] C.H. Lee and T. Altan, "Influence of flow stress and friction upon metal flow in upset forging of rings and cylinders," in Journal of Engineering for Industry, 1972, pp. 780.

[48] H.S. Valberg, *Applied Metal Forming Including FEM Analysis*. New York: Cambridge University Press, p.52, 2010.

[49] Y. Xue, Z.M. Zhang, and Y.J. Wu, "Study on critical damage factor and the constitutive model including dynamic recrystallization softening of AZ80 magnesium alloy," *Science of Sintering* vol. 45, pp**.**199-208, 2013.

[50] P. Skubisz, J. Sinczak, and S. Bednarek, "Forgeability of Mg–Al–Zn magnesium alloys in hot and warm closed die forging," *Journal of Materials Processing Technology*, vol. 177, pp. 210-213, 2006.

[51] H. Jeon, J. Yoon, and J. Lee, "Forging test of Mg-Sn-Al-Zn series alloy under warm forming conditions," *International Journal of Precision Engineering and Manufacturing*, vol. 15, No. 10, pp. 2127-2132, 2014.

[52] H.S. Valberg, *Applied Metal Forming Including FEM Analysis*. New York: Cambridge University Press, p.271, 2010.

[53] APC Project's Sharepoint\UWaterloo\Task 2 – Design, website

[54] H.S. Valberg, *Applied Metal Forming Including FEM Analysis*. New York: Cambridge University Press, p.281, 2010.

[55]   T. Altan, F.W. Boulger, J.R. Becker, N. Akgerman, and H.J. Henning, *Forging Equipment, Materials, and Practices*. Virginia: National Technical Information Service, p119, 1973.

[56]   Alex Strong, "Optimization of forged magnesium structural automotive components," MASc thesis, Department of Mechanical Engineering, University of Waterloo, Waterloo, ON, 2016.

Appendix A

Material Models

The flow stress in material definition is rate and temperature sensitive. However the Hill's anisotropic coefficients are not. They have to be defined for each forging rate accordingly. One figure of flow stress for each extruded material is presented here. Anisotropic coefficients for all rates are presented.

1. Extruded AZ31 flow stress @ 500ºC, 0.001, 0.01, 0.1, and 1/s:
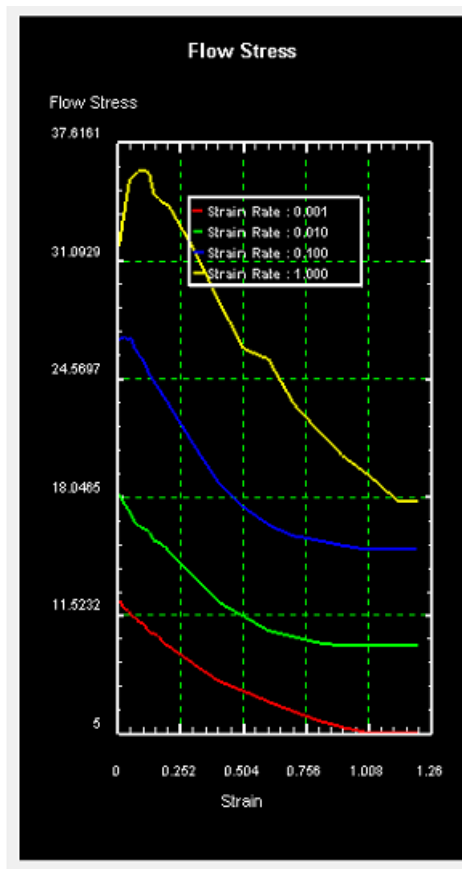
500C	Strain rate			
Strain	0.001	0.01	0.1	1
0	12.326	18.21	26.678	31.875
0.02	11.856	17.678	26.878	33.722
0.03	11.8	17.463	26.731	
0.04	11.665	17.243	26.744	35.427
0.05	11.445	17.005	26.784	35.638
0.06	11.427	16.691	26.293	
0.07	11.246	16.533	26.116	
0.08	11.116	16.48	25.844	36.05
0.09	11.062	16.284	25.718	
0.1	10.977	16.305	25.457	36.063
0.12	10.552	16.081	24.822	35.916
0.14	10.499	15.613	24.42	34.788
0.16	10.298	15.484	24.017	34.5
0.18	9.897	15.338	23.535	34.234
0.2	9.784	15.027	23.121	34.109
0.3	8.797	13.598	20.895	31.709
0.4	7.848	12.215	18.804	28.834
0.5	7.309	11.429	17.47	26.23
0.6	6.705	10.648	16.486	25.621
0.7	6.189	10.3	15.876	23.188
0.8	5.663	9.965	15.614	21.668
0.9	5.3	9.8	15.334	20.263
1	5	9.8	15.121	19.26
1.2	5	9.8	15.121	17.804

Extruded AZ31 anisotropic coefficients @ 500ºC, 0.01, 0.1, and 1/s:

	F	G	H	L	M	N
0.01/s	0.414	0.414	0.701	0.449	0.449	0.517
0.1/s	0.39	0.431	0.655	1.092	1.092	1.938
1/s	0.431	0.431	0.655	1.029	1.029	1.741

2. Extruded AZ80 flow stress @ 400ºC, 0.001, 0.01, 0.1, and 1/s
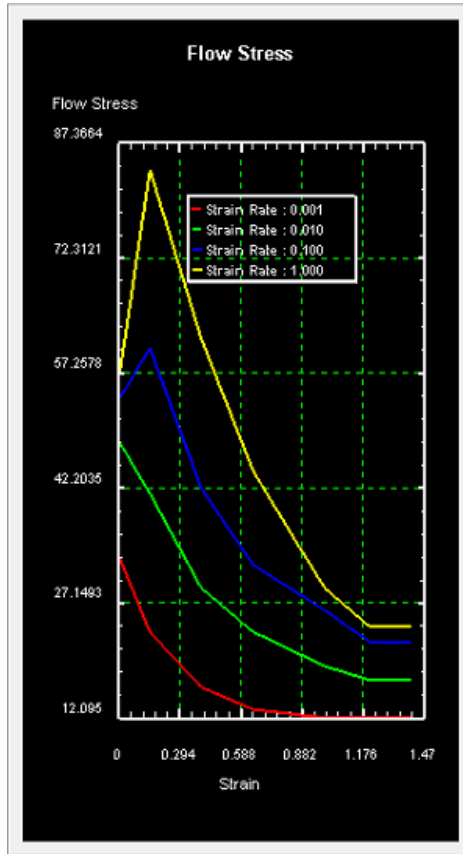
500C	Strain rate			
Strain	0.001	0.01	0.1	1
0	32.88	47.98	53.93	57.26
0.02775			61.08	
0.03144		49.46		
0.07148		47.84		
0.07975				79.39
0.0837			65.58	
0.13666				84.52
0.14459	23.23			
0.20669		35.91		
0.33186			44.51	
0.35602				64.17
0.39091	16.03			
0.4919		25.24		
0.62452				45.05
0.63518			32.15	
0.64033	13.14			
0.87009	12.38			
0.98112				29.1
0.98585	12.09			
0.99734		18.61		
0.99864			25.88	
1.2	12.09	17	22	24
1.4	12.09	17	22	24

Extruded AZ80 anisotropic coefficients @ 400ºC, 0.01, 0.1, and 1/s

	F	G	H	L	M	N
0.01/s	0.42	0.42	0.684	4.506	4.506	1.789
0.1/s	0.439	0.439	0.637	2.153	2.153	1.715
1/s	0.41	0.41	0.716	2.5	2.5	1.836

3. Extruded ZK60 flow stress @ 450ºC, 0.001, 0.01, 0.1, and 1/s
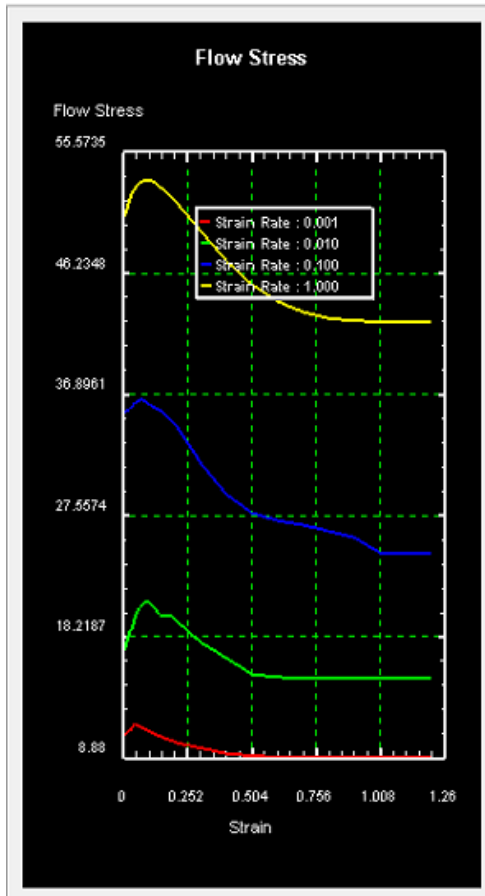
450C	Strain rate			
Strain	0.001	0.01	0.1	1
0	10.6	17.05	35.46	50.5
0.02	10.9	18.6	35.73	51.93
0.03	11.25	18.87	36	52.4
0.04	11.4	19.65	36.17	52.7
0.05	11.32	20.16	36.3	53
0.06	11.2	20.44	36.4	53.16
0.07	11.1	20.62	36.4	53.25
0.08	11	20.8	36.33	53.33
0.09	10.9	20.86	36.2	53.35
0.1	10.85	20.72	36	53.35
0.12	10.65	20.26	35.8	53.15
0.14	10.48	19.8	35.6	52.8
0.16	10.3	19.8	35.3	52.5
0.18	10.2	19.78	34.9	52.1
0.2	10	19.44	34.5	51.7
0.3	9.57	17.7	31.5	49.4
0.4	9.14	16.5	29.1	47.1
0.5	9	15.27	27.7	45.3
0.6	8.88	15.05	27.1	44
0.7	8.88	14.99	26.77	43.2
0.8	8.88	14.99	26.3	42.7
0.9	8.88	14.99	25.8	42.5
1	8.88	14.99	24.65	42.48
1.2	8.88	14.99	24.65	42.48

Extruded ZK60 anisotropic coefficients @ 450ºC, 0.01, 0.1, and 1/s

	F	G	H	L	M	N
0.01/s	0.442	0.442	0.628	7.721	7.721	1.698
0.1/s	0.423	0.423	0.677	4.1	4.1	1.777
1/s	0.42	0.42	0.686	2.722	2.722	1.792

Appendix B
Small-Scale Forging Results

1. Test matrix

Trial	Material	Billet Temperature °C	Tooling Temperature °C	Displacment Rate mm/s	Lubricant
SF1	AZ31extruded	500	500	0.004	graphite
SF2	AZ31extruded	500	500	0.04	graphite
SF3	AZ31extruded	500	500	4	graphite
SF4	AZ31extruded	500	500	40	graphite
SF5	AZ80extruded	400	400	0.004	graphite
SF6	AZ80extruded	400	400	0.04	graphite
SF7	AZ80extruded	400	400	---	graphite
SF7b	AZ80extruded	400	400	4	graphite
SF8	AZ80extruded	400	400	40	graphite
SF9	ZK60extruded	450	450	0.004	graphite
SF10	ZK60extruded	450	450	0.04	graphite
SF11	ZK60extruded	450	450	4	graphite
SF12	ZK60extruded	450	450	40	graphite
SF13	AZ31extruded	500	500	0.4	graphite
SF14	AZ80extruded	400	400	0.4	graphite
SF15	ZK60extruded	450	450	0.4	graphite

2. AZ31

- Experiment
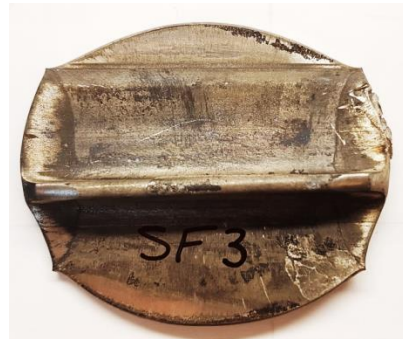
SF2 – 0.04mm/s   SF3 – 0.4mm/s

SF4 – 4mm/s   SF13 – 40mm/s

- Simulation
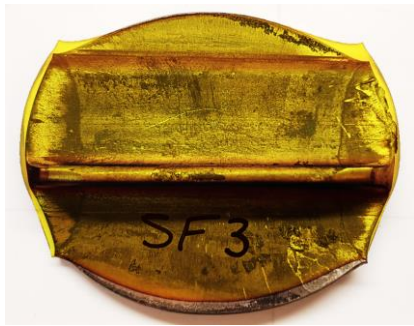
SF3 – 0.4mm/s   SF4 – 4mm/s

- Dimensional comparison

SF3		0.4mm/s	Step 193		
AZ80	1	2	3	4	5
Aniso	54.15	67.67	56.01	51.31	38.55
Exp	55.61	65.21	57.25	54.27	36.42
% dif	-2.63	3.77	-2.17	-5.45	5.85

SF4		4mm/s	Step 190		
AZ80	1	2	3	4	5
Aniso	54.71	67.35	56.86	48.96	36.43
Exp	54.55	62.86	53.25	53.64	38.15
% dif	0.29	7.14	6.78	-8.72	-4.51

98

- Load comparison
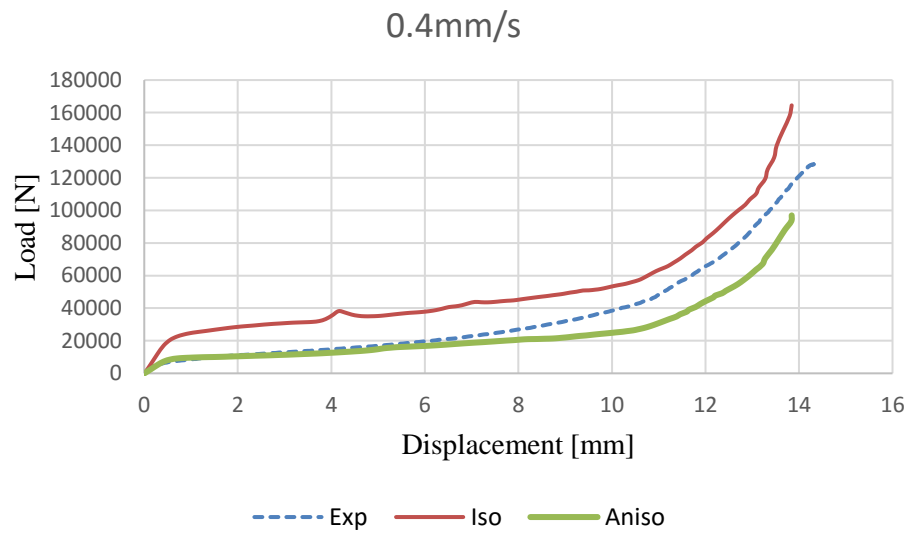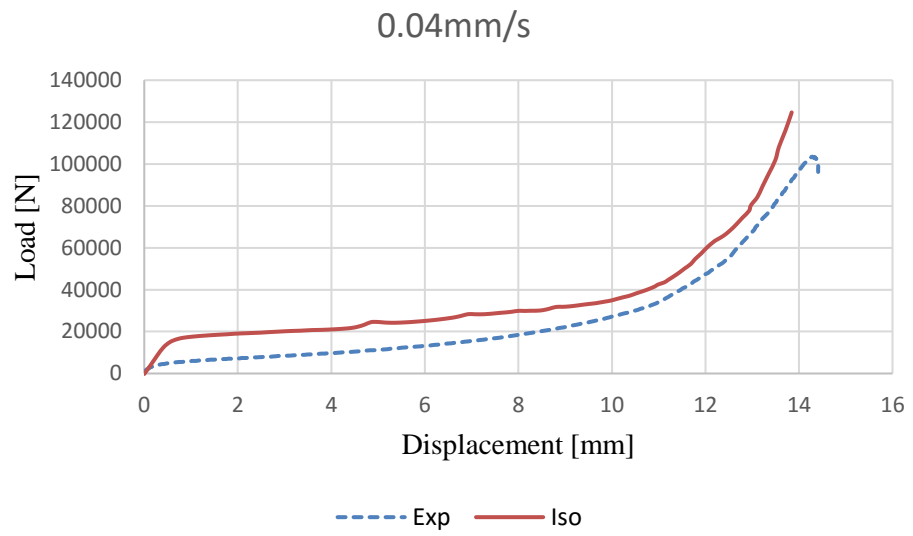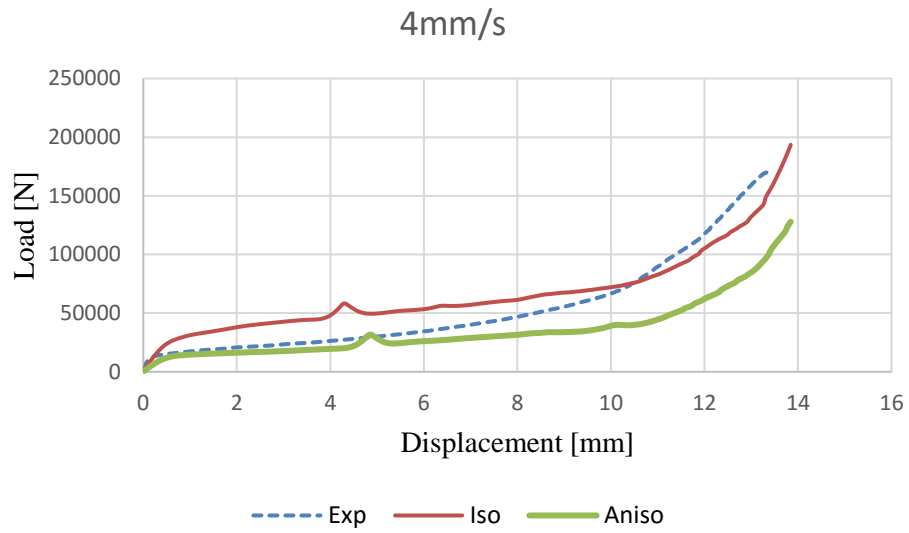
0.04mm/s

0.4mm/s

4mm/s

3. AZ80

- Experiment

SF6 – 0.04mm/s

SF14 – 0.4mm/s



SF7b – 4mm/s

SF8 – 40mm/s

- Simulation
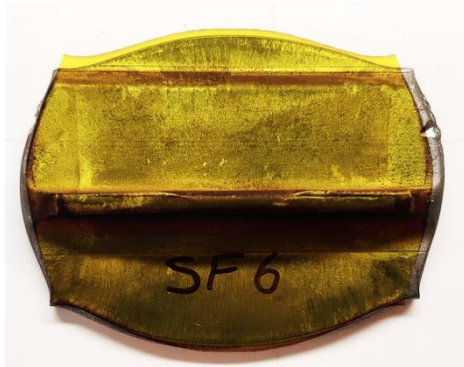
SF6 – 0.04mm/s

SF14 – 0.4mm/s

SF7b – 4mm/s

- Dimensional comparison

SF6		0.04mm/s	Step 195		
AZ80	1	2	3	4	5
Aniso	51.79	63.47	54.65	50.35	39
Exp	56.23	64.41	55.59	48.88	35.54
% dif	-7.91	-1.46	-1.69	3.01	9.74

SF14		0.4mm/s	Step 193		
AZ80	1	2	3	4	5
Aniso	51.81	62.81	54.83	49.14	38.19
Exp	53.13	62.63	55.17	49.98	36.44
% dif	-2.48	0.29	-0.62	-1.68	4.80

SF7b		4mm/s	Step 190		
AZ80	1	2	3	4	5
Aniso	50.98	61.68	53.87	48.18	37.58
Exp	52.02	60.67	51.96	48.26	37.12
% dif	-2.00	1.66	3.67	-0.18	1.25

- Load comparison
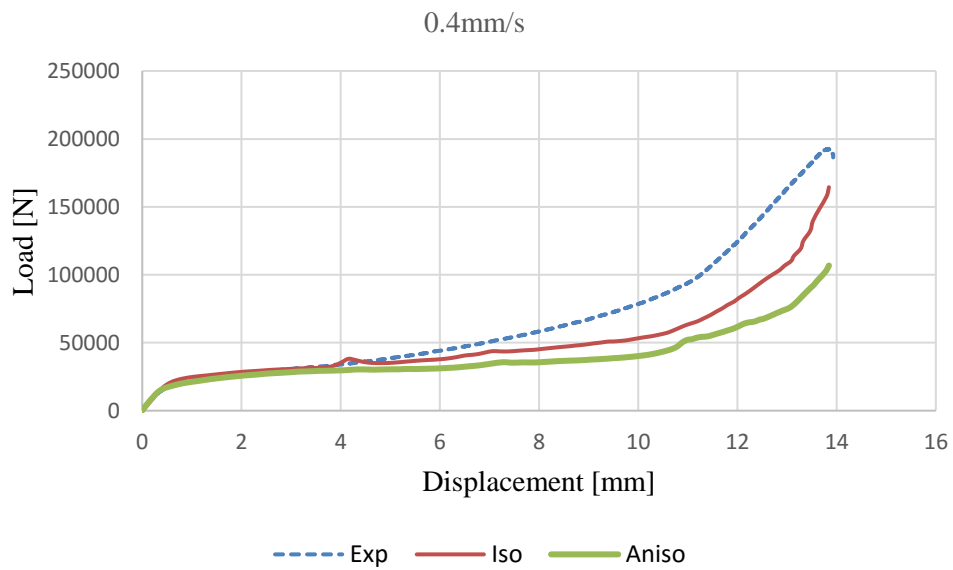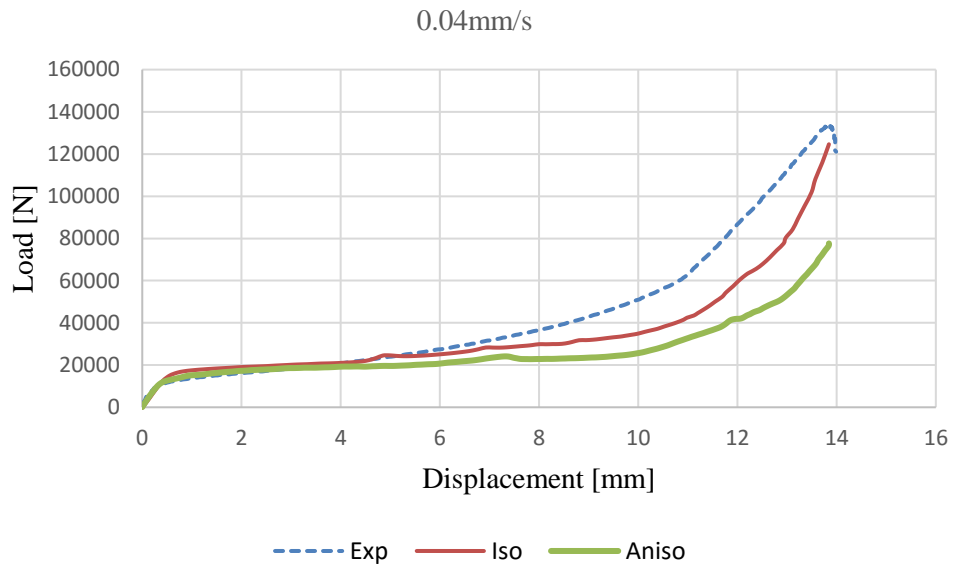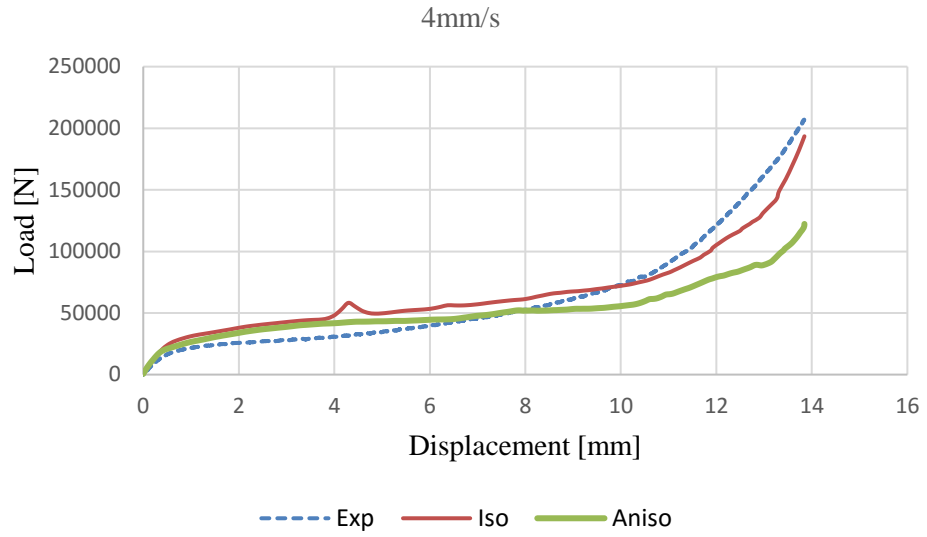
0.04mm/s

0.4mm/s

4mm/s

4. ZK60

- Experiment

SF10 – 0.04mm/s

SF11 – 0.4mm/s
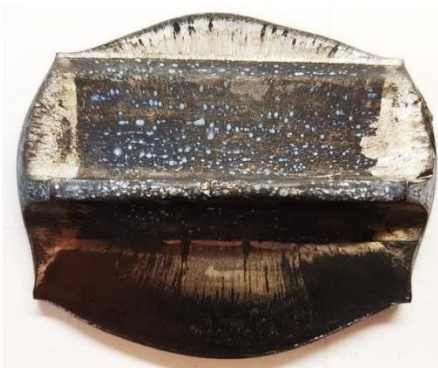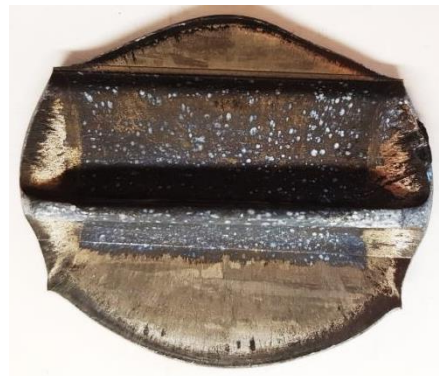
SF12 – 4mm/s

SF15 – 40mm/s

- Simulation
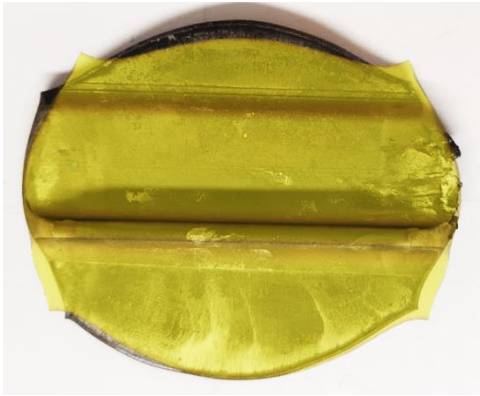
SF10 – 0.04mm/s
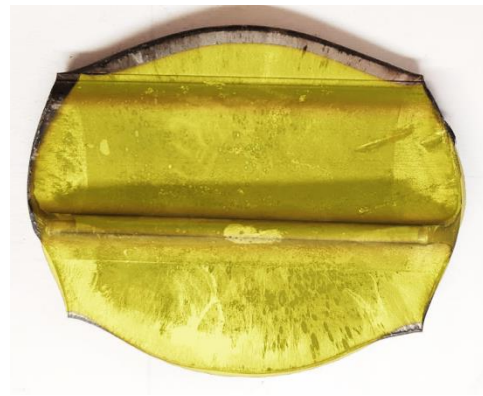
SF11 – 0.4mm/s

SF12 – 4mm/s

- Dimensional comparison

SF10		0.04mm/s	Step 109		
ZK60	1	2	3	4	5
Aniso	52.75	70.41	60.83	54.90	41.93
Exp	60.03	69.46	57.8	57.89	36.85
% dif	-12.12	1.37	5.24	-5.16	13.79

SF11		0.4mm/s	Step 105		
AZ80	1	2	3	4	5
Aniso	53.9	67.65	56.29	50.54	37.5
Exp	56.37	65.95	55.45	53.78	39.08
% dif	-4.38	2.58	1.51	-6.03	-4.04

SF12		4mm/s	Step 105		
AZ80	1	2	3	4	5
Aniso	55.22	67.88	56.87	50.41	38.41
Exp	55.17	65.39	57.92	54.15	38.27
% dif	0.09	3.81	-1.81	-6.91	0.37

- Load comparison

0.04mm/s

0.4mm/s

4mm/s
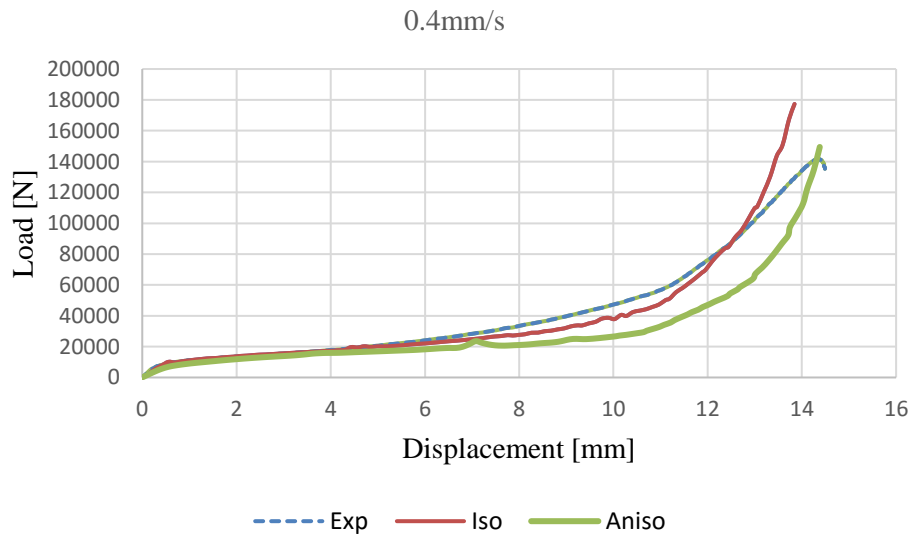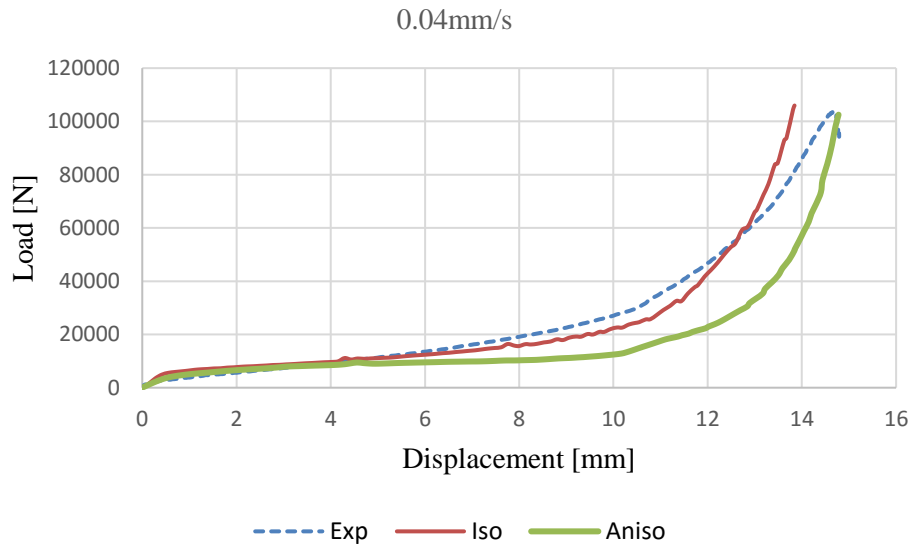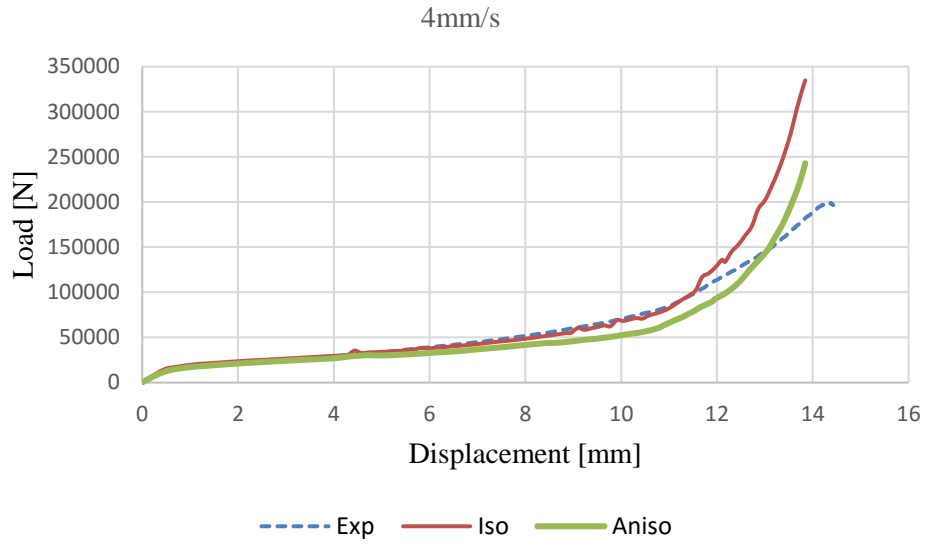
Appendix C

I-Beam Forging Die Design

Ø 9.53 ▽ 12.70

4 x Ø 11.9 THRU
⌴ Ø 20 ▽ 25

161.93
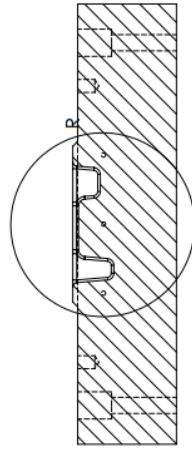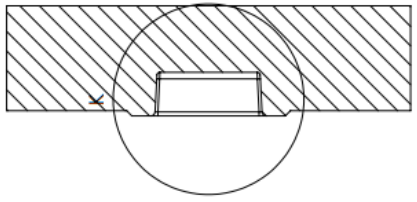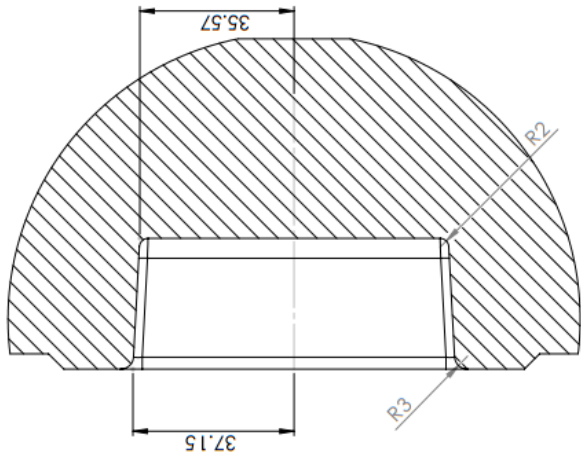133.35
101.60
50.80

101.60
111.13
139.70
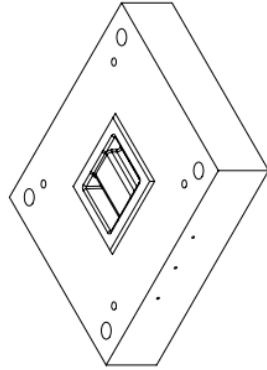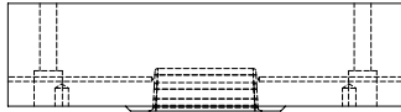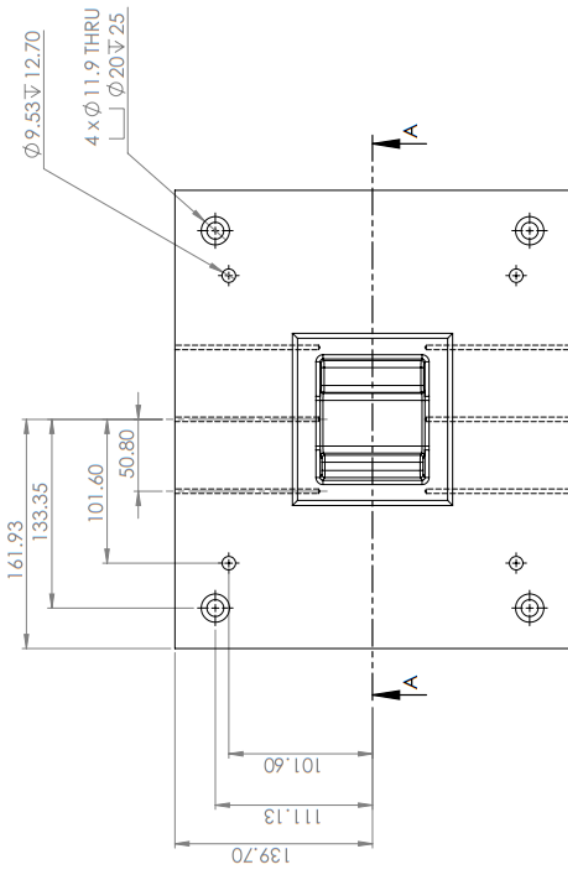
3x Ø 3.18 ▽ 102.6
Both Sides

SECTION A-A
SCALE 1 : 3

UNLESS OTHERWISE SPECIFIED:
DIMENSIONS ARE IN MILLIMETERS
SURFACE FINISH:
TOLERANCES:
LINEAR:
ANGULAR:

	NAME	SIGNATURE	DATE			
DRAWN	Hugo					
CHK'D						
APPV'D						
MFG						
Q.A						

FINISH:

DEBUR AND
BREAK SHARP
EDGES

DO NOT SCALE DRAWING

REVISION

TITLE:

Upper Die

MATERIAL:
HOTVAR

DWG NO.
01

A3

WEIGHT:

SCALE:1:2

SHEET 1 OF 6

108

DETAIL R
SCALE 2 : 1

R5
R3
R5
R5
R5
R3
R5

SECTION A-A
SCALE 1 : 3

	NAME	SIGNATURE	DATE
DRAWN	Hugo		
CHK'D			
APPV'D			
MFG			
Q.A			

TITLE:

UpperDie

MATERIAL:
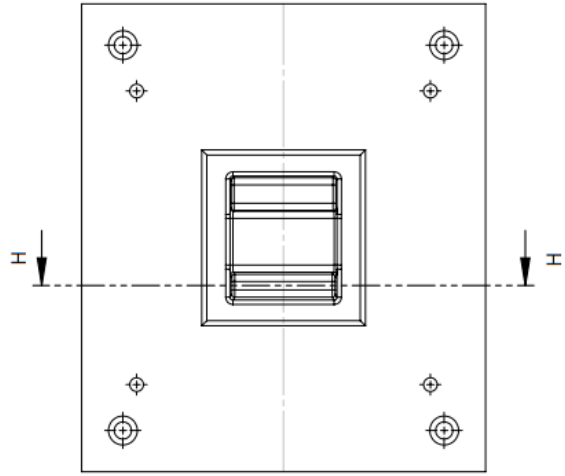HOTVAR

DWG NO.
02

WEIGHT:

SCALE:1:5   SHEET 2 OF 6

A3

DETAIL P
SCALE 2 : 1

SECTION A-A
SCALE 1 : 3

UNLESS OTHERWISE SPECIFIED:
DIMENSIONS ARE IN MILLIMETERS
SURFACE FINISH:
TOLERANCES:
  LINEAR:
  ANGULAR:

	NAME	SIGNATURE	DATE
DRAWN	Hugo		
CHK'D			
APPV'D			
MFG			
Q.A			

FINISH:

DEBUR AND
BREAK SHARP
EDGES

DO NOT SCALE DRAWING

REVISION

MATERIAL:
HOTVAR

WEIGHT:

TITLE:

Upper Die

DWG NO.
03

SCALE:1:2   SHEET 3 OF 6

A3

76.20
72.67
19.05
16.61
5 x 45°
57.31
42.97
18.01
23.41
43.33
57.31
3.54
26.61
41.21
19.41
25.69
40.69

DETAIL K
SCALE 1 : 1

35.57

37.15

R2

R3

SECTION H-H
SCALE 1 : 3

H

H

UNLESS OTHERWISE SPECIFIED: DIMENSIONS ARE IN MILLIMETERS SURFACE FINISH: TOLERANCES: LINEAR: ANGULAR:		FINISH:		DEBUR AND BREAK SHARP EDGES		DO NOT SCALE DRAWING	REVISION
	NAME	SIGNATURE	DATE		TITLE:		
DRAWN	Hugo						
CHK'D						Upper Die	
APPV'D							
MFG							
Q.A				MATERIAL: HOTVAR	DWG NO. 04	
				WEIGHT:	SCALE:1:5	SHEET 4 OF 6
						A3

111

DETAIL M
SCALE 1 : 1

0.61

R2
R3

SECTION L-L
SCALE 1 : 3

M

L
L

112

DETAIL O
SCALE 1 : 1

SECTION N-N
SCALE 1 : 3

R3
R2

O

N
N

Upper Die

HOTVAR

DWG NO. 06

SCALE:1:5   SHEET 6 OF 6

A3

113

Appendix D
I-Beam Forging Results

1. Test matrix

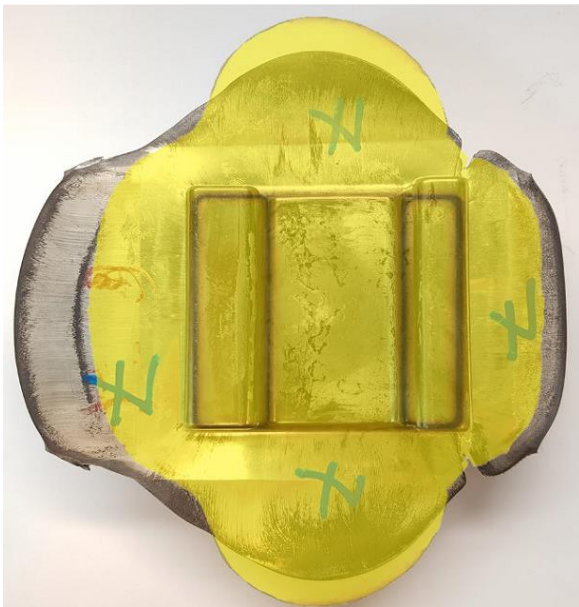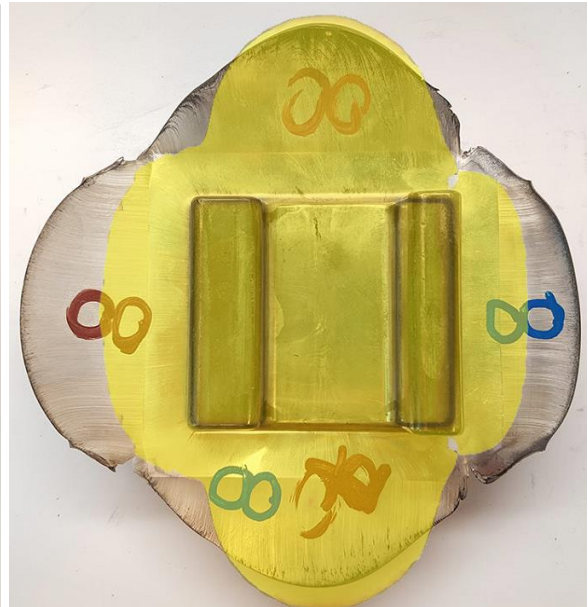| Trial	Material	Billet Temperature	Tooling Temperature	Displacment Rate	Lubricant	Test Date
		°C	°C	mm/s		
IF1	AZ31extruded	500	500	0.006	graphite	
IF2	AZ31extruded	500	500	0.06	graphite	08-Jun-16
IF3	AZ31extruded	500	500	0.6	graphite	03-Jun-16
IF3b	AZ31extruded	500	500	0.6	copper sheath / graphite	06-Jun-16
IF3c	AZ31extruded	500	500	0.6	graphite	06-Jun-16
IF4	AZ31extruded	500	500	6	graphite	07-Jun-16
IF5	AZ80extruded	400	400	0.006	graphite	
IF6	AZ80extruded	400	400	0.06	graphite	01-Jun-16
IF6b	AZ80extruded	400	400	0.06	graphite	14-Jun-16
IF7	AZ80extruded	400	400	0.6	graphite	01-Jun-16
IF7b	AZ80extruded	400	400	0.6	graphite	14-Jun-16
IF8	AZ80extruded	400	400	6	graphite	01-Jun-16
IF8b	AZ80extruded	400	400	6	graphite	14-Jun-16
IF9	AZ80extruded	400	400	0.006	graphite	
IF10	ZK60extruded	450	450	0.06	graphite	02-Jun-16
IF10b	ZK60extruded	450	450	0.06	graphite	22-Jun-16
IF11	ZK60extruded	450	450	0.6	graphite	02-Jun-16
IF11b	ZK60extruded	450	450	0.6	graphite	22-Jun-16
IF12	ZK60extruded	450	450	6	graphite	02-Jun-16
IF12b	ZK60extruded	450	450	6	graphite	22-Jun-16
IF13	AZ80extruded	400	25	0.06	graphite	07-Jun-16
IF14	AZ80extruded	400	25	6	graphite	07-Jun-16
IF15	ZK60extruded	450	25	6	graphite	11-Jun-16
IF16	AZ31Bextruded	500	25	6	graphite	10-Jun-16
IF17	AZ80extruded	400	200	6	graphite	15-Jun-16
IF18	ZK60extruded	450	200	6	graphite	15-Jun-16
IF19	AZ31Bextruded	500	200	6	graphite	16-Jun-16
IF20	AZ80extruded	400	400	24	graphite	23-Jun-16
IF21	AZ80extruded	400	400	??? - tbd	graphite	23-Jun-16

2. AZ31

IF3c – 0.6mm/s
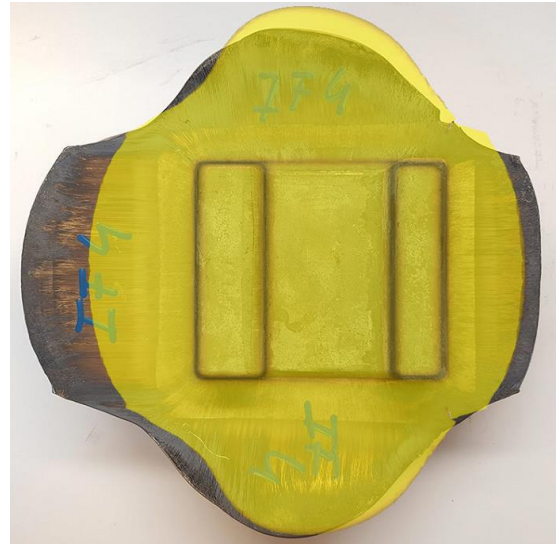
IF4 – 6mm/s

3. AZ80

IF7b – 0.6mm/s

IF8b – 6mm/s